Volume 1
Issue 1

September 2024

eISSN: 3063-640X

INTERNATIONAL JOURNAL OF MARINE ENGINEERING AND APPLICATIONS

Published by
Department of Marine Engineering
Universitas Hang Tuah

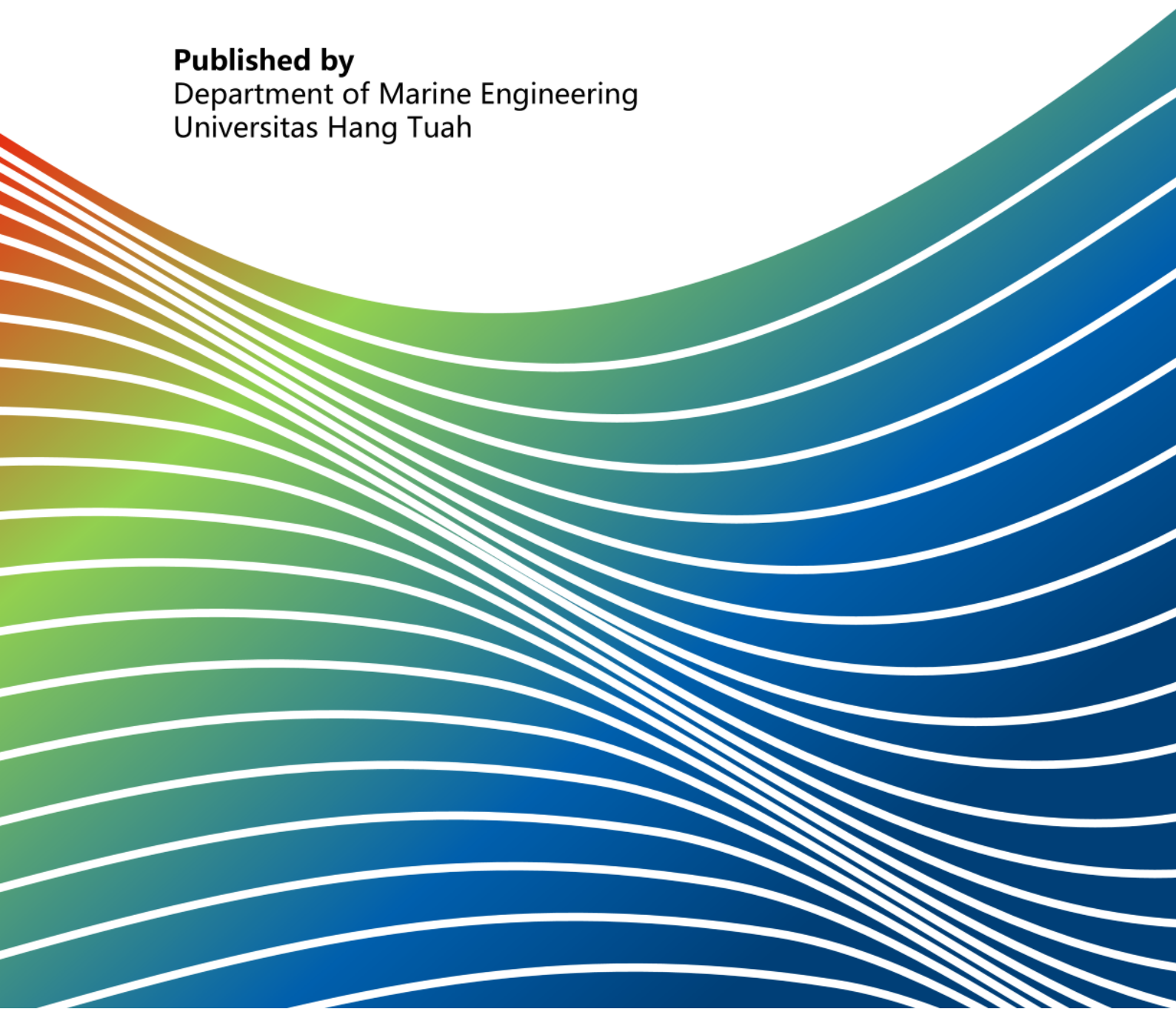

INTERNATIONAL JOURNAL OF MARINE ENGINEERING AND APPLICATIONS

VOLUME 1, ISSUE 1, SEPTEMBER 2024
DOI: https://doi.org/10.30649/ijmea.v1i1

TABLE OF CONTENT

ARTICLE

INTERNATIONAL JOURNAL OF MARINE ENGINEERING AND APPLICATIONS

International Journal of Marine Engineering and Applications
Volume 1, Number 1, September 2024
e-ISSN: 3063-640X

Date of Received:
July 18, 2024

Date of Accepted:
August 1, 2024

Date of Published:
September 1, 2024
DOI: doi.org/10.30649/ijmea.v1i1.374

TECHNICAL STUDY ON THE COMPARATIVE PLANNING OF A WASTE COLLECTION VESSEL PROPULSION SYSTEM: CONVENTIONAL ENGINE AND SOLAR PANELS

Betty Ariani[1*], Burhana Robby[2]

[1] Department of Naval Architecture, Universitas Muhammadiyah Surabaya, 60113, Indonesia
[2] Department of Marine Engineering, Universitas Hang Tuah, 60111, Indonesia

*Corresponding Author: betty.ariani@ft.um-surabaya.ac.id

ABSTRACT

Conventional diesel engines, also known as mechanical direct injection systems, represent a traditional approach to fuel delivery in engines. In contrast, solar panels convert sunlight into electrical energy using the photovoltaic effect. This research aims to conduct a technical comparative study on the planning of a waste collection vessel propulsion system using both conventional diesel engines and solar panels. The vessel system design requires 3.78 hp. The battery capacity calculated for this system is 84.24 Ah, with an operational duration of 6.4 hours for the diesel engine. The waste capacity is 0.371 m^3/ton, with a power requirement of 3.75 hp, and the chosen engine for this setup is the Yamaha 5CHMS. For the solar panel system, the potential calculation is 5.47 hours of sunlight, with a similar vessel system design of 3.78 hp. The battery usage duration is 6 hours, with the same waste capacity and power requirement. The selected solar panel is the Hangkai DNYSJYSJ. Based on technical calculations, it can be concluded that a waste collection vessel with a conventional diesel engine is more efficient due to its consistent technical performance requirements.

Keywords: Diesel, propulsion, solar panels, technical comparative analysis, waste collection vessel.

Introduction

Environmental issues have become increasingly critical in recent years, with aquatic pollution being one of the major concerns [1]. Rivers and oceans worldwide are plagued with floating debris and waste, severely impacting marine ecosystems and human health. Tackling this problem requires innovative and effective solutions to maintain clean waterways and preserve aquatic life [2].

One straightforward yet impactful approach to mitigate water pollution is the deployment of waste collection vessels [3]. These vessels play a vital role in cleaning up floating debris, thereby reducing pollution levels and preventing the spread of contaminants [4]. However, the efficiency and sustainability of these vessels depend significantly on their propulsion systems. This study aims to compare the technical aspects of two propulsion systems: conventional engines and solar panels [5].

Conventional engines, known for their mechanical direct injection systems, have been the traditional choice for marine propulsion [6]. They are renowned for their reliability and performance. However, the environmental impact of diesel engines, including greenhouse gas emissions and fuel consumption, has raised concerns about their long-term viability [7]. As a result, there is a growing interest in exploring alternative, more sustainable propulsion methods [8].

Solar panels, which convert sunlight into electrical energy through the photovoltaic effect, offer a promising alternative [9]. Solar-powered vessels produce zero emissions during operation,

Figure 1. Vessel Hull Shape

making them an environmentally friendly option [10]. The ability to harness renewable energy from the sun presents an opportunity to reduce the carbon footprint of marine operations significantly [11]. However, the practicality and efficiency of solar panels in marine applications require thorough investigation.

This research will conduct a technical comparative analysis of waste collection vessel propulsion systems powered by conventional engines and solar panels. By evaluating key performance indicators such as power output, operational duration, energy efficiency, and environmental impact, this study aims to provide valuable insights into which system offers a more viable solution for future applications. The findings will help guide the design and implementation of more sustainable marine vessels, contributing to cleaner waterways and a healthier planet.

In conclusion, this study not only addresses the pressing issue of aquatic pollution but also explores innovative solutions to enhance the sustainability of waste collection vessels. By comparing diesel and solar-powered systems, we seek to identify the most effective propulsion method, paving the way for cleaner and more efficient marine operations. The results of this research will be instrumental in shaping the future of marine environmental conservation efforts.

Methodology

a. Vessel Specification

The first step in the methodology involves specifying the waste collection vessel used in this study. The chosen vessel is a small 4-meter waste collection boat, as shown in Figure 1. This boat is designed for efficiency in navigating narrow waterways and collecting floating debris, making it an ideal candidate for waste collection in various aquatic environments [12]. The vessel's main dimensions, weight, and waste capacity are detailed in Table 1, providing a clear overview of its specifications.

This particular vessel model was selected based on its proven performance in previous research and practical applications. Its compact size allows it to operate effectively in confined spaces, such as canals and rivers, where larger vessels would struggle. Additionally, the design and construction of the vessel have been optimized for stability and maneuverability, ensuring it can handle the demands of waste collection without compromising safety or efficiency.

The specifications outlined in Table 1 include key parameters such as the vessel's length, width, depth, weight, and maximum waste capacity. These parameters are critical for understanding the operational limits and capabilities of the vessel, which in turn influence the propulsion system requirements. By providing a detailed specification, this study ensures that all subsequent analyses and comparisons between the conventional diesel engine and solar panel systems are grounded in a realistic and practical context.

Furthermore, the vessel's waste capacity is a crucial factor in this study. The capacity determines how much debris the vessel can collect before needing to return for unloading, directly impacting the efficiency and effectiveness of the waste collection process. By selecting a vessel with a

known and tested waste capacity, this study builds on a foundation of reliable data, enhancing the validity of the comparative analysis.

Table 1. Vessel Specification

Specification	Value
Length of Overall (LOA)	4,000 m
Length of Waterline (LWL)	3,858 m
Breath (B)	1,200 m
Height (H)	0,600 m
Draft (T)	0,300 m
Volume Displacement	0,36 m^3

In summary, the specification of the waste collection vessel is a foundational step in this methodology. It establishes the baseline parameters for the vessel's performance and ensures that the study is rooted in practical, real-world conditions. This careful selection and detailed documentation of the vessel's specifications enable a robust comparison of the propulsion systems under consideration, providing valuable insights into their respective efficiencies and operational characteristics.

b. Vessel Power Selection

The power selection process is critical for ensuring the vessel's operational efficiency. For this study, two power systems are compared: a conventional diesel engine and a solar panel system. The conventional diesel engine, specifically the Yamaha 5CHMS, was chosen for its proven reliability and compact design, making it suitable for small vessels. This engine is known for its robust performance, ease of maintenance, and availability, making it a practical choice for waste collection operations.

In contrast, the solar panel system was selected for its capability to provide a sustainable and environmentally friendly power source. The chosen solar panel, the Hangkai DNYSJYSJ, is designed to harness solar energy efficiently and convert it into electrical power. This system offers the advantage of reducing fuel consumption and emissions, aligning with modern environmental standards and sustainability goals [13].

The vessel's power requirements were meticulously calculated to ensure both systems can meet the operational demands. These calculations consider factors such as the vessel's speed, operational duration, and the power needed to drive the propulsion system and auxiliary equipment. By ensuring that both power systems can deliver the required performance, this study provides a fair basis for comparing their efficiency and suitability for waste collection applications.

c. Engine Performance Calculation

A series of performance calculations were conducted to evaluate the diesel engine's suitability [14]. These include determining the effective horsepower (EHP), shaft horsepower (SHP), brake horsepower (BHP), and delivered horsepower (DHP). The calculations are based on standard engineering principles, taking into account factors such as fuel efficiency, mechanical losses, and engine load conditions. These performance metrics are essential for understanding the engine's operational efficiency and reliability.

- Effective Horsepower (EHP): This metric measures the actual power delivered to the propeller, considering the losses in the drivetrain.
- Shaft Horsepower (SHP): This represents the power available at the engine shaft before any losses due to the propeller or other mechanical components.
- Brake Horsepower (BHP): This measures the engine's power output before losses due to friction and other mechanical inefficiencies.
- Delivered Horsepower (DHP): This final metric represents the power that effectively reaches the water to propel the vessel.

These calculations are based on standard engineering principles and take into account factors such as fuel efficiency, mechanical losses, and engine load conditions. By evaluating these performance metrics, the study provides a comprehensive understanding of the diesel engine's operational efficiency and reliability.

d. Solar Panel System Calculation

The solar panel system's feasibility was assessed by calculating its energy production capabilities and storage requirements [15]. This involves evaluating the potential sunlight exposure, typically measured in peak sunlight hours per day, and determining the solar panel's ability to generate the necessary power. The solar panels' placement and orientation on the vessel were optimized to maximize energy capture, ensuring that the system

can operate effectively even in varying sunlight conditions.

Additionally, the battery storage capacity was calculated to ensure the vessel can operate continuously, even during periods of low sunlight. This includes considerations for battery type, storage efficiency, and overall system integration to meet the operational power requirements. The chosen battery type, capacity, and expected performance metrics are detailed to provide a clear understanding of the solar power system's capabilities and limitations.

By conducting these detailed calculations, the study ensures that the solar panel system is not only theoretically viable but also practical for real-world application. The combination of optimized solar energy capture and adequate battery storage ensures that the vessel can maintain its operational efficiency and reliability, making the solar panel system a viable alternative to the conventional diesel engine.

Result and Discussion

a. Technical Calculation of Ship Powering Using Conventional Engine

In the calculation of the main engine power for this vessel, Break Horse Power (BHP) was considered. The initial calculation involved determining the service speed used. To calculate the service speed, the formula used was Vp plus 1, multiplied by 0.5144. The result of this calculation was 4.629 knots.

Vp = (Vd + 1) × 0.5144
= (18 + 1) × 0.5144
= 4.629 knots

In addition, the vessel's resistance was calculated based on the ship's speed. The resistance calculation had already been performed, yielding a result of 28.056 N. This hull resistance value was then used to calculate the Effective Horsepower (EHP). To calculate EHP, the ship's resistance (Wo) was multiplied by the service speed (Vp) and then divided by 75, resulting in 1.731 hp.

$$EHP = \frac{Wo\ x\ VP}{75} = \frac{28.056\ x\ 4.629}{75} = 1.73 \text{ hp}$$

Wake Friction is assessed by comparing the ship's speed with the propeller's rotational speed. To calculate W, 0.5 was multiplied by Cb, which was 0.8, and then 0.05 was subtracted. Hence, the calculated result for wake friction was 0.35.

W = (0.5 x 0.8) – 0.05 = (0.5 x 0.228) – 0.05 = 0.35

The Thrust Deduction Factor, which signifies the loss of thrust in the propulsion system, was calculated. It was determined by multiplying 0.6 by W. Consequently, the thrust deduction factor was found to be 0.21.

t = 0.6 x W
t = 0.6 x 0.35 = 0.21

From the calculations of wake friction and thrust deduction factor, the hull efficiency was determined. To calculate the hull efficiency (ηh), the thrust deduction factor (t) was subtracted from 1 and then divided by 1 minus the wake fraction (w). The result of this calculation was 1.21.

$$\eta h = \frac{1-t}{1-w} = \frac{1-0.21}{1-0.35} = 1.21$$

From these calculations, the coefficient of propulsion (Pc) can be determined to find the Delivered Horse Power (DHP). Pc is calculated by multiplying the propulsion efficiency ηp by the hull efficiency ηh and then by the relative rotational efficiency ηrr. Here, the propulsion efficiency is taken as 0.419, and the relative rotational efficiency as 1.03. Thus, the coefficient of propulsion Pc is determined to be 0.523.

Pc = $\eta p\ x\ \eta h\ x\ \eta rr$
= 0.419 x 1.21 x 1.03 = 0.523

Following this, the propeller shaft power is calculated based on the ratio of Effective Horsepower (EHP) to the coefficient of propulsion (Pc). From this calculation, the Delivered Horsepower (DHP) is determined to be 3,309 hp.

$$DHP = \frac{EHP}{Pc} = \frac{1.731}{0.523} = 3.309 \text{ hp}$$

Following that, the Thrust Horsepower (THP) was calculated, which represents the power delivered by the driving engine (shaft power). THP was calculated by dividing DHP by 0.98, resulting in 3.376 hp.

$$THP = \frac{DHP}{0.98} = \frac{3.309}{0.98} = 3.376 \text{ hp}$$

Table 2. Comparison of Conventional Engine Options

Specification	**Option 1**	**Option 2**	**Option 3**
Engine	Maritime 10DO1	Yamaha 5CMHS	Outboard MOB-803G
Fuel	Diesel	Gasoline	Gasoline
Engine Type	Inline 1	1 Cylinder – 2 Stroke	2 - Stroke
Power (hp)	10	5	3
Engine Speed (rpm)	3600 – 4000	4500 – 5500	6500
Displacement (cc)	406 cc	103 cc	52 cc
Transmission	Forward – Neutral - Backward	Forward – Neutral - Backward	Forward
Weight (kg)	60	21	10
Physical Figure			

To calculate Shaft Horse Power (SHP), DHP increased by 3% and is multiplied by DHP. The result is 3.408 hp.

SHP = DHP + (3% x DHP)
= 3.309 + (3% x 3,309) = 3.408 hp

In this system, the vessel does not use a reduction transmission system, so the calculated BHP_{scr} is equal to SHP, which is 3.408 hp.

BHP_{scr} = SHP = 3.408 hp

BHP_{mcr} is the output power of the propulsion motor sought for the main engine of the ship. To calculate BHP_{scr} BHP_scr is divided by 0.85, resulting in a value of 4.26 hp.

$BHP_{mcr} = BHP_{scr}/0.85$ = 4.26 hp

From the results obtained, it is known that the power required for the conventional engine to be used on this ship is 4.26 hp. This power is categorized as relatively small compared to larger vessels. After researching several engines within this power range, three engines were found that fit this requirement for the ship. Table 2 presents a comparison of several conventional engines found within this power range.

It was found that the Yamaha 5CMHS engine closely matches the required power. This gasoline-powered engine has a maximum power output of 5 hp. The other two engines, Maritime 10DO1 and Outboard MOB-803G, are still significantly outside the required power range. Several other options are displayed in Table 2.

Engines that are too large or too small can be disadvantageous for their use on the ship, affecting both capital expenditure and operational costs. Additionally, oversized engines increase the weight of the ship, potentially reducing payload capacity [16]. Engines with insufficient power cannot effectively meet the operational needs of the ship, aligning with the intended purpose of the vessel construction [17].

b. Technical Calculation of Ship Powering Using Solar Panel Battery Selection

Battery Selection

Batteries store electrical energy received from solar panels and distribute it to loads. They also provide power to loads when there is no sunlight. There are specific specifications to evaluate solar battery options, such as how long the solar battery will last and how much power it can supply [18]. For this study, the IDrive2 magnetic motor battery has been chosen, as shown in Figure 2 with detailed specifications in Table 3.

The data provided outlines the specifications for a battery system intended for use in the waste collection vessel's solar panel power setup. The battery dimensions are 522 mm in length, 239 mm in width, and 221 mm in height, making it compact enough to fit within the vessel's designated space for energy storage components. This compact size ensures that the battery can be easily integrated without compromising the vessel's design or functionality. With a weight of 25 kg, the battery is also relatively lightweight, minimizing the impact on the vessel's overall weight and stability.

Figure 2. Visual Construction of IDrive2 Battery

The battery operates with a nominal voltage of 24 V and a nominal capacity of 100 Ah. This capacity indicates that the battery can store a substantial amount of energy, essential for ensuring the vessel can operate for extended periods, even during cloudy days or when sunlight is limited. The charge voltage is specified at 57.6 V, with a standard charge current of 15 A, providing a clear guideline for the charging infrastructure required to maintain optimal battery performance. These specifications are critical for designing the solar panel system and ensuring that the energy storage is efficient and reliable.

Moreover, the battery's depth of discharge (DoD) is 80%, which means that 80% of the battery's total capacity can be used before recharging is necessary. This higher DoD allows for more efficient use of the stored energy, ensuring that the vessel can make the most out of each charging cycle. The balance between nominal capacity and DoD is crucial for maintaining battery health and longevity, making this battery a robust choice for the vessel's energy needs. These specifications collectively contribute to the effectiveness and sustainability of the solar-powered propulsion system.

Vessel Power Requirement

To calculate the solar panel requirements, data on power needs and the potential solar energy output specific to the location where the ship will operate, in Surabaya, Indonesia, are necessary. Table 4 presents the required data for this calculation.

Table 3. Battery Specification

Specification	Value
Dimension (mm)	522 x 239 x 221
weight (kg)	25
Charge Voltage (V)	57,6
Charge Current Standard (A)	15
Nominal Voltage (V)	24
Nominal Capacity (Ah)	100 Ah
Depth of Discharge (%)	80

Table 4. The Primary Data for Calculating Solar Panel Requirements

Basic Consideration	Value	Unit
Pload	1850	Watt
PSI	1000	Watt/m^2
Gav	5473	Wh/m^2 per day
ΔT	7	^{o}C
PSH	5.473	Hour

With this data, the efficiency of solar panels at each capacity can be determined by calculating ηpv. In this study, selections were made for several solar panel capacities: 200 Wp, 300 Wp, and 450 Wp, using the following method. The calculated ηpv for a 200 Wp solar panel is 15.27%, for a 300 Wp solar

panel is 18.45%, and for a 450 Wp solar panel is 21.65%. From these results, it was found that the 450 Wp solar panel exhibits the highest efficiency.

ηpv = (Pmax)/(PSI x A)(100%)

Pmax = 200 wp

PSI = 1000 watt/m^2
A = 1,309 m^2

ηpv = $(\frac{200}{1000\ x\ 1,309})$x100%
= 15,27 %

Pmax = 300 wp

PSI = 1000 watt/m^2
A = 1,626 m^2

Hpv = $(\frac{300}{1000\ x\ 1,626})$x100%
= 18,45 %

Pmax = 450 wp

PSI = 1000 watt/m^2
A = 2,078 m^2

NPv = $(\frac{450}{1000\ x\ 2,078})$x100%
= 21,65 %

After obtaining the efficiency values for each solar panel capacity, the power generated by each capacity can be determined to identify which solar panel can meet the power requirements of the electric conveyor motor. The power required (Pwp) is calculated as the product of peak solar irradiation (PSI), which is 1000 Watt/m^2, multiplied by the effective solar energy absorption time (PSH), the area of the solar panel (A), and the solar panel efficiency. The PSH value is derived from the global horizontal irradiance (GHI), which is 5478, divided by 1000, resulting in an energy absorption time of 5.478 hours.

Pwp = PSI x A x ηpv x PSH

PSH = $(\frac{GHI}{PSI})$
PSH = $\frac{5478}{1000}$
PSH = 5,478 hour

From the calculation of PSH, the power generated by each solar panel can be determined. The solar panel with a capacity of 200 Wp generates a power output of 1094 Wp, while the 300 Wp solar panel generates 1643 Wp, and the 450 Wp solar panel generates 2464 Wp.

Pwp solar panel 200 wp

PSI = 1000 watt/m^2
A = 1,309 m^2
Npv = 15,27 %
PSH = 5,478 jam

Pwp 200 wp = 1000 x 1,309 x (15,27%) x 5,478
= 1094 wp

Pwp solar panel 300 wp

PSI = 1000 watt/m^2
A = 1,626 m^2
Npv = 18,45 %
PSH = 5,478 jam

Pwp 300 wp = 1000 x 1,626 x (18,45%) x 5,478
= 1643 wp

Pwp solar panel 450 wp

Pmax = 450 watt
PSI = 1000 watt/m^2
A = 2,078 m^2
PSH = 5,478 jam
Npv = 21,65 %

Pwp 300 wp = 1000 x 2,078 x (21,65%) x 5,478
= 2464 wp

The calculations from the equation above show the power generated by solar panels during their effective operating time in Surabaya. According to the Solar Global Atlas website, the effective solar energy absorption time in Surabaya is approximately 5.47 hours, occurring between 09:00 and 14:47, which is the optimal period for energy absorption.

The power generated by solar panels is influenced by the location's temperature

If the location where the solar panels are used exceeds 25°C, the panels will experience a power loss of 0.5%. In this study, the solar panels are deployed in the sea near Surabaya, with daily temperatures averaging 28.1°C according to the data in the image. Thus, the difference between the

standard panel temperature and the sea temperature in Surabaya is 7°C.

To determine the total power (Pmpp) generated by each solar panel capacity after accounting for the temperature difference, it can be calculated as follows: Pwp multiplied by (1 - 0.005) multiplied by the temperature difference.

Pmpp = Pwp - (0.5% x Pwp x ΔT)

Pmpp solar panel 200 wp

Pwp =1000 wp
ΔT = 3°C

Pmpp = 1094 – (0,5% x 1094 x 3)
= 1055 wp

Pmpp solar panel 300 wp

Pwp = 1077 wp
ΔT = 3°C

Pmpp = 1643 – (0,5% x 1643 x 3)
= 1618.4 wp

Pmpp solar panel 450 wp

Pwp = 2250 wp
ΔT = 3°C

Pmpp = 2464 – (0,5% x 2250 x 3)
= 2430.25 wp

After obtaining the total power generated, the temperature correction factor (TCF) can be calculated using the following equation.

$$TCF = \frac{Pmpp}{Pwattpeak}$$

TCF of 200 wp

$$TCF = \frac{1055}{1094}$$
= 0.96 %

TCF of 300 wp

$$TCF = \frac{1618,4}{1643}$$
= 0.98%

TCF of 450 wp

$$TCF = \frac{2430,5}{2464}$$
= 0.98%

From the calculations, it is found that the temperature correction factors are similar, at 0.96% and 0.98%. Next, based on several previous calculation results, the number of solar panels needed for the ship's power requirements is determined based on the area of the solar panels [19]. Based on the power to be generated (Wpeak) with an assumed inverter efficiency of 0.9, the required number of solar panels (Npv) can be calculated as follows: Npv is equal to the total required power divided by the total power generated by a solar panel (EL).

EL = Pv area x GSI x ηpv x TCF x ηout

The number of 200 Wp solar panels needed can be calculated using the formula

EL = 1.309 m^2 x 5478 x (15.27%) x 0.96 x 0.9
EL = 946 wattpeak

$$Npv = \frac{1850}{946}$$
Npv = 1.95 pieces

Thus, the result of the calculation shows that 2 units of 200 Wp solar panels are needed.

The number of 300 Wp solar panels needed can be calculated using the formula

EL = 1.676 m^2 x 5478 x (18.45%) x 0.98 x 0.9
EL = 1494.03 wattpeak

$$Npv = \frac{1850}{1494,03}$$
Npv = 1.2 pieces

Thus, the result of the calculation shows that 2 units of 300 Wp solar panels are needed.

The number of 450 Wp solar panels needed can be calculated using the formula

EL = 2.16 m^2 x 5478 x (18.45%) x 0.98 x 0.9
EL = 1925 wattpeak

$$Npv = \frac{1850}{1925}$$
Npv = 0.96 pieces

Thus, the result of the calculation shows that 1 unit of 450 Wp solar panels is needed.

In this study, the available area for solar panels on the waste collection vessel is 2.76 m^2. Therefore, it is determined that the solar panel suitable for use

Table 5. Solar Panel Specification

Specification	**Value**	**Unit**
Maximum Power	450	wp
Maximum Power Voltage	41.40	V
Maximum Power Current	10.87	A
Operating Temperature	-40 – 85	*℃*
Dimension	2108 x 1048 x 35	*mm*
Weight	24,50	Kg
Open Circuit Voltage	50	V
Short circuit current	11,36	A

on the waste collection vessel is a 450 Wp solar panel. This is because a 450 Wp solar panel can adequately cover the available area for solar panel installation, which is sufficient for one solar panel.

Battery Capacity Requirement

To meet the electric motor's power requirements using solar energy, the next step is to determine the energy storage device, namely batteries. The suitable battery type for the solar photovoltaic system (PLTS) is a Deep Cycle Battery VRLA, such as VRLA Absorbent Glass Mat (AGM) or VRLA Gel, due to their long charge and discharge cycles, leak-free, and maintenance-free characteristics. To calculate the required battery capacity based on the load to be supplied, the following considerations are made: the autonomy day is one day, with a battery voltage of 24 V and a depth of discharge (DOD) of 0.9.

$$\text{AH} = \left(\frac{(\text{Pload x } Autonomy\ day)}{(Vbattery\ x\ Depth\ of\ Discharge)}\right)$$

$$\text{AH} = \frac{(1850\ x\ 1)}{(24\ x\ 0.9)} = 84.24 \text{ Ah}$$

The calculated battery capacity required is 84.24 Ah.

It has been determined that to meet the load requirements, a battery capacity of 84 Ah is necessary. However, batteries commonly available in the market are rated at capacities of 50 Ah, 100 Ah, and 150 Ah. Therefore, a 100 Ah battery capacity is selected. The electric conveyor motor operates at 230 V, hence 10 pieces of 100 Ah batteries are connected in series. This series configuration is chosen to increase the voltage output while keeping the current constant.

Subsequently, calculations are performed using the selected battery data from the previous calculation to determine the duration the conveyor power requirements can be met. This calculation yields the following result.

$$\text{Tbattery} = \left(\frac{(\text{Ah battery x V battery x PSH})}{\text{Pload}}\right)$$

$$\text{Tbattery} = \frac{(100\ x\ 24\ x\ 5)}{1850} = 6{,}4 \text{ (calculated as 6 hours)}$$

Thus, the calculated battery runtime required is 6.4 hours (rounded to 6 hours).

In this study, a 450 Wp solar panel is used, as shown in Figure 3. To determine the Voc (Open Circuit Voltage) and Isc (Short Circuit Current) values of the solar panel, refer to the panel's specifications in Table 5.

Vmaxin > 1,25 × 50 = 62,5 V

Imaxin > 1,25 × 11,36 = 14 ,2 A

Figure 3. Solar Panel with 450 Wp Monocrystalline (m.icasolar.com)

Based on the above calculations, the electric conveyor requires a minimum current of 14.2 A and a minimum voltage of 62.5 V. In this study, an SCC (Solar Charge Controller) with a maximum input current of 20 A is used, as SCCs commonly available in the market are sold in multiples of 10 A.

Apart from the conveyor, another electric motor is required for driving purposes in this study, which operates independently from the conveyor. Even if used together, it does not require power exceeding that of the conveyor, as specified in Table 6.

Table 6. Electric Motor Specification

Specification	**Value**
Type	Hangkai DNYSYSJ
Material	Aluminium
Operation	Electric
Model	DD-48V-1000W
Voltage	48V
Ampere	18A
Motor Speed	3000 rpm

c. Comparison of Diesel Engine and Solar Panel

From the calculation above about the power selection, it should be considered that for small vessels, such as a 4-meter waste collection boat, the comparison between conventional combustion engines and solar power becomes distinctively nuanced. Conventional small vessels powered by combustion engines, typically running on gasoline or diesel, offer reliable and powerful performance crucial for consistent operation, especially in areas with fluctuating waste collection needs. These engines are compact and can be easily maintained, but they require a supply of fuel, which adds to the operational costs and environmental impact due to emissions [20]. In contrast, small solar-powered vessels harness solar panels' energy, providing an environmentally friendly and sustainable power source. However, the power output from solar panels can be variable and dependent on sunlight availability, which might not be sufficient for consistent daily operations, especially in areas with limited sunlight.

From an investment and operational cost perspective, small conventional combustion engine vessels are generally less expensive to purchase initially due to the lower cost of small engines and the minimal infrastructure required [21]. However, the ongoing fuel and engine maintenance costs can accumulate over time, making them potentially more expensive in the long run. Solar-powered vessels require a higher initial investment due to the cost of solar panels and battery storage systems [22]. Nonetheless, they benefit from minimal operational costs as they do not require fuel and have lower maintenance needs, primarily focused on the upkeep of solar panels and battery systems. The long-term cost savings from reduced fuel expenses can be significant, especially for small vessels with regular use.

Space utilization is also a critical consideration for small vessels. Conventional engines require space for the engine itself and fuel storage, which can be substantial even on a small vessel, reducing the available space for waste collection. Solar panels, on the other hand, can be mounted on the vessel's roof or deck without taking up significant interior space, preserving more room for waste collection. However, battery storage systems for solar power can occupy space within the vessel, although advancements in battery technology are making these systems more compact and efficient [23]. Overall, for a small 4-meter waste collection vessel, solar power offers a promising alternative with environmental benefits and potential long-term cost savings, but it is limited by power availability and storage capacity compared to conventional combustion engines.

Conclusion

In conclusion, for small waste collection vessels, there is a trade-off between the reliability of conventional combustion engines and the sustainability of solar power. Conventional engines, such as the Yamaha 5CHMS, provide dependable performance but incur higher long-term costs and environmental impacts, requiring 3.78 hp and a battery capacity of 84.24 Ah for 6.4 hours of operation. Solar-powered vessels, using systems like the Hangkai DNYSJYSJ, offer an environmentally friendly and cost-effective alternative with better space utilization, needing 3.78 hp and providing 6 hours of operation from solar energy. However, their effectiveness depends on sunlight and advancements in battery technology. This research highlights the importance of continued innovation in solar technology to improve its feasibility for small marine vessels.

References

[1] J. F. Hansen and F. Wendt, “History and State of the Art in Commercial Electric Ship Propulsion, Integrated Power Systems, and Future Trends,” *Proceedings of the IEEE*, vol. 103, no. 12, pp. 2229–2242, Dec. 2015, doi: 10.1109/JPROC.2015.2458990.

[2] E. Sugianto, J. H. Chen, and N. P. Purba, "Cleaning technology for marine debris: A review of current status and evaluation," *International Journal of Environmental Science and Technology 2022*, pp. 1–20, Jul. 2022, doi: 10.1007/S13762-022-04373-8.

[3] G. Duan and K. Zhang, "Optimization on hybrid energy vessel routing and energy management for floating marine debris cleanup," *Transp Res Part C Emerg Technol*, vol. 138, p. 103649, May 2022, doi: 10.1016/J.TRC.2022.103649.

[4] M. Compa, D. March, and S. Deudero, "Spatio-temporal monitoring of coastal floating marine debris in the Balearic Islands from sea-cleaning boats," *Mar Pollut Bull*, vol. 141, pp. 205–214, Apr. 2019, doi: 10.1016/J.MARPOLBUL.2019.02.027.

[5] A. Del Pizzo, R. M. Polito, R. Rizzo, and P. Tricoli, "Design criteria of on-board propulsion for hybrid electric boats," *19th International Conference on Electrical Machines, ICEM 2010*, 2010, doi: 10.1109/ICELMACH.2010.5607817.

[6] B. Jeong, E. Oguz, H. Wang, and P. Zhou, "Multi-criteria decision-making for marine propulsion: Hybrid, diesel electric and diesel mechanical systems from cost-environment-risk perspectives," *Appl Energy*, vol. 230, pp. 1065–1081, Nov. 2018, doi: 10.1016/J.APENERGY.2018.09.074.

[7] C. A. Reusser and J. R. Pérez Osses, "Challenges for Zero-Emissions Ship," *Journal of Marine Science and Engineering 2021, Vol. 9, Page 1042*, vol. 9, no. 10, p. 1042, Sep. 2021, doi: 10.3390/JMSE9101042.

[8] H. Lan, S. Wen, Y. Y. Hong, D. C. Yu, and L. Zhang, "Optimal sizing of hybrid PV/diesel/battery in ship power system," *Appl Energy*, vol. 158, pp. 26–34, Nov. 2015, doi: 10.1016/J.APENERGY.2015.08.031.

[9] G. de Freitas Viscondi and S. N. Alves-Souza, "A Systematic Literature Review on big data for solar photovoltaic electricity generation forecasting," *Sustainable Energy Technologies and Assessments*, vol. 31, pp. 54–63, Feb. 2019, doi: 10.1016/j.seta.2018.11.008.

[10] C. S. Chin, Y. J. Tan, and M. V. Kumar, "Study of Hybrid Propulsion Systems for Lower Emissions and Fuel Saving on Merchant Ship during Voyage," *Journal of Marine Science and Engineering 2022, Vol. 10, Page 393*, vol. 10, no. 3, p. 393, Mar. 2022, doi: 10.3390/JMSE10030393.

[11] H. Pestana, "Future trends of electrical propulsion and implications to ship design," *Maritime Technology and Engineering*, pp. 811–820, Sep. 2014, doi: 10.1201/B17494-85.

[12] E. Sugianto, J. H. Chen, and N. V. A. Permadi, "Effect of Monohull Type and Catamaran Hull Type on Ocean Waste Collection Behavior Using OpenFOAM," *Water 2022, Vol. 14, Page 2623*, vol. 14, no. 17, p. 2623, Aug. 2022, doi: 10.3390/W14172623.

[13] N. Planakis, G. Papalambrou, and N. Kyrtatos, "Predictive power-split system of hybrid ship propulsion for energy management and emissions reduction," *Control Eng Pract*, vol. 111, p. 104795, Jun. 2021, doi: 10.1016/J.CONENGPRAC.2021.104795.

[14] A. Iswantoro, I. M. Ariana, and M. Syuhri, "Analysis of Performance, Emission, Noise and Vibration on Single Cylinder Diesel Engine After Installing Dual Fuel Converter-Kit Based on ECU," *Kapal: Jurnal Ilmu Pengetahuan dan Teknologi Kelautan*, vol. 19, no. 1, pp. 42–49, Mar. 2022, doi: 10.14710/KAPAL.V19I1.44126.

[15] N. Bennabi, J. F. Charpentier, H. Menana, J. Y. Billard, and P. Genet, "Hybrid propulsion systems for small ships: Context and challenges," *Proceedings - 2016 22nd International Conference on Electrical Machines, ICEM 2016*, pp. 2948–2954, Nov. 2016, doi: 10.1109/ICELMACH.2016.7732943.

[16] C. Nuchturee, T. Li, and H. Xia, "Energy efficiency of integrated electric propulsion for ships – A review," *Renewable and Sustainable Energy Reviews*, vol. 134, p. 110145, Dec. 2020, doi: 10.1016/J.RSER.2020.110145.

[17] W. Litwin, W. Lesniewski, D. Piatek, and K. Niklas, "Experimental Research on the Energy Efficiency of a Parallel Hybrid Drive for an Inland Ship," *Energies 2019, Vol. 12, Page 1675*, vol. 12, no. 9, p. 1675, May 2019, doi: 10.3390/EN12091675.

[18] B. Jeong *et al.*, "Is electric battery propulsion for ships truly the lifecycle energy solution for marine environmental protection as a whole?," *J Clean Prod*, vol. 355, p. 131756, Jun. 2022, doi: 10.1016/J.JCLEPRO.2022.131756.

[19] M. Altosole, U. Campora, and V. Vigna, "Energy efficiency analysis of a flexible marine hybrid propulsion system," *2020 International Symposium on Power Electronics, Electrical Drives, Automation and Motion, SPEEDAM 2020*, pp. 436–441, Jun. 2020, doi: 10.1109/SPEEDAM48782.2020.9161873.

[20] E. K. Dedes, D. A. Hudson, and S. R. Turnock, "Assessing the potential of hybrid energy technology to reduce exhaust emissions from global shipping," *Energy Policy*, vol. 40, no. 1, pp. 204–218, Jan. 2012, doi: 10.1016/J.ENPOL.2011.09.046.

[21] H. Doukas, E. Spiliotis, M. A. Jafari, S. Giarola, and A. Nikas, "Low-cost emissions cuts in container shipping: Thinking inside the box," *Transp Res D*

Transp Environ, vol. 94, p. 102815, May 2021, doi: 10.1016/J.TRD.2021.102815.

[22] Y. Yuan, J. Wang, X. Yan, B. Shen, and T. Long, "A review of multi-energy hybrid power system for ships," *Renewable and Sustainable Energy Reviews*, vol. 132, p. 110081, Oct. 2020, doi: 10.1016/J.RSER.2020.110081.

[23] P. Wu and R. Bucknall, "Hybrid fuel cell and battery propulsion system modelling and multi-objective optimisation for a coastal ferry," *Int J Hydrogen Energy*, vol. 45, no. 4, pp. 3193–3208, Jan. 2020, doi: 10.1016/J.IJHYDENE.2019.11.152.

International Journal of Marine Engineering and Applications
Volume 1, Number 1, September 2024
e-ISSN: 3063-640X

Date of Received:
June 24, 2024

Date of Accepted:
July 10, 2024

Date of Published:
September 1, 2024
DOI: doi.org/10.30649/ijmea.v1i1.366

MAINTENANCE ANALYSIS OF ANCHOR CHAIN AGAINST CORROSION RATE BY PAINTING METHOD

Fariz Maulana Noor [1*], Rizal Ruliyanto[1]

[1] Hydrodynamics Technology Research Centre, National Research and Innovation Agency, 60111, Indonesia

*Corresponding Author: farizmaulana@gmail.com

ABSTRACT

One of the damages to the anchor and its chain is caused by being exposed to various environmental loads from the sea every time the anchor is lowered or when the anchor is raised, so that it will gradually experience fatigue due to dynamic loads that occur repeatedly in a long period of time. However, there has not been an analysis that combines anchor chain maintenance of the corrosion rate with the painting method and a comparison between before painting and after painting. Therefore, the researchers proposed a study, "Analysis of Anchor Chain Maintenance of Corrosion Rates Using the Painting Method". This study aims to carry out an analysis to reduce the corrosion factor on the anchor chain by using marine coatings or painting processes so that the operability and capability of the system can be maintained. The research design is based on an experimental method that seeks to posit and solve the problem of the condition of a ship's anchor chain made of steel or metal. based on both visual data and literacy. The existing data is then analyzed and interpreted, which is comparative. The interval for each coat of paint depends on the drying power. What can you do with the next coat of paint if the previous paint layer is dry, it should not exceed the specified paint allowance, because it will give poor adhesion. From the analysis of the anchor chain structure, the resulting stress is 168.73 MPa. If it is estimated with a period of 3 years from the anchor chain structure, the stress result is 192.75 MPa, and if it occurs at this time in 2022 with a period of 5 years, the stress result is 213.95 MPa.

Keywords: Anchor chain, corrosion, marine coating, maintenance, analysis.

Introduction

An anchor is one component of ship equipment that plays a very important role in the marine transportation system. Ship anchors are used so that the ship does not move due to gusts of wind, currents, or waves. The anchor is designed in such a way and connected with a chain made of cast iron so that it can withstand the movement of the ship [4]. The anchor chain is equipment that is useful for connecting the ship's anchor to the ship so that it is not released if the anchor is lowered from the ship [3].

One of the damages to the anchor and its chain is caused by being exposed to various environmental loads from the sea every time the anchor is lowered or when the anchor is raised, so it will eventually experience fatigue due to dynamic loads that occur repeatedly over a long period of time. The risk of breaking the anchor chain is due to wear on the anchor chain material. Wear basically has several mechanisms, namely abrasion, erosion, adhesive, fatigue, and corrosion. Damage to the anchor and its chain is caused by environmental loads from the sea when the anchor is lowered or when it is raised, so that over time it will cause deformation in the anchor structure and its chain [4].

Based on previous research from Andarum Septianto, it has been stated that the absence of a

good anchor chain maintenance role in its implementation can have several impacts that can become a problem on the ship, such as corrosion, depletion of wildcat serrations, influence on the anchor feeding process, the heavy up anchor process is disrupted and from several impacts that can occur resulting in hampering ship operations [1].

In a study conducted by Mardawiah, it was shown that the stress result was 168.73 MPa when estimated with a period of 3 years from the installation of the chain line installation, the stress result was 192.75 MPa, and if it occurs at this time in 2022 with a period of 5 years, the stress result is 213.95 MPa. The strength of the chain line structure when receiving loads that work on safe criteria and do not exceed the maximum Yeild Strength according to the DNV OS E301 standard reference of 265.5 MPa, as well as the deformation results of 0.35101 mm, when estimated with a time period of 3 years from the installation of the chain line installation, the deformation results are 0.65605 mm. The results of the deformation value obtained do not exceed the maximum limit of deformation according to the DNV OS E301 standard reference of 0.8 mm [2].

Based on research, it can be concluded that the largest Von Mises stress value is found in the area between joints, which is 242.71 MPa under maximum loading conditions. The stress value is still below the yield strength value of the material used, which is 680 MPa, and the largest deformation value in the end shackle structure due to environmental loads is 0.103 mm. Based on this, it can be said that the end shackle structure used to withstand loads from anchors and environmental loads is in a safe condition for use and does not exceed the allowable stress set by the Indonesian Classification Bureau, which is 400 MPa [4].

Government and international organizations have been spurred by this to make significant pledges to decrease marine debris in many nations. Plans for regional and national garbage management have been created in numerous nations [5]. This has encouraged the emergence of various innovations and technologies for cleaning marine debris, one of which is a catamaran-type garbage collection ship and which uses conveyors with several conveyor wing variations [6].

Various studies on garbage collection vessels using catamaran vessels have been conducted. Research on the numerical investigation of the effect of conveyor wing type on marine garbage collection behavior has been conducted. This study discusses the effect of wing shape on garbage collection in calm waters. The three wing shape variations used in the numerical simulation are solid wing shape, square hollow wing shape, and circular hollow wing shape. As a result, from the simulation results, the circular hollow wing is faster in collecting marine debris, followed by the square hollow wing and the solid wing. From the flow pattern analysis, the circular hollow wing model is easier to get the marine debris closer to the winged conveyor than the square wing and solid wing models [7].

Other research is an experiment on the hollow wing technique to improve conveyor performance in marine debris collection [8]. Debris collection ratio than other models. A study on the effect of placing a portable conveyor on a garbage collection vessel on marine garbage collection behavior has been conducted [9].

According to research conducted by Alfafa and Zuan Syafa, the results of the calculation of the corrosion rate with the obtained factors, causing the diameter of the chain to decrease, namely corrosion and maintenance factors. The result of the reduction in the diameter of the anchor chain of the right X container ship is 0.549 mm, the corrosion rate is 0.198 mm/y, the left is 0.970 mm, and the corrosion rate is 0.232 mm/y. The right Y container ship is 0.054 mm, corrosion rate is 0.018 mm/y, the left is 1.392 mm, corrosion rate is 0.464 mm/y, and the right Z container ship is 1.088 mm, corrosion rate is 0.363 mm/y, the left is 2.267 mm, corrosion rate is 0.882 mm/y [10].

However, no analysis has been found that combines the maintenance of the anchor chain against the corrosion rate with the painting method and the comparison between before being subjected to painting and after painting. Therefore, the researcher proposed the research "Analysis of Anchor Chain Maintenance on Corrosion Rate by Painting Method". This research aims to conduct an analysis to reduce the corrosion factor of the anchor chain with the use of marine coating or painting processes, so that the operability and capability of the system can be maintained.

Methodology

Corrosion

Corrosion is the deterioration of metals due to electrochemical reactions with their environment. NACE (National Association of Corrosion

Engineers) defines corrosion as a decrease in the quality of a material (usually steel) or its properties caused by a reaction with its environment [11-12]. Meanwhile, Trethewey (1988) provides a definition of corrosion as a decrease in the quality of steel due to electrochemical reactions with the environment [1]. Furthermore, the ASM Materials Engineering Dictionary states corrosion as a chemical or electrochemical reaction between the anode and cathode of steel with an electrolyte environment that results in a decrease in material quality and chemical properties [13].

In many cases, corrosion attacks cannot be avoided, but they can be controlled so that the steel structure or component has a longer service life. Every structure or component generally goes through a three-stage process: design, manufacture, and use. Corrosion control plays an important role in each of these stages. Failure in any of the corrosion control stages can lead to premature failure of the component. In principle, corrosion control can be done in various ways, including: [14]

- Component design modification.
- Environment modification.
- Material selection.
- Cathodic and anodic protection.
- Application of protective coatings.

Protective or barrier coatings applied to steel surfaces aim to separate the steel from its environment or to control the microenvironment at the steel surface. There are many coating methods used for this purpose, including paints, organic coatings, varnishes, steel coatings, and enamels. However, by far, the most common and widely used method is paint [15].

The research design is based on an experimental method that tries to suggest and solve problems from the condition of the ship's anchor chain, made of steel or metal. based on data, both visual and literary. The existing data is then analyzed and interpreted, which is comparative in nature. This study uses research materials, including:

Research materials

The materials needed for research are as follows:

1. Anchor chains

An anchor chain is a critical component in a ship's mooring system that serves to connect the anchor to the ship. It has several special characteristics, such as high tensile strength, corrosion resistance, and flexibility, which allow the anchor to hold the vessel securely in place despite ocean currents, wind, and waves. Anchor chain materials are usually made of high-quality steel coated with anti-corrosion materials to increase durability against harsh marine environments. The anchor chain is shown in Figure 1.

Figure 1. Anchor chain

2. Anti-corrosive (AC)

Anti-corrosion paint is a type of paint specifically designed to protect metal surfaces from corrosion or rust. These paints contain chemicals that create a protective layer on the metal surface, preventing reactions between the metal and corrosive elements such as oxygen, water, salt, and other chemicals. The use of anti-corrosion paints is very common in the maritime industry, construction, automotive, and other sectors where metal protection from rust is essential. These include epoxy paints and zinc-rich primers. The function of epoxy is anti-corrosion protection, strong adhesion, mechanical strength, and abrasion resistance. The function of the zinc-rich primer is Cathodic Protection, good adhesion, Barrier Protection, and coating repair. The combination of epoxy, zinc-rich primer is very influential because, by using zinc-rich primer as the base coat and epoxy as the final protective layer, this combination provides very effective corrosion protection. Zinc-rich primer provides cathodic protection while epoxy protects against mechanical damage and corrosive elements, ensuring the anchor chain remains in optimal condition for a longer period of time. It is then painted with a protective marine anti-corrosion coating.

3. Salt Solution (NaCl)

Salt solution (NaCl) is a solution formed when table salt (sodium chloride) is dissolved in water as shown in Figure 2. Table salt consists of sodium ions (Na^+) and chloride ions (Cl-), which dissociate in water to form an electrolyte solution. Salt solutions are very important in various fields due to their distinctive electrolyte properties and their ability to simulate corrosive environments. NaCl is used to create environmental conditions that accelerate the corrosion process of metals. NaCl helps in checking how well protective coatings or paints protect metals from corrosion. And comparing the corrosion resistance of different types of metals or coatings under controlled conditions. NaCl is therefore very useful for simulating corrosive environments, for example, to test the corrosion resistance of materials and coatings.

Figure 2. Salt solution

Test equipment

The equipment needed for research is as follows:

1. Spray gun

A spray gun is a device used to spray liquids, such as paint, varnish, or other coatings, onto the surface of an object, as shown in Figure 3. It works by using air pressure to atomize the liquid into small particles, which are then sprayed in the form of a fine mist. Spray guns are essential tools in a variety of painting and coating applications, providing professional and efficient results.

Figure 2. Spray gun

2. Air compressor

An air compressor is a device used to increase air pressure by compressing the air entering the system, as shown in Figure 4. This pressurized air is then stored in a tank and can be used for a variety of industrial, repair, and maintenance applications, including as a power source for pneumatic tools such as spray guns, air drills, and lifting equipment. The compressor was used to assist with the painting process of the anchor chain.

Figure 4. Air compressor

3. Sandblasting tools

Sandblasting is the process of cleaning or smoothing the surface of a material by firing abrasive particles using high air pressure. Sandblasting tools are devices used to apply this technique. Sandblasting is usually used to clean ship hulls and steel structures from rust and dirt. The advantages of using sandblasting are high efficiency because it can clean surfaces quickly and effectively, accurate results because it provides smooth and uniform cleaning results, and flexibility because it can be used on various materials such as metal, wood, glass, and concrete. Therefore, by using sandblasting tools, the cleaning and surface preparation process becomes faster and more efficient, and provides a high-quality finish.

4. Micrometer for measuring paint thickness

A micrometer is a precision measuring device used to measure thickness or small dimensions with high accuracy. To measure the thickness of a paint layer, a special micrometer known as a coating thickness gauge is used. Micrometers are also commonly used to control the thickness of paint layers on various products to ensure quality and durability. The advantages of micrometers are high accuracy, ease of use, and flexibility. Therefore, by using a special micrometer to measure paint thickness, quality control becomes more efficient, and production or maintenance results are more reliable.

5. Corrosion rate measuring instrument

A corrosion rate meter is a device used to measure the degree of degradation or damage caused by corrosion to a particular material. It is generally designed to provide information about the speed of corrosion under various environmental conditions. Corrosion rate meters have the ability to control environmental conditions (such as temperature, humidity, and pH), make accurate and consistent measurements, and the ability to record data and analyze it for further evaluation. The use of corrosion rate meters is important in various industries such as manufacturing, construction, and metal treatment industries to identify and reduce the impact of corrosion on material reliability and service life.

6. Digital scales

Digital scales are measuring devices used to determine the weight of material samples before and after exposure to corrosive conditions. This weight difference helps calculate the corrosion rate or the rate of material loss due to corrosion. The digital scales are shown in Figure 5. Digital scales are measuring devices used to determine the weight of material samples before and after exposure to corrosive conditions. This weight difference helps calculate the corrosion rate or the rate of material loss due to corrosion. The digital scales are shown in Figure 5.

Figure 5. Digital scales

Marine Coating Methods with Epoxy Paint is one of the most popular marine coating options due to its strength and resistance to corrosion and abrasion. Epoxy can be applied to metal, concrete, and wood surfaces and provides long-lasting protection. Several studies have shown that epoxy paints are very effective in protecting ship surfaces from corrosion and the effects of the marine environment [16].

Marine Coating Method with Fluorinated Polymer is a marine coating material that is resistant to corrosion and highly resistant to the effects of harsh marine environments. It is often used for the protection of tankers and marine platforms due to its UV resistance and long-lasting performance [17].

Polyurethane Marine Coating Method is a marine coating material that is highly resistant to the effects of the marine environment, including corrosion and UV light. This material is resistant to abrasion and is easily applied to ship surfaces. Several studies have shown that polyurethane provides excellent protection and can increase the longevity of ships and marine structures [18].

Research Procedure

a. Sample preparation

1. Site Identification and Initial Preparation

In the site identification and preliminary preparation phase of corrosion testing, steps include selecting a representative and relevant test site, such as a maritime area with aggressive seawater conditions or a corrosion-prone industrial environment. In addition, the initial preparation includes collecting anchor chain samples from the site, as well as cleaning and smoothing the surface of the samples to remove any dirt, rust, or previous corrosion layers, to ensure consistent initial conditions ready for further treatment in the test. Proper site selection and preparation are critical to obtaining accurate and reliable test results.

2. Painting Method Selection

In the painting method selection stage of corrosion testing, different types of paints and coatings are considered based on the environmental conditions and material properties of the anchor chain. Considerations include paint resistance to seawater, adhesion ability, and durability under extreme operational conditions. Application methods such as brushing, spraying, or immersion were also evaluated to determine the most effective technique for providing maximum protection against corrosion. The selection of an appropriate painting method aims to ensure an optimal protective coating, so as to minimize the corrosion rate and extend the service life of the anchor chain.

3. Surface Preparation

The surface preparation stage in corrosion testing involves cleaning and smoothing the surface of the anchor chain to remove dirt, rust, and remnants of previous corrosion. This process includes the use of mechanical methods such as sandblasting, as well as chemical cleaning to ensure the surface is free of contaminants. Optimal surface preparation is essential to ensure strong adhesion of the paint protection layer, thereby increasing the effectiveness of corrosion protection and providing accurate and consistent test results.

4. Anchor Chain Painting

The process of painting the anchor chain in corrosion testing involves first applying an anti-corrosion primer coat, such as using an epoxy, zinc-rich primer to provide basic protection and improve the adhesion of the main paint. Thereafter, the main marine paint coating is applied by the chosen method, such as spraying or immersion, to ensure uniform coverage and appropriate thickness. Each coat of paint is given sufficient drying time to achieve optimum hardness and durability. Afterward, measure the thickness of the paint layer using a micrometer to ensure uniform thickness. Careful painting aims to form an effective barrier against corrosive elements, thereby reducing the corrosion rate and extending the service life of the anchor chain in aggressive environments.

5. Observation and Monitoring:

The observation and monitoring stage of corrosion testing involves regular visual inspections and detailed measurements of the condition of the painted anchor chain. Observations are made to detect surface changes, such as the appearance of cracks, peeling paint, or early signs of corrosion. In addition, paint thickness measurements and microstructure analysis using an electron microscope are conducted periodically to obtain quantitative data on corrosion rates. Careful and continuous monitoring is essential to assess the effectiveness of the painting method in protecting the anchor chain from corrosion, as well as to identify areas that require further repair or adjustment while recording visual changes and corrosion rate-related measurements.

methodology can be divided into one or more parts according to the research requirements.

b. Corrosion testing

Test Environment Setup:

1. Prepare a container containing a 3.5% NaCl solution to simulate a marine environment.
2. Place the sample in the container and keep it under controlled conditions (temperature and humidity) for 30 days.

Corrosion Rate Measurement:

1. Take samples at regular intervals (e.g., every 7 days) to measure weight changes using a digital balance.
2. Use a corrater to measure the corrosion rate directly.

c. Data analysis

Data Processing:

1. Calculate the corrosion rate based on the weight change of the sample and the data from the crater.
2. Compare the corrosion rate between painted and unpainted samples.

Effectiveness Evaluation:

1. Analyze the effectiveness of the protective paint in reducing the corrosion rate.
2. Use statistical analysis to determine the significance of the difference between the painted and unpainted samples.

d. Flow chart

The flowchart of the corrosion testing steps illustrates the stages of the process systematically from site identification and initial preparation, selection of painting method, and surface preparation, to painting application. Thereafter, steps include periodic observation and monitoring of the anchor chain condition, as well as analysis of test data. This diagram helps visualize a structured workflow, ensures each stage is properly executed, and facilitates the identification of critical points that affect the effectiveness of corrosion protection of the anchor chain. The research steps are shown in the flow chart of Figure 6.

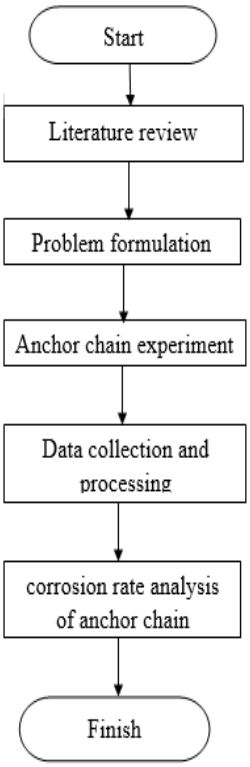

Figure 6. Research flow chart

The selection of ship equipment, such as anchors, anchor chains, and other mooring tools, depends on the equipment items regulated by several classifications [19]. According to BKI 2014 Volume II Section 18 B.1

$$Z = D\frac{2}{3} + 2hB + \frac{A}{10} \quad (1)$$

Where:
Z = modulus (m^3),
D = displacement (ton),
B = ship width (m),
h = sum of freeboard to superstructure height (m)
A = lateral plane area of the body and building (m^2).

Corrosion can be said to be a decrease in the quality of metal. Corrosion can occur due to electrochemical reactions between metals and the environment. One of the environmental conditions that often causes corrosion of iron is seawater. Seawater contains a variety of salts, with the largest percentage of salt being NaCl [20].

The corrosion rate can generally be measured using two methods, namely: the weight loss method or immersion test, and the electrochemical method. The weight loss method is to calculate the weight loss that occurs after some immersion time. In this study, the weight loss method was used, where the difference between the initial weight and the final weight was calculated.

Unit of corrosion rate:

1. Weight reduction = g or mg
2. Weight/unit of metal surface area = mg/mm^2
3. Weight expansion per time = mg/dm^2 day (mdd), g/dm^2. day, g/cm^2.hour, g/m^2 .h, moles/cm^2 .h
4. In penetration per time: inch/year, inch/month, mm/year, miles/year (mpy), 1 milli = 0,001 inch

The corrosion rate by immersion test is based on weight loss. The weight loss method is carried out by calculating the difference between the initial weight and the final weight that occurs after some immersion time [21].

$$CR = (87{,}6 \times W)/(D \times A \times T) \quad (2)$$

Where:
CR = corrosion rate (mmpy)
W = lost weight (gram)
D = density of corrosion test piece ($gram/cm^3$)
A = surface area (in^2)
T = time (hour).

Corrosion rate according to Faraday's Law, which relates the corrosion rate to the amount of charge involved in the electrochemical reaction [22].

$$I = (m) / (nFt) \quad (3)$$

Where:
I = Corrosion rate (g/yr atau mm/yr)
m = Mass of corroded metal (g)
n = The number of electrons involved in an electrochemical reaction
F = Faraday Constant (96.485 C/mol)
t = Time (s)

Result and Discussion

Results

1. Surface Preparation
- Sandblasting Process:

The surface of the anchor chain is cleaned of rust, old paint, and other contaminants using sandblasting. This process ensures a clean and rough surface, which is essential for good paint adhesion.
- Visual Inspection:

After sandblasting, the surface of the anchor chain is visually inspected to ensure that no rust or contaminants remain. This rough and clean surface is ready for primer application.

2. Application of Zinc-Based Primer
- Primer Application:

A zinc-based primer is applied to the cleaned anchor chain. This primer provides a sacrificial coating that protects the steel from corrosion.
- Coating Consistency:

The thickness of the primer layer is checked using a micrometer, ensuring consistent thickness according to predetermined specifications.

3. Application of Epoxy Coating
- Epoxy Application:

An epoxy coating is applied over the zinc-based primer. This coating provides additional protection by offering excellent adhesion and chemical resistance.
- Coating Inspection:

The thickness and consistency of the epoxy coating are checked to ensure complete coverage and optimal protection.

4. Final Coating Application
- Final Coating Application:

The finish coat is applied as additional protection against environmental factors such as UV radiation and mechanical abrasion.
- Final Result:

The finish coat is checked to ensure good adhesion and a durable finish, providing long-term protection against corrosion.

5. Testing and Measurements
- Thickness Measurement:

A micrometer is used to measure the total thickness of the coating system (primer, epoxy, and finish), ensuring that the thickness meets the set standards.
- Corrosion Resistance Testing:

The coated anchor chain was tested under simulated marine conditions to evaluate its resistance to corrosion. Results showed that the protective coating significantly reduced the corrosion rate compared to the uncoated anchor chain. From the experimental observations of the addition of marine anti-corrosive coatings, compared to before adding marine anti-corrosive coatings to anchor chain materials in seawater fluid, data and corrosion rates on anchor chains with different conditioning.

Discussion

1. Effectiveness of Surface Preparation:

Thorough surface preparation through sandblasting is critical to the success of the painting method. Without adequate preparation, the paint will not adhere well to the steel surface, reducing the effectiveness of the coating.

2. Importance of Zinc-Based Primer:

Zinc-based primers provide initial protection against corrosion by acting as a sacrificial layer. This means that the zinc will corrode before the steel, protecting the anchor chain from more severe corrosion damage.

3. Benefits of Epoxy Coatings:

Epoxy coatings enhance protection by offering excellent adhesion and chemical resistance. Epoxy also acts as an additional barrier, extending the life of the anchor chain.

4. Role of the Finish Coat:

The finish coat protects against environmental factors such as UV radiation and mechanical

abrasion. This ensures that the coating system remains effective for a longer time, even in harsh marine conditions.

5. Effect of Coating Thickness:

Consistent coating thickness is critical to the effectiveness of the coating system. Precise measurements ensure that each layer is of sufficient thickness to provide the required protection without compromising flexibility or adhesion.

6. Performance under Load Conditions:

Coated anchor chains exhibit improved corrosion resistance during operational use. This improvement translates into longer service intervals and lower maintenance costs, ensuring the anchor chain remains functional and reliable.

painting can prevent corrosion of the anchor chain. The painting methods used include painting with anti-corrosion paint. Painting can increase the resistance of the anchor chain to wear and mechanical damage.

Strength analysis of the anchor chain structure using some of the data has different dimensions. The strength analysis of the anchor chain structure is carried out using a dimensional reduction due to the corrosion rate of the anchor chain material.

The interval of each coat of paint depends on its drying power. The next coat of paint can be applied when the previous coat is dry, but it should not exceed the specified allowance, as it will give poor adhesion. The interval required by each painting is different. Primer paints have a 10-hour allowance and a maximum of 3 months. Anti-corrosive paints allow 50 minutes at the earliest and 8 hours at the latest, while anti-animal and marine plant paints require 24 hours for the next painting.

Conclusion

A painting method consisting of thorough surface preparation, the application of a zinc-based primer, an epoxy coating, and a final coat proved effective in controlling corrosion of the anchor chain. Results show that this coating system significantly increases the service life and reliability of anchor chains, making it a valuable approach to marine equipment maintenance. Regular inspections and strict quality control are essential to ensure the continued effectiveness of the protective coating.

Based on the research that has been done, conclusions can be drawn such as, not implementing the role of good anchor chain maintenance in its implementation can have several impacts that can become a problem on the ship, such as corrosion, exhaustion of wildcat serrations, influence on the anchor feeding process, the process of the heavy up anchor is disrupted and from several impacts that can occur resulting in hampering ship operations.

Anchor chain painting is an effective method to prevent corrosion and improve chain durability. Various painting methods can be used, depending on the type of metal and environmental conditions. By using the right painting method, the anchor chain can remain in good working order and ensure the safety of the ship. The method of painting with zinc-rich primer and epoxy coating proved effective in reducing the corrosion rate of the anchor chain. Regular maintenance and periodic repainting is highly recommended to maintain the stability and service life of the anchor chain under corrosive marine environmental conditions.

It is hoped that research that can be developed in future studies can be in the form of analyzing the maintenance of anchor chains and windlasses against corrosion rates, with other methods that are more effective than the painting method used in this study.

References

[1] Andarum Septianto, 2022. Peranan Pemeliharaaan Rantai Jangkar Di MT. Griya Flores.

[2] Mardawiah, 2022, Analisa Kekuatan Rantai Jangkar Setelah Mengalami Korosi.

[3] Source from https://www.suzuki.co.id/tips-trik/ayo-mengenal-jangkar-kapal-dan-apa-saja-jenisnya?pages=all (diakses pada 01 Mei 2023)

[4] Irianto, P.T., dkk. 2020. Analisa Kekuatan Struktur End Shackle Rantai Jangkar Akibat Adanya Beban Lingkungan pada Kapal Perintis 1200 GT. *Jurnal Teknik Perkapalan*. Volume 8(4). pp 509

[5] Sugianto, E., Chen, J. H., & Purba, N. P. Cleaning technology for marine debris: A review of current status and evaluation. (2023). International Journal of Environmental Science and Technology, 20(4), 4549-4568. https://doi.org/10.1007/s13762-022-04373-8

[6] Sugianto, E., & Chen, J. H. Experimental Study of the Effect of a Solid Wing Conveyor on Marine Debris Collection. (2022). Journal of Marine Science and Technology, 30(6), 2. https://doi.org/10.51400/2709-6998.2584

[7] Sugianto, E., Horng-Chen, J., & Purba, N. P. Numerical investigation of conveyor wing shape type effect on ocean waste collection behavior. (2021). In E3S Web of Conferences (Vol. 324, p.

01005). EDP Sciences. https://doi.org/10.1051/e3sconf/202132401005

[8] Sugianto, E., & Chen, J. H. Hollow Wing Technique to Enhancing Conveyor Performance on Marine Debris Collection. (2022). Evergreen. 9(4), 1160-1167. https://doi.org/10.5109/6625727

[9] Sugianto, E., Chen, J. H., Sugiono, R., & Prasutiyon, H. Effect of portable conveyor placement in ship on ocean waste collection behavior. (2022). In IOP Conference Series: Earth and Environmental Science (Vol. 1095, No. 1, p. 012015). IOP Publishing. doi:10.1088/1755-1315/1095/1/012015

[10] Alfafa. Syafa, Z. 2022. Analisis Pengurangan Diameter Rantai Jangkar Ditinjau Dari Laju Korosi Pada Kapal Baja Di Galangan Kapal Lamongan.

[11] Kenneth R. Trethewey, John Chamberlain, Korosi untuk Mahasiswa dan Rekayasawan, Terjemahan Alex Tri Kantjono Widodo, PT. Gramedia Pustaka Utama, Jakarta, 1991.

[12] Van Vlack, H. Lawrence, Ilmu dan Teknologi Bahan (Ilmu Baja dan Bukan Baja), 5 th ed, PT. Erlangga, 1994.

[13] ASM Handbook, vol. 5, Surface Engineering, The Material Information Society.

[14] Fontana, Mars Guy, Corrosion Engineering, International edition, Mc. Graw Hill Inc, 1987.

[15] Zdunek, A.D., Shubinsky, G., & Kwan, H.J., Inspection and Evaluation of Protective Coatings by Visual Imaging Techniques, Northwestern University,1995.

[16] Rabiee, A., Soltani, R., & Ariannejad, M. M. (2018). Comparative study of anticorrosive coatings in marine environments. Journal of Coatings Technology and Research, 15(5), 1027-1038.

[17] Venkatesh, R., & Elango, A. (2019). Performance evaluation of fluoropolymer coatings for offshore structures in marine environment. Surface Review and Letters, 26(03), 1850003.

[18] Ma, Z., & Chen, S. (2018). Corrosion protection performance of a polyurethane coating containing zinc phosphate in marine environments. Progress in Organic Coatings, 118, 51-59.

[19] BKI, "Rules for the Classification and 2016 Edition Biro Klasifikasi Indonesia," Volume III.

[20] Ludiana Y, Handani S., Pengaruh Konsentrasi Inhibitor Ekstrak Daun Teh (Camelia Sinensis) Terhadap Laju Korosi Baja Karbon Schedule 40 Grade B Erw. Jurnal Fisika Unand, 2012. Volume 1(1).

[21] Pattireuw, K.J., dkk. 2013. Analisis laju korosi pada baja karbon dengan Menggunakan air laut dan H2SO4. *Jurnal Online Poros Teknik Mesin Unsrat*. Volume 2(1).

[22] Uhlig, H. H., & Revie, R. W. (2020). Corrosion and corrosion control: An introduction to corrosion science and engineering. John Wiley & Sons Inc. Neew York. 9-19

International Journal of Marine Engineering and Applications
Volume 1, Number 1, September 2024
e-ISSN: 3063-640X

Date of Received:
June 23, 2024

Date of Accepted:
July 4, 2024

Date of Published:
September 1, 2024
DOI: doi.org/10.30649/ijmea.v1i1.365

NUMERICAL SIMULATIONS OF TURBULENT GAS-SOLID FLOW IN A GRADUAL EXPANSION

Mahendra Indiaryanto[1*], Cahya Kusuma[2], Roy Mansyah Arsad[3]

[1] Research Center for Hydrodynamics Technology, National Research and Innovation Agency (BRIN), Surabaya, 60111, Indonesia
[2] College of Naval Technology, Bumi Moro, Morokrembangan, Surabaya, 60178, Indonesia
[3] Ministry of Law and Human Rights, Probolinggo, 67217, Indonesia
*Corresponding Author: mahe002@brin.go.id

ABSTRACT

The dwindling availability of petroleum fuels encourages the use of fuel from renewable and environmentally friendly natural resources. This study focused on the iodine value in used biodiesel methyl ester and its effect on the performance of the main components of a diesel motor, such as power, torque, brake mean effective pressure (BMEP), and specific fuel oil consumption (SFOC). Numerical research was carried out on the YANMAR TF85-MH engine model using computational fluid dynamics (CFD). The variations used are biodiesel B20, 20A, and 20B at three different engine rotation speeds: 1900 RPM, 2000 RPM, and 2100 RPM. The results show that the performance of biodiesel B20 is better compared to others. It produces 4.01 kW of power, 19.79 N.m of torque, 82065.12 Pa of BMEP, and 270.43 g/kWh of SFOC. While the B20A produces 4.61 kW of power, 20.44 N.m of torque, 84067.31 Pa of BMEP, and 288.76 g/kWh of SFOC. Then, the B20B produces 4.12 kW of power, 20.57 N.m of torque, 83244 Pa of BMEP, and 316.57 g/kWh of SFOC. So, it can be seen that the mixture of biodiesel fuel with iodine slightly affects the increase in diesel motor performance. In addition, the use of renewable energy fuels must be encouraged because their availability is maintained.

Keywords: Numerical investigation, biodiesel, motor performance, eco-friendly ship

Introduction

The fuel crisis for diesel motorbikes derived from petroleum is the biggest issue that occurs globally. To respond to this issue is to use alternative fuels, one of which is biodiesel. Biodiesel is an alternative fuel that is now increasingly being developed and can reduce the use of petroleum fuels. The development of biodiesel, apart from solving the problem of providing energy in the world, is also a hope for the future because biodiesel is based on agriculture, which will not run out as long as there are still people growing the raw material. In recent years, biodiesel has become a popular topic of conversation as an alternative material that can replace petroleum [1]. Technological advances such as the development of direct injection systems and turbocharging have made light-duty diesel-equipped motors even more enjoyable to drive. However, drastic reductions in pollutant emissions must be achieved to achieve future emission standards. This can only be done by optimizing the combustion process [2]. However, the oil crisis and global warming have caused research to be oriented toward finding suitable alternative fuels for petroleum. Now biodiesel is produced from vegetable oil, which cannot be consumed because of the high price of edible vegetable oil, becoming an alternative fuel to replace diesel oil [3].

Biodiesel is considered an effective replacement fuel to be developed. It is considered a prominent fuel because it is non-toxic, biodegradable, and renewable. Apart from that, its environmentally friendly nature is also the main reason, as well as abundant natural resources and even the existence of raw materials, which have spread globally. The raw materials needed to produce biodiesel also vary, namely soybean oil, palm oil, used cooking oil, animal fat, and several other sources [4]. Air pollution will, of course, have an impact on human health, as well as on other living creatures such as animals and plants. So that the diesel motor used does not cause excessive air pollution, research needs to be carried out [5].

Exhaust gas from the combustion process has an impact on air and environmental pollution, especially from diesel motorbikes. The diesel motor was invented in 1892 by Rudolf Diesel. The working principle of a diesel motor is to inject fuel into a combustion chamber where the air inside has been compressed. Lack of homogeneous mixing of fuel with air and high combustion temperatures cause the appearance of exhaust gases in diesel motors, for example, PM [6].

Biodiesel is an alternative fuel that has different characteristics from other fuels, therefore there is a need for experiments on exhaust gases and feasibility studies related to the greenhouse effect when used as an alternative fuel to replace fossil fuels in diesel motors, so, numerical modeling and simulation of fluid flow through the intake valve using CFD (Computational Fluid Dynamics) is the right choice of method considering the constraints mentioned previously. In this research process, it is hoped that biodiesel and methyl ester waste cooking can be used with added iodine and then simulated using computational software fluid dynamics because the addition of fuel has an effect on a more optimal diesel motor combustion process and lower exhaust gas [7].

In a diesel motor, only air is sent into the combustion chamber during induction, namely, channeling clean air into the combustion chamber (cylinder). combustion chamber (cylinder). This air is compressed during the compression stroke, and towards the end of the compression stroke, fuel is injected by the fuel injection system into the cylinder just before the desired start of combustion. Liquid fuel is injected at high speed through a small hole or nozzle at the end of the injector. The fuel is atomized into small droplets and penetrates into the combustion chamber, then evaporates and mixes with high-temperature and high-pressure cylinder air [8]. On the other hand, knowing the phenomena in the combustion chamber when the chemical combustion process occurs can help us in designing optimal combustion chamber geometry or operating the gas turbine system more efficiently. Two ways can be used to determine phenomena in the combustion chamber, namely the experimental method and the simulation method. The experimental method is a method where data collection is carried out experimentally in the field on test equipment, while the simulation method is a method that does not require direct experimentation, but is carried out by analyzing and creating simulations using CFD (Computational Fluid Dynamics) software [9] .

Recently, Computational Fluid Dynamics (CFD) has gained reliability in predicting emissions and combustion characteristics using properly calibrated and validated models. Then, CFD modeling is a very attractive alternative compared to experimental approaches, especially for diesel motor hardware optimization due to its lower requirements in terms of time and resources. Therefore, it is necessary to develop an optimization methodology based on CFD modeling that is suitable not only to define the optimal diesel motor hardware configuration/setup but also to identify qualitatively and quantitatively the most relevant effects of the variables to be optimized [11].

Research on the effect of differences in injection pressure on the amount of torque, power, and BMEP in single-cylinder diesel motors with a mixture of diesel fuel, used cooking methyl ester (JME) from coconut oil, and candlenut oil was confirmed by Francisco Pinto [12]. The results. The higher the concentration of vegetable oil in the mixture, the lower the performance of the diesel motor. Coconut oil and candlenut oil can be used as alternative ingredients to be mixed with diesel in certain mixtures. Using a mixture of used cooking oil (JME) and diesel in a ratio of 10:90 increases the effective power of a diesel motor when compared to using pure diesel fuel at rpm and load. certain. The increase also occurred in the 20:80 and 30:70 mixtures. Even with a JME fuel composition of 100% at 2000 rpm, there is an increase in the effective power of 30.34% when compared to using diesel fuel. JME will be promoted as a substitute for diesel fuel and will then be widely used as a fuel in the future [13].

However, research on exhaust gas analysis in diesel motors using waste cooking biodiesel methyl ester fuel containing iodine is still limited. So this research will be carried out with the variations used, namely biodiesel from waste cooking methyl ester (used cooking oil) with variations in iodine content with the composition B20 (a mixture of 80% diesel, 20 percent biodiesel, with no iodine) B20A (a mixture of 80% diesel, 20 percent biodiesel, 10 grams of iodine) B20B (mixture of 80% diesel, 20 percent biodiesel, 20 grams of iodine). The diesel engine speed is 1800 rpm, 1900 rpm, 2000 rpm, 2000 rpm, and 2200 rpm.

Methodology

This study uses a method utilizing the Ansys CFD program to carry out simulations. The main objective of this research is to gain an in-depth understanding of the effects of variations in engine combustion chamber design and biodiesel fuel selection on diesel engine performance. The main focus is on the effect on engine power, torque, braking mean effective pressure (BMEP), and specific fuel consumption (SFOC). In this research, the biodiesel fuel used was methyl ester (B20) without iodine, and B20 with the addition of iodine (B20A, B20B).

The data used in this research comes from previous findings that used experimental techniques to understand combustion characteristics in engines. This method involves collecting data from Ansys CFD simulation results to support the analysis carried out.

Furthermore, after the data has been collected, this research will involve using SolidWorks software to design an engine combustion chamber model and carry out simulations. By using SolidWorks, researchers will be able to visualize and analyze how different combustion chamber designs affect overall diesel engine performance.

The engine used in this research is a Yanmar TF85 MH diesel engine, which uses a Hopper water cooling system and does not use a turbo system (naturally aspirated). The components to be evaluated include the intake valve, intake manifold, exhaust valve, and cylinder of the Yanmar TF85 MH engine. Images of this diesel engine are shown in Figure 1 for analysis and evaluation purposes.

This research will also consider the use of dual-fuel diesel, by testing three different types of fuel: conventional diesel, biodiesel made from methyl ester, and biodiesel with the addition of iodine (B20, B20A, B20B). This variation aims to evaluate how the chemical composition of the fuel affects combustion efficiency and overall engine performance.

It is hoped that the results of this research will not only provide deeper insight into combustion optimization in diesel engines but also provide a basis for the development of more efficient and environmentally friendly technologies in the future. In conclusion, this research has the potential to make a significant contribution to the understanding and development of better diesel engine technology.

Figure 1. Yanmar TF85 MH. Diesel Engine

a. Modeling

Numerical research was carried out on the YANMAR TF85-MH engine model using computational fluid dynamics (CFD). SolidWorks software is used for modeling; Figure 2 shows the diesel motor combustion 3D model.

Figure 2. Diesel Motor Combustion 3D Model

b. Model Simulation Using CFD

The computational fluid dynamics (CFD) program is then used to simulate the internal combustion model of the diesel engine that was created in the previous stage. When different air and fuel mixtures are incorporated into the model, the objective is to establish the distribution of mixing speed. In this step, the location of the air inlet and outlet, as well as the intake and exhaust valves, are chosen. The biodiesel B20, B20A, and B20B geometries are listed below and can be seen in Figure 3.

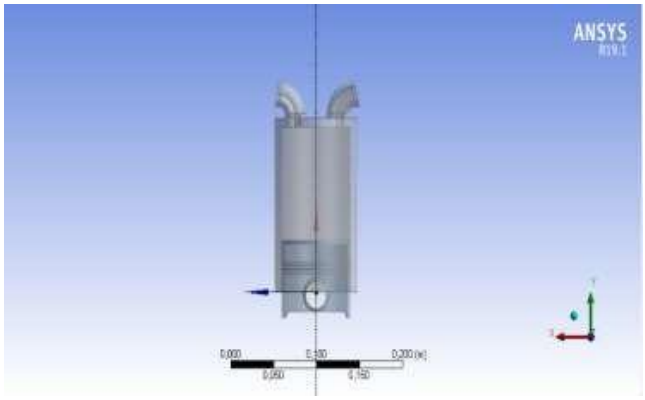

Figure 3. Biodiesel geometry stage

The meshing procedure will then be resumed. Mesh creation is a crucial step in the CFD simulation since it affects the caliber and outcome of the modeling process [14-16]. Static meshing is frequently employed in simulations for systems that are solid or immovable [17-18]. The meshing outcomes for the B20, B20A, and B20B biodiesel models are illustrated in Figure 4.

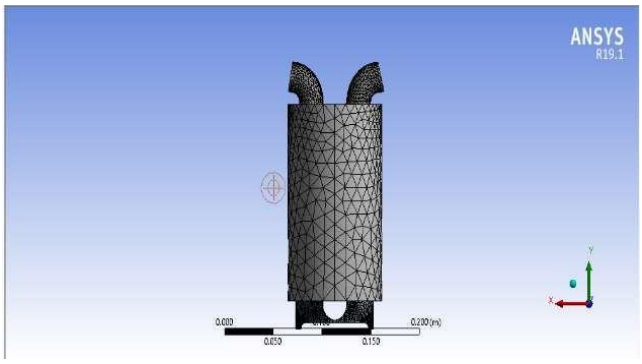

Figure 4. Biodiesel Meshing Stage

The setup stage should then be completed. This is the most crucial stage because it involves processing nearly all research parameters, including models, materials, cell zone conditions, boundary conditions, mesh interfaces, dynamic mesh, reference values, solution methods, solution controls, solution initialization, calculation activities, and calculation runs [19-21]. Figure 5 depicts the outcome of the model biodiesel B20, B20A, and B20B

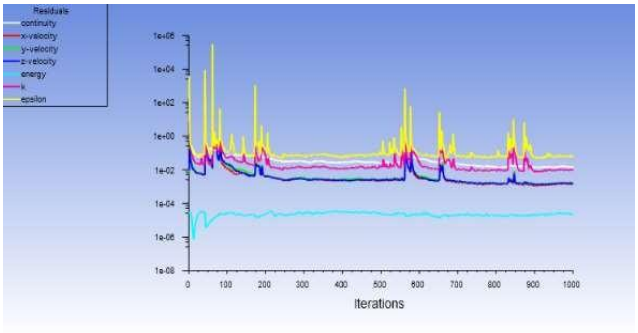

Figure 5. Residual iterations

Result and Discussion

This section examines the findings of the simulation process, data in the form of Power, Torque, Brake Mean Effective Pressure (BMEP), and Specific Fuel Oil Consumption (SFOC) per rotation of RPM, which were simulated with CFD software, particularly Ansys Fluent, at 1900, 2000, and 2100 RPM. In the results stage, we can view the outcomes of what is being examined by showing visuals, photos, and animations after the running or simulation process is complete [22].

a. B20 fuel

80% diesel and 20% biodiesel make up B20 fuel, which is variant 1 and was developed in response to the CFD stage's findings. Figure 6 depicts the combustion chamber of a diesel engine running at 1900 RPM; the pressure velocity color contour is green, and the pressure speed is 2.62 N/m. 2. While there is a pressure of -3.45 N/m2 at the inflow valve, there is a pressure of 6.01 N/m2 at the output valve. The diesel engine will experience overheating more quickly, the higher the pressure value in the combustion chamber. The fluid velocity color contour ranges from blue to red; the closer a color is to the top red, the higher the pressure or increasing pressure is. After going through the selection of several vessels, it is further determined how much power will be used on the vessel. The dimensions of the main sizes of vessels can be seen in Table 1.

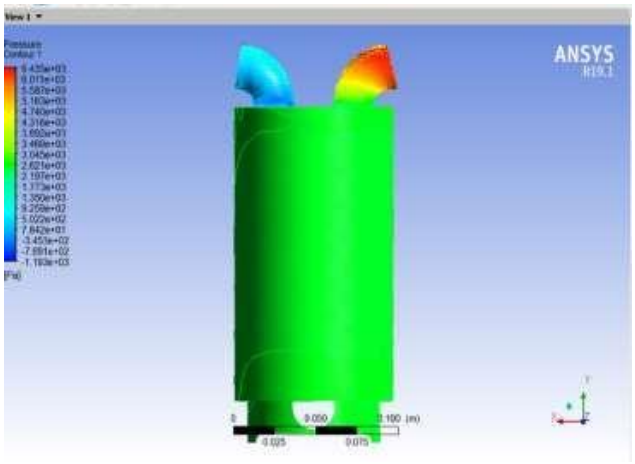

Figure 6. B20 Biodiesel Setup Stage

b. B20A fuel

Following the findings of the CFD stage, B20A fuel is variant 2, namely B20A (a blend of 80% diesel, 20% biodiesel, and 10 grams of iodine). Figure 7 depicts the combustion chamber of a diesel engine with a 1900 RPM rotation variation. The pressure speed is shown as a yellow contour with a pressure speed of 1.49 N/m2. While there is a pressure of -3.09 N/m2 at the inflow valve, there is a pressure of 6.08 N/m2 at the output valve. The combustion chamber of a diesel engine will experience overheating more quickly the higher the pressure is. The fluid velocity color contour ranges from blue to red; the closer the color is to red at the top, the higher the pressure.

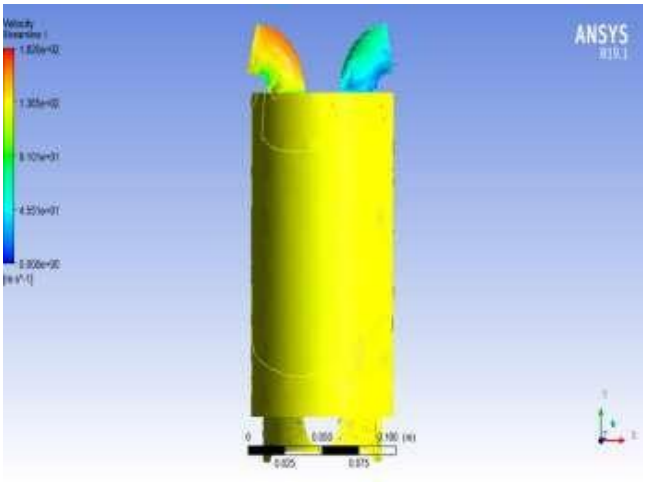

Figure 7. B20A Biodiesel Setup Stage

c. B20B fuel

B20B fuel is variation 3, (a mixture of 80% diesel, 20% biodiesel, 20 grams of iodine.

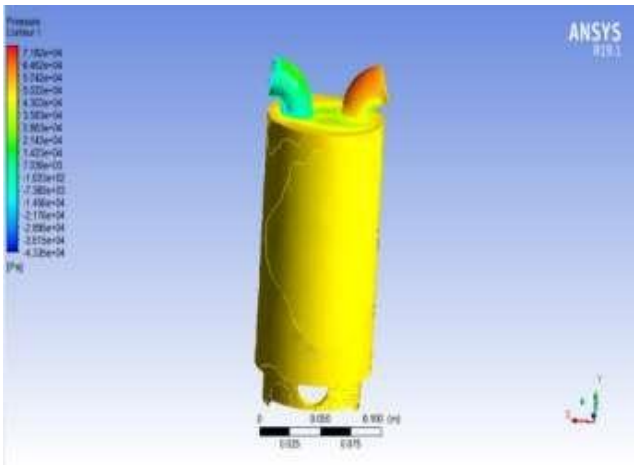

Figure 8. B20B Biodiesel Setup Stage

Diesel engine combustion chamber with a rotation variation of 1900 Rpm, the color contour of the pressure speed is yellow, the pressure speed is 4.43 N/m2. While the pressure at the inlet valve is 1.47 N/m 2, the pressure at the outlet valve of 6.45 N/m2. The greater the pressure value in the diesel engine combustion chamber, the faster it will experience overheating. The color contour of the fluid velocity is blue to red; the closer the color is to the top red, the higher the pressure.

d. Effect of Biodiesel B20, B20A, B20B on Power

The findings of the simulation demonstrate that the iodine number has an impact on the power produced by the engine at each level of rotation since the power produced by the engine at each level of load and rotation is almost the same. The biodiesels B20, B20A, and B20B are compared in Table 1. The results of the simulation show that the iodine value has no effect on engine power at any level of load and that at every level of rotation, the power generated increases along with an increase in engine speed.

Table 1. Power Comparison B20, B20a And B20b

Fuel	**1900 Rpm**	**2000 Rpm**	**2100 Rpm**
Biodiesel B20 (kW)	4.01	4.37	5.10
Biodiesel B20A (kW)	4.17	4.61	5.19
Biediesel B20B (kW)	4.12	4.63	4.99

e. Effect of Biodiesel B20, B20A, B20B on Torque

A simulation study was carried out to identify how the iodine number affects the torque produced by the engine at various rotation levels. Table 2 shows the torque produced by the engine at the highest load at each engine speed with various types of fuel. The results show that the engine produces almost the same amount of torque at the highest load at each engine speed, regardless of the type of fuel used, because the iodine number does not influence this torque.

Basically, the torque produced by the engine is not greatly influenced by the chemical characteristics of the fuel, such as the iodine number. Torque is influenced more by the design of the engine itself and other factors, such as load and engine rotation speed.

The table also shows that as engine speed increases, the torque produced tends to be inversely proportional to the rotation variation. This means that the higher the engine speed, the torque produced tends to decrease. This is a common phenomenon in engines, where the engine torque characteristics can vary depending on the engine rotation regime.

In this context, it is important to understand that although the fuel iodine number has an important role in combustion properties and its possible impact on engine performance, such as emissions or deposit formation, in the case of specific torque at certain engine speeds, the simulation results show that differences in the iodine number are not significant.

Table 2. Torque Comparison B20, B20a And B20b

Fuel	**1900 Rpm**	**2000 Rpm**	**2100 Rpm**
Biodiesel B20 (Nm)	19.79	21.07	22.31
Biodiesel B20A (Nm)	20.48	21.18	22.83
Biediesel B20B (Nm)	20.57	21.96	22.05

This research provides important insight that when evaluating engine performance, especially in terms of torque at a given engine speed, other factors such as engine design and operational load may have a greater influence than the type of fuel used. Therefore, to optimize engine performance, adjusting design and operational settings may be more crucial than considering specific chemical variations of the fuel.

f. Effect of Biodiesel B20, B20A, B20B on BMEP

The following Table 3 shows the effects of the iodine number on the BMEP generated by the engine at various rotation rates. It is well known that BMEP is basically unaffected by iodine number at each load and rotation level with different iodine variants in each type of fuel. Table 3 displays the BMEP at maximum load for each level of rotation. As can be observed, there are no appreciable differences in the types of fuel utilized at either low speed (1900 rpm) or maximum speed (2100 rpm). Additionally, it can be seen that, aside from the increase from low to high rotation, the increase in BMEP is fairly steady as the rotation increases.

Table 3. Comparison of BMEP B20, B20a And B20b

Fuel	**1900 Rpm**	**2000 Rpm**	**2100 Rpm**
Biodiesel B20 (Pa)	19.79	21.07	22.31
Biodiesel B20A (Pa)	20.48	21.18	22.83
Biediesel B20B (Pa)	20.57	21.96	22.05

g. Effect of Biodiesel B20, B20A, B20B on SFOC

The simulation findings show that the SFOC is relatively unaffected by the iodine value at each degree of load and rotation with different iodine variants in each type of fuel. There is no discernible difference between the types of fuel consumed at low speed (1900 rpm) and at maximum speed (2100 rpm), as seen in Table 4's SFOC at maximum load at each level of rotation.

Additionally, it is observed that, aside from the increase from low rotation to high rotation, the increase in SFOC is largely consistent with the higher spin.

Based on the simulation results of speed contours in the engine combustion chamber with three fuel variations, B20 biodiesel was proven to be the best choice because it showed better performance compared to other variations, namely B20A and B20B biodiesel. This simulation reveals that variations B20A and B20B experience high-pressure contours around the engine exhaust valve area. This high pressure can accelerate the

occurrence of "overhead" events in the diesel engine combustion chamber, which has the potential to damage engine components, especially due to the interaction between Fe (iron) and Al (aluminum) materials.

Table 4. Comparison Of BMEP B20, B20a And B20b Sfoc

Fuel	**1900 Rpm**	**2000 Rpm**	**2100 Rpm**
Biodiesel B20 (g/kWh)	270.43	263.52	260.91
Biodiesel B20A (g/kWh)	288.76	291.97	273,56
Biediesel B20B (g/kWh)	316.57	274.12	253.33

The effect of the three types of fuel on engine performance is measured through the parameters power, torque, BMEP (Brake Mean Effective Pressure), and SFOC (Specific Fuel Oil Consumption). The results show significant differences in characteristics between these three types of fuel.

In terms of power, B20A biodiesel or fuel with a mixture of iodine numbers shows a striking difference compared to B20 biodiesel and other conventional fuels at engine speeds of 1900, 2000, and 2100 rpm. This suggests that the chemical characteristics of the fuel can significantly influence the engine's ability to produce power.

Meanwhile, in terms of torque, there is no significant variation between the three versions of B20 and B20A biodiesel. This shows that engine torque is not greatly influenced by the type of fuel used in this simulation.

In terms of BMEP parameters, the simulation results show slight variations between the three fuel variations at engine speeds of 1900 rpm, 2000 rpm, 2100 rpm, and 2200 rpm. This indicates that the BMEP performance of the three types of fuel does not show significant differences in the results.

Although B20 biodiesel was found to have advantages in reducing the risk of high pressure around the engine exhaust valve area, the simulation results also highlight that fuel characteristics can influence various aspects of engine performance. This study provides important insights for the development of greener fuel technologies and more efficient engine designs in the future by considering the effects of fuel variations on diesel engine performance and reliability.

Conclusion

Get the following findings based on simulation results utilizing variations in biodiesel fuel B20, B20A, and B20B using computational fluid dynamics: 1. Biodiesel outperforms B20A and B20B biodiesel in performance. 2. The power, torque, and BMEP of the engine are not considerably impacted by the iodine value. 3. At a specific rate of rotation, there is enough iodine to alter the SFOC. The power produced by the engine increases along with the rotational speed as the rotation increases. 4. With increased load and rotation, BMEP increases. 5. While there are variations in SFOC, there are none in power, torque, or BMEP at each level of rotation.

Acknowledgments

We thank the UHT marine engineering study program for launching its first journal, IJMEA; hopefully, it will be useful. thank you also for the publication of the results of this research. congratulations.

References

[1] Oemar K S 2018 Analisa Performa Berbasis Eksperimen dan Kelayakan Ekonomis Baha Bakar Biodiesel Biji Kemiri pada Mesin Satu Silinder (Experiment-Based Performance Analysis and Economic Feasibility of Candlenut Biodiesel Fuel in Single Cylinder Engines), ITS Press, Surabaya.

[2] Prasutiyon H 2017. Pengaruh Angka Iodin Terhadap Ketahanan Komponen Utama Motor Diesel Dengan Bahan Bakar Jelantah Methyl Ester B20 The Influence of Iodine Number on the Resistance of Main Components of Diesel Motors Using Waste Cooking Fuel Methyl Ester B20), ITS Press, Surabaya.

[3] Muhammad U L, Shamsuddin I M, Danjuma A, Musawa R S and Dembo U H 2018 Biofuels as the Starring Substitute to Fossil Fuels Petroleum Science and Engineering 2 (1) pp 44-49

[4] Pinto F 2018 Analisa Pengaruh Angka Iodin Terhadap Emisi NOx Pada Motor Diesel Dengan Bahan Bakar Biodiesel Dari Waste Cooking Oil Dengan StandarIMO TIER III (Analysis of the Effect of Iodine Number on NOx Emissions in Diesel Motors Using Biodiesel Fuel from Waste Cooking Oil with IMO TIER III Standards), ITS Press, Surabaya.

[5] Schober S and Mittelbach M 2007 Iodine value and biodiesel: Is limitation still appropriate? Lipid Technology 19 (12) pp 281-284.

[6] Li Q, Backes F and Wachtmeister G 2015 Application of canola oil operation in a diesel engine with common rail system Fuel 159 pp 141-149.

[7] Suziki T, Sumimoto K, Fukada K and Kayatama T 2021 Iodine value of tung biodiesel fuel using Wijs method is significantly lower than calculated value Journal of Wood Science 67:55.

[8] Yasar F 2020 Comparision of fuel properties of biodiesel fuels produced from different oils to determine the most suitable feedstock type Fuel 264 116817.

[9] Sugianto E, Chen J-H, and Permadi NVA 2022 Effect of Monohull Type and Catamaran Hull Type on Ocean Waste Collection Behavior Using OpenFOAM. Water 14 (17):2623.

[10] Sugianto E, Winarno A, Indriyani R, and Chen J-H 2021 Hull Number Effect in Ship Using Conveyor on Ocean Waste Collection. Kapal: Jurnal Ilmu Pengetahuan dan Teknologi Kelautan 18 (03) pp 128-139.

[11] Sugianto E, Chen J-H and Puba NP 2021 Numerical investigation of conveyor wing shape type effect on ocean waste collection behavior E3S Web of Conferences 324:01005

[12] A. Iswantoro, I. M. Ariana, B. G. Luqmananto, and M. F. Maulana, "Performance and Emission Analysis of Four- Stroke Diesel Engine Single Cylinder on Toroidal Piston Modification with B30 Fuel," vol. 7, no. 4, pp. 198–212, 2022.

[13] H. Ikhwani, D. Satrio, W. Umari, Y. S. Hadiwidodo, and R. Muhammad, "The Analysis of Coastal Society Vulnerabilities Against the Spread of Covid-19 in Surabaya Using the Analytical Hierarchy Process (AHP)," vol. 7, no. 4, pp. 218–224, 2022.

[14] E. Sugianto, J.-H. Chen, and N.V.A Permadi, "Effect of Monohull Type and Catamaran Hull Type on Ocean Waste Collection Behavior Using OpenFOAM," Water, 14 (17), 2623 (2022). https://doi.org/10.3390/w14172623

[15] E. Sugianto, J.-H. Chen, "Hollow Wing Technique to Enhancing Conveyor Performance on Marine Debris Collection," Evergreen, 9 (4) 1160–1167 (2022). https://www.tj.kyushu-u.ac.jp /evergreen/contents/ EG2022-9_4_ content/pdf/p1160-1167.pdf

[16] E. Sugianto, J.-H. Chen, "Experimental Study of the Effect of a Solid Wing Conveyor on Marine Debris Collection," Journal of Marine Science and Technology, 30 (06) 278–286 (2022). https://doi.org/10.51400/2709-6998.2584

[17] E. Sugianto, A. Winarno, "Computational model tahanan kapal untuk menentukan kebutuhan daya kapal bulk carrier 8664 DWT," Jurnal Kelautan, 10 (02) 168–173 (2017). https://doi.org/10.21107/jk.v10i2.3411

[18] E. Sugianto, H.P. Haditama, "Penggunaan Metode Komputerirasi dalam Penentuan Tahanan Kapal Tanker," Jurnal Rotor, 10 (02) 54-57 (2017). https://doi.org/10.19184/rotor.v10i2.6392.

[19] E. Sugianto, Chen J-H, Permadi NVA. Effect of Monohull Type and Catamaran Hull Type on Ocean Waste Collection Behavior Using OpenFOAM. Water. 2022; 14(17):2623. https://doi.org/10.3390/w14172623.

[20] E. Sugianto.; Chen, J.H.; Purba, N.P. Numerical investigation of conveyor wing shape type effect on ocean waste collection behavior. E3S Web Conf. 2021, 324, 01005. https://doi.org/10.1051/e3sconf/202132401005{

[21] E. Sugianto, A. Winarno, R. Indriyani, and J. H. Chen. 2021. Hull Number Effect in Ship Using Conveyor on Ocean Waste Collection. Kapal: Journal of Marine Science and Technology,vol. 18, no. 3, pp. 129-142. https://doi.org/10.14710/kapal.v0i0.40744.

[22] E. Sugianto, J.-H. Chen, R. Sugiono, H. Prasutiyon. Effect of portable conveyor placement in ship on ocean waste collection behavior. IOP Conf. Series: Earth and Environmental Science, 1095:012015 (2022). doi:10.1088/1755-1315/1095/1/012015

International Journal of Marine Engineering and Applications
Volume 1, Number 1, September 2024
e-ISSN: 3063-640X

Date of Received:
June 26, 2024

Date of Accepted:
July 4, 2024

Date of Published:
September 1, 2024
DOI: doi.org/10.30649/ijmea.v1i1.368

IMPLEMENTATION OF FISH DISTRIBUTION QUALITY WITH COLD CHAIN SYSTEM (CASE STUDY: PRIGI TO TULUNGAGUNG)

Nor Sa'adah[1*], Dian Sari Maisaroh[2], Raka Nur Sukma[3], Prasetyo Bayu Aji[4]

[1] Politeknik Bumi Akpelni, 50235, Indonesia
[2] Sunan Ampel State Islamic University, 60237, Indonesia
[3] PGRI Ronggolawe University, 62391, Indonesia
[4] Warehousing, CV Kelola Mina Tawar, 66482, Indonesia

*Corresponding Author: saadah1809@gmail.com

ABSTRACT

Prigi Nusantara Fishing Port is a port located in the south of Java Island. The production of fishermen's catches that can be landed at the Prigi Nusantara Fishing Port is 24,928,229 kg. It is necessary to have a management plan and identification of cold chain system distribution costs to maximize the distribution of catches, in this study, to the Tulungagung area. Cold storage also has an important role in the cold chain system. Thus, this study plans to identify the management process, identify distribution costs, and assess the role of cold storage. This research aims to identify the management process and distribution costs as well as assess the role of cold storage. The results of this management mapping plan are from fishermen to cold storage, cold storage processing, and transportation to markets and consumers. With a total cost of IDR 173,382,000/year, including operational costs of IDR 82,950,000/year and vehicle travel costs of IDR 90,43,000/year, using a Thermo King truck. Assessment of the role of government cold storage obtained a score of 45.8% while private cold storage obtained 43.6%. The role of cold storage is still not optimal for storing fish to stabilize prices.

Keywords: Fisheries, fishermen's catch, cold chain system, cold storage

Introduction

Indonesia is one of the largest maritime countries in the world. Located on the Asian continent, flanked by the Indian and Pacific Oceans, Indonesia consists of 17,504 islands, with two-thirds of the country's territory consisting of oceans. Indonesia's ocean area is 6.4 million km2. The land area is 1.9 million km^2. The vast area of the ocean shows that Indonesia is a very large Maritime Country (Statistics Center, 2021). As a maritime country, the marine natural resources produced are certainly very abundant. Mining resources, marine tourism energy, coral reefs, and capture fisheries resources [1], [2].

Captured fish resources are one of the leading resources produced by fishermen throughout Indonesia. The Ministry of Maritime Affairs and Fisheries (KKP) noted that Indonesia's marine capture fisheries production has increased from year to year [3]. The latest data in 2020, marine capture fisheries production reached 7.1 million tons (KKP, 2021). For East Java Province, the production of captured fish in 2017 was 395,254.64 tons, in 2018 it was 467,959.99 tons, in 2019 as much as 481,490.85 tons, and in 2020 as much as 395,254.64 tons [4]. Fish is one of Indonesia's marine wealth as an archipelago [5]. Therefore, most of the coastal residents are fishermen, ranging from small fishermen who only fish with makeshift equipment to fishermen who have many fishing boats, even though they are still small. Fishermen who have many fishing boats, even though they are

still simple. Most of these vessels are made with makeshift equipment and are not well structured [6], [7], [8].

Marketing of fishery products from PPN Prigi is in the form of fresh fish and processed fish products. Distribution destinations include local areas, namely Trenggalek, and inter-city distribution, including Tulungagung, Surabaya, Jombang, Malang, Nganjuk, and other cities. Fishery production from PPN Prigi is distributed in the form of fresh fish, frozen fish, and processed fish, which include Pindang fish, salted fish, fish flour, smoked fish, and other processed fish [9].

In addition to fish prices that tend to be uncontrollable, Prigi Beach fishermen cannot get maximum results. What can be known is that the above areas have a standard price that already meets the standard market price of the region; this is unfortunate because the potential of capture fisheries in the Prigi Coast region cannot be maximized.

Therefore, there needs to be a solution to enable fishermen's catches can be sold at maximum prices, and help the economy of Prigi Beach fishermen and the surrounding areas. This factor is very influential and formulating an integrated cold chain management or research from the time of capture to the hands of consumers with distribution from Prigi Beach to Tulungagung. As well as how the management mapping process and identification of distribution costs from the Prigi Beach area to Tulungagung using a cold temperature Thermo King truck, so that the quality of the fish can be maintained.

Prigi Perikanan Nusantara Port (PPN) has four cold storage units, consisting of three private and one government-owned. However, until now, the cold storage located at PPN Prigi has not functioned optimally, where only part of the cold storage is being used. This is because fishermen during the fish season, and fishery entrepreneurs, immediately sell the catch landed at PPN Prigi, even though the price is low. Based on this information, it is necessary to assess the role of cold storage in PPN Prigi, adjusted to the catch of fishermen.

Methodology

Research methodology is the basic framework of the stages of completing a thesis, which includes all activities that will be carried out to solve problems or carry out the process of analyzing research problems. The methodology used in this research is a case study and field research.

The data needed in this research process uses primary data and secondary data. Primary data is obtained from interviews based on questionnaires directly by respondents who know the conditions related to cold storage at PPN Prigi, and interviews directly with those who know the process of the fish distribution chain at PPN Prigi. Secondary data is obtained from private and government cold storage industry managers and reproduced with other sources such as journals, books, and others.

a. Problem Identification and Formulation

The initial stage in working on this research is to identify existing problems and also the formulation problems that will be resolved during this research. In addition, there are also problem boundaries whose function is to make the topic of discussion more detailed and not widespread, also this will make it easier for the author to analyze the problem.

b. Literature Study

A literature study is carried out by collecting various references to support the writing of this thesis. The necessary references can be found through various media, including books (cold chain fish, cold storage, fish cooling system), journal of Cold Chain System Simulation on Fish Distribution Chain to Measure Fish Quality Improvement in Semarang City), Paper (Cold Chain Fish), Article (Variation of iodine number with diesel fuel and biodiesel), final project (Cold storage fisheries in Indonesia), internet (cold chain fish, fresh and frozen fish quality, fisheries cold storage).

c. Data Collection

Data collection or retrieval is done by directly reviewing the research location to obtain the required data. Data collection in this study used a collection method in the form of purposive sampling. Purposive sampling is a method of taking respondents according to the characteristics determined by the researcher [6], [7]. The selection of respondents was carried out with the consideration that the respondent has an important position in the existing field at the relevant agency and has more knowledge in the field that is the object of research. Apart from the above data collection methods in writing this final project, it is carried out in 2 (two ways, namely:

1. Direct data collection (Primary)
   This direct data collection is done by methods:
   a) Direct interview
      Interviews were conducted with related parties in this final project, namely the manager of cold storage at PPN Prigi
   b) Survey of field conditions. Survey of field conditions at PPN Prigi.
2. Indirect data collection (Secondary data)
   Secondary data collection is done by taking data sourced from the Prigi VAT Statistical Report, cold storage annual work report, performance report, and 10 respondents.
3. Fish distribution data
   Marketing of Prigi Beach fishery products in the form of fresh fish products or processed fish, including frozen fish. The distribution area covers the local area of Trenggalek and the surrounding cities.
4. Fishermen's catch
   The following are the top 9 fish productions landed at PPN Prigi are of pelagic fish species such as Tongkol Lisong (Bullet Tuna), Layang Deles (Shortfin Scad), Cakalang (Skipjack Tuna), Tembang (Deepbody Sardinella), Layur (Hairtails), Layang Anggur (Redtail Scad), Tongkol Krai (Frigate tuna), Tuna Madidihang (Yellowfin Tuna), and Tongkol Komo (Eastern little tuna) [9]
5. Government and private cold storage data
   After we know the number of fleets and how much the catch of fishermen is, knowing the capacity of government and private cold storage, this determination aims to find out how much the catch of fishermen can be utilized by cold storage in PPN Prigi.

d. Data Collection

After getting the necessary data is complete, the next step is data analysis and discussion, namely comparing the data that has been obtained from the most effective and efficient previous calculations.

1. Distribution chain from VAT Prigi to Tulungagung market.
   This analysis discusses how the distribution process chain from the Prigi VAT area to the Tulungagung market. It identifies the stages and mapping of distribution management, as well as which parties are involved in the distribution management process.
2. Cost analysis of fish distribution from Prigi Beach to Tulungagung.
   This analysis discusses how to identify the cost of fish distribution from Prigi Beach to Tulungagung. In this case, using truck transportation (truck Thermo King).
3. Analysis of the role of government and private cold storage
   This analysis discusses how much the role of cold storage in PPN Prigi both the government and the private sector through questionnaires, using the Likert scale method.

e. Data Collection

After analyzing the data, the next step is to conclude the data analysis and discussion. It is hoped that the conclusions can answer the problems that are the objectives of this thesis. In addition, suggestions are needed based on the research results to improve this research so that it is more perfect [10].

Result and Discussion

The success of a fishing operation cannot be separated from the facilities and infrastructure of a complex fishing unit. A fishing unit is a technical unit consisting of a fishing fleet, fishing gear, and fishermen.

The fish catch resources in PPN Prigi are strongly supported by the success of its fishing fleet structure (Figure 1). The fishing fleet operating in PPN Prigi consists of vessels measuring less than 10 GT up to 30 GT, and is dominated by vessels under < 10 GT with 490 vessels (73.80%).

The use of fishing gear is usually adjusted to the characteristics of the fishing area and the target catch. The types of fishing gear used by fishermen in PPN Prigi are hand line, purse seine, Tonda fishing rod, gill net, and seine.

The fishing fleet in PPN Prigi (Figure 2) in 2021 is 664 units, consisting of 449 units of Fishing Rods (67.20%), 2-boat Ring Trawlers 130 units (18.95%), Trolling Lines 67 units (9.77%), Gill Net 7 units (2.48%), Payang 7 units (1.02%) and 1-ship purse seine 4 units (0.58%). The highest number of fishing gear operating in Prigi waters, namely in 2021, was 664 units. This year was recorded in the period 2017 - 2021 as the year with the largest number of fishing fleets in the Prigi PPN, while the number of fishing gear operating was the highest.

This occurred slightly in 2020, amounting to 608 units, because there were not many private fishing industries that entered the Prigi PPN environment, and the cause of the coronavirus outbreak that has hit many fishermen, experiencing financial disruption, as well as the cycle of changes to normalization after the virus outbreak that hit the Prigi Beach area in particular.

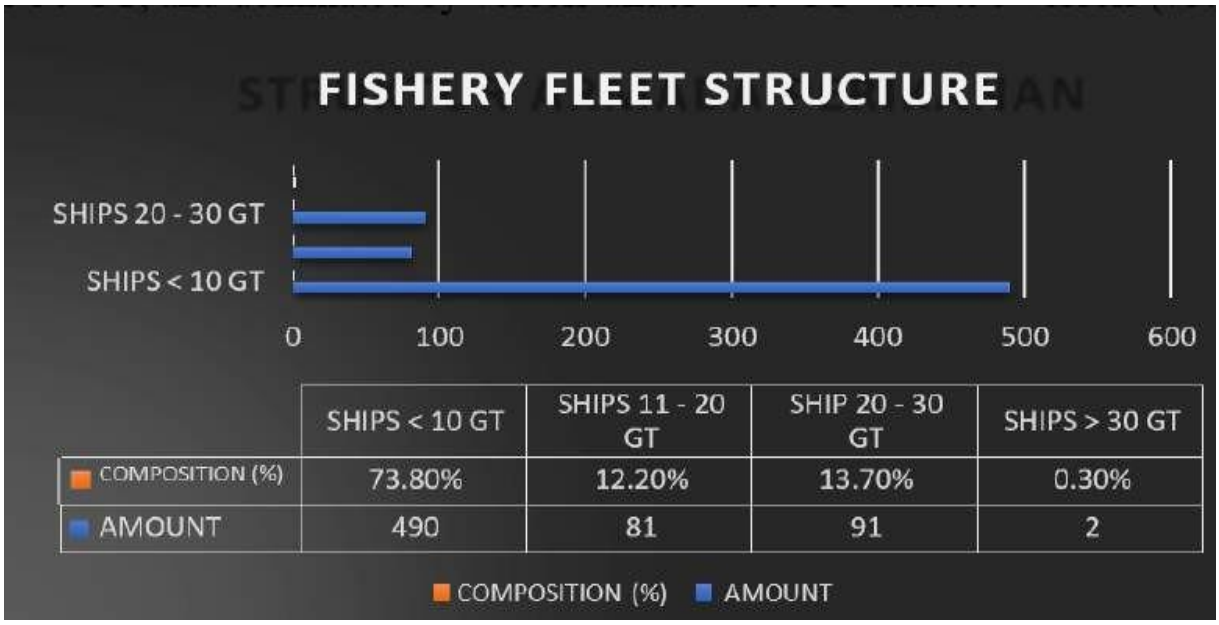

Figure 1. Fishing Fleet Structure

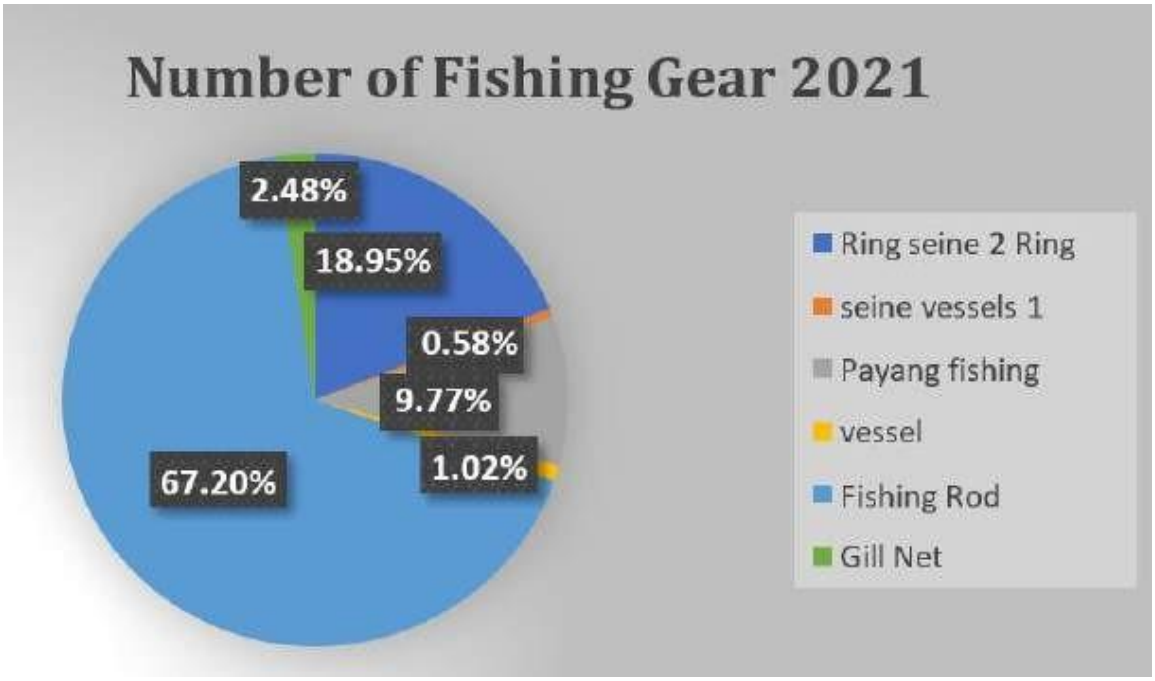

Figure 2. Number of Fishing Gears in 2021

In 2020, the recorded volume of fisheries production landed at PPN Prigi was 28,822,884 kg. with a production value of Rp. 198.339.137.750. while in 2021 it will be 24,928,229 Kg with a production value of IDR. 219,419,964,000, so this year there was a decrease in the volume of fisheries production of 3,894,655 Kg or 13.51% due to a significant decrease in the volume of the Deles Fly species, namely 70%, while the production value increased by Rp. 21.080.826.250 or 10.63% because fish prices tend to be stable. In the period between 2017 and 2021, 2019 was also the year

with the highest production amount and production value, namely Rp. 233,308,498,100 and 28,472,852 kg, while the lowest was in 2017, namely the production amount was 4,165,068 kg with a production value of Rp. 79,243,899,200 (Figure 3). Catch productivity has fluctuated from year to year. The biggest decline occurred in 2017 which was quite drastic. Based on information obtained from the management of PPN Prigi and fishermen, this is thought to be because in that year many fishing fleets did not go to sea. The number of fishing fleets that do not go to sea is due to the issue of tsunami waves that often occur in the southern waters of Java, affecting the productivity of fishermen.

Distribution and marketing of fishery products from PPN Prigi consists of fresh fish products and processed fish products (Figure 4). The distribution destination area includes the local area, namely Trenggalek, and also inter-city distribution, including Tulungagung, Surabaya, Jombang, and other cities. Fisheries production from PPN Prigi which was distributed in the form of Fresh Fish amounted to 10,807,487 kg (43.35%), Frozen Fish 2,359,669 kg (9.47%), and processed fish which included Fish Pindang 9,227,443 kg (37.02%), Salted Fish 1,937,857 kg (7.77%), Fish Meal 26,450 kg (0.11%), smoked fish 565,463 kg (2.27%) and other processed products 3,860 kg (0.02%).

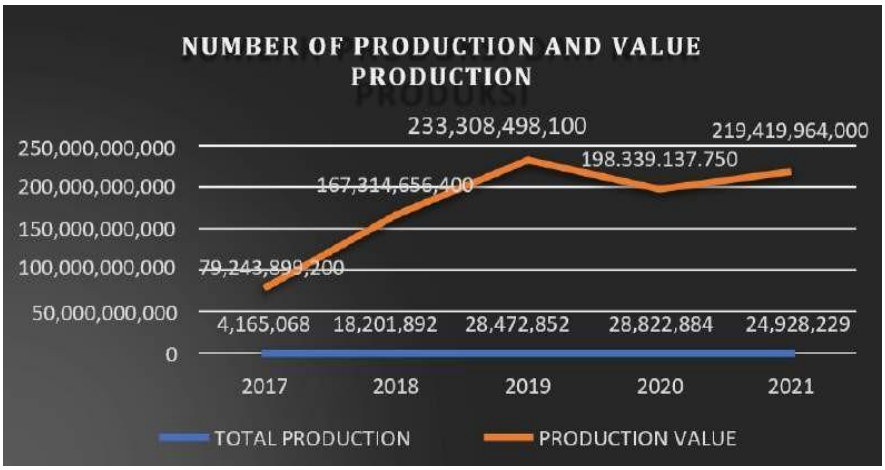

Figure 3. Production Amount and Production Value

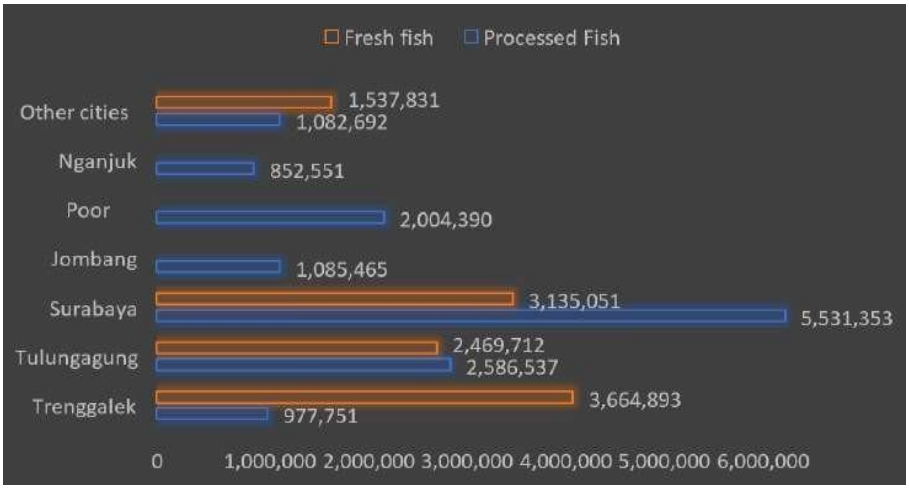

Figure 4. Distribution of Prigi VAT Fishery Products

The concept or pattern of distribution of fish catches before entering cold storage (Figure 5). There are several parties involved in the marketing of caught fish at PPN Prigi, ranging from collectors, dealers, large traders, small traders, and retailers to consumers. Collectors are traders who collect or buy caught fish from fishermen, while dealers are collecting traders with larger capital and scale than collectors. Besides being able to buy fish directly from fishermen, dealers can also collect catches from collectors. Wholesalers are also collector traders, but are engaged in a larger and wider business sector with legal entities and have been organized such as supermarkets, supermarkets,

and wholesale supermarkets. Retailers are stall traders or kiosk owners, vegetable vendors, restaurants, hotels, and caterers who can buy fish from large traders. Consumers are final consumers who buy fish caught for consumption and not for resale.

Marketing of fish catches by fishermen in PPN Prigi can be done directly or indirectly. Direct marketing is carried out by fishermen to large traders, while for consumption, fish marketing channels are carried out by large traders, as well as retailers, to end consumers (household consumers). Indirect marketing is done through intermediaries (collectors, dealers, wholesalers, and retailers). Indirect distribution patterns vary, using one to four intermediaries. So that each intermediary can take advantage, the more intermediaries result in the price of fish obtained by the final consumer will be higher (Hermawan, 2018). Apart from the above concept, fishermen also have the right to distribute their catches directly to consumers without any intermediaries.

Fishery product production from PPN Prigi is in the form of fresh fish products and processed fish (Figure 5). The distribution destination area includes the local area, namely Trenggalek, and inter-city distribution, including Tulungagung, Surabaya, Jombang, and other cities. Fisheries production from PPN Prigi which was distributed in the form of Fresh Fish amounted to 10,807,487 kg (43.35%), Frozen Fish 2,359,669 kg (9.47%), and processed fish including Pindang Fish 9,227,443 kg (37.02 %), Salted fish 1,937,857 kg (7.77%), Fish Flour 26,450 kg (0.11%), Smoked Fish 565,463 kg (2.27%) and other processed products 3,860 kg (0.02%).

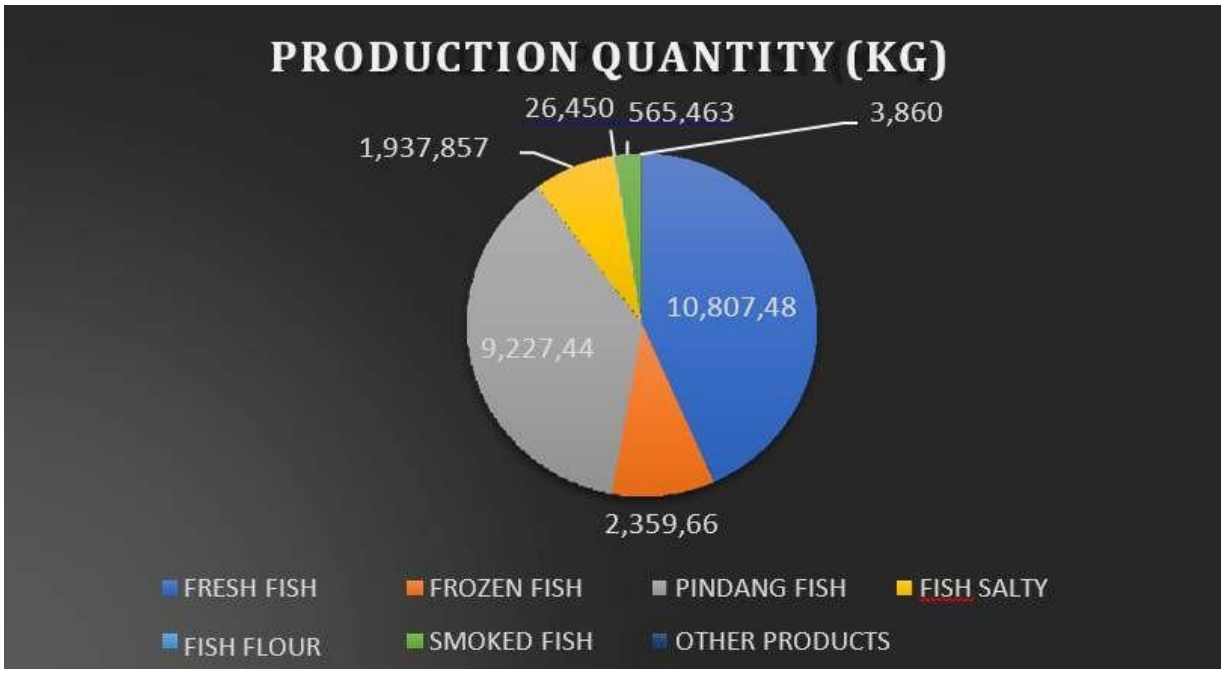

Figure 5. PPN Prigi Processed Products

Next is a fish distribution chain mapping model. This mapping consists of, among other things: starting from the fishermen's catch, then transportation to the cold storage place, then the processing process in cold storage, then transportation to the market, and finally into the hands of consumers. This mapping model aims to maintain the quality of fish during the distribution process while the fish is frozen and the quality is maintained [10].

The delivery process, in this process, consists of two stages, namely from the fish auction place to the cold storage place using private transportation (pick up) and from the cold storage place to the Tulungangunng market using government-owned transportation (Thermo King truck). First, from the fish auction place to the cold storage using a pick-up vehicle with a capacity of 1500 kg at a distance of 1 km. Where one trip takes 4.6 hours, including loading and unloading. The total cost of a pick-up vehicle, consisting of operating costs and annual voyage costs, is IDR 55,529,920. Next is delivery from the cold storage place to the Tulungagung market using a Thermo King truck transportation with a fish storage temperature during the distribution of (-11) – (-12) °C with a capacity of 6000 kg over a distance of 60 Km. Where 1 trip takes 5 hours, including processing, loading, and

unloading. The total cost of a Thermo King truck vehicle, consisting of operating costs of IDR 82,950,000 and voyage costs of IDR 90,432,000 per year, is IDR 173,382,000.

The potential for capture fisheries in PPN Prigi reaches 24,928,229 Kg. Of the total catch by fishermen, no more than 9% can be used in cold storage. So far, catches in the form of fish, shrimp, and other biota are often sold directly by fishermen without any technological touch, namely cold storage, which functions for freezing and cooling, as an effort to maintain the quality of fishery products. The advantages of using cold storage are guaranteeing supplies of materials for the continuity of factory operations, extending the life of stored products, contributing to reducing unemployment through employment, training facilities, internships, and development of science and technology in the field of fishery product processing to increase economic value, regional income, and regulating distribution and stabilizing prices.

The Nusantara Prigi Fishing Port has four units of fish cooling and freezing facilities (cold storage), consisting of one owned by the government and three owned by the private sector. There are currently only two active cold storage units operating, each with an Air Blass Freezer (ABF) and cold room. The cold storage owned by the government has a capacity of 100 tons, consisting of one ABF room unit with a load of 50 tons and a 100-ton cold room. Meanwhile, privately owned cold storage has a capacity of 300 tons, consisting of four Air Blass Freezer (ABF) units with a capacity of 5 tons each and a 300-ton cold room.

The process of handling fish and storing fish in cold storage is carried out by workers provided by service users who will store the caught fish in cold storage. The Prigi Archipelago Fisheries Port (PPN) only provides officers who record the type of fish and the weight of the fish that will be stored in cold storage. Before entering cold storage, the caught fish go through several handling processes, including when the fish arrives, the fish must be washed first after the fish is clean, then put in a fiberglass box for temporary storage with ice cubes given to it to maintain temperature. the fish remains stable. Next, the fish are sorted according to type and size and then placed in a van/pan with a capacity of 1 pan containing 10 kg of fresh fish. After sorting, the fish are put into the ABF room for freezing. Freezing 1 ton of fish takes 4 to 4.5 hours. Freezing fresh fish is usually done for 14 to 16 hours per day (until the fish is frozen) with a

Table 1. Government Cold Storage Performance

No.	Year	Quarterly	Production Capacity Cold Storage (Ton)	Cold storage capacity (Tons)
1	2017	1	0	100
		2	41	100
		3	49	100
		4	72	100
2	2018	1	0	100
		2	7	100
		3	5	100
		4	29	100
3	2019	1	0	100
		2	41	100
		3	49	100
		4	16	100
4	2020	1	0	100
		2	57	100
		3	10	100
		4	0	100
5	2021	1	0	100
		2	0	100
		3	62	100
		4	31	100

Description: 1 (January, February, March), 2 (April, May, June), 3 (July, August, September), 4 (October, November, December).

temperature range of -25°C to -40°C. After the fish is frozen, the fish is then put into a cold room with a temperature range of (-17°C) to (-30°C) until the desired storage time.

Assessment of the role of cold storage capacity can be determined by production in the period 2017 - 2021 for government cold storage and 2020 - 2021 for private cold storage (Table 1 and Figure 6).

The performance results of the government's cold storage capacity based on the weight of fish stored during the period 2017 - 2021, from the first to the fourth quarter, showed that none of them reached the cold storage capacity of 100 tons. Most storage was only in the fourth quarter of 2017, with a total storage production of 72 tons. The availability of fish in the first quarter of 2017-2021 is 0, which means that fish is not available in cold storage.

The results of the performance of private cold storage capacity based on the weight of fish stored during the period 2020 - 2021, from quarters one to four, show that none of them reached a cold storage capacity of 100 tons. The largest storage was in 2020 in the fourth quarter with a capacity of 84 tons. In 2020, in quarters one to three, the production capacity did not exceed 50% of the cold storage capacity. This also occurred in the second to fourth quarter of 2021, with fish availability not reaching 50% of the cold storage capacity (Table 2).

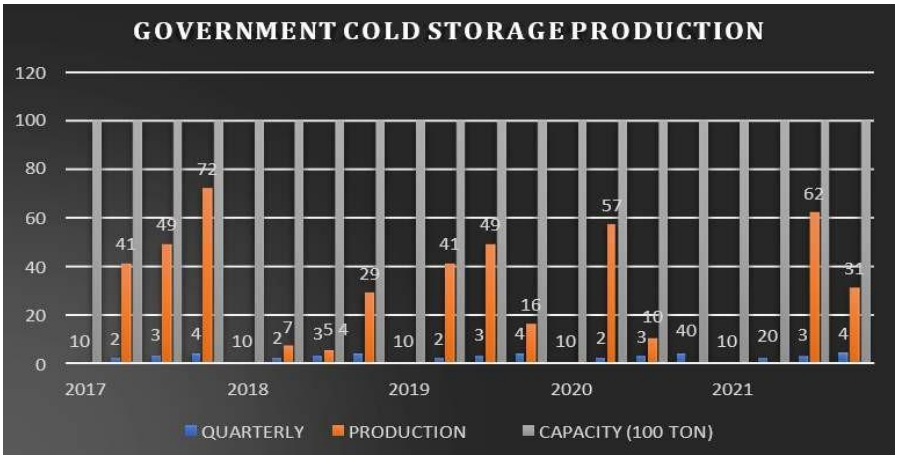

Figure 6. Government Cold Storage Production

Table 2. Private Cold Storage Performance

No.	Year	Quarterly	Production Capacity Cold Storage (Ton)	Cold storage capacity (Tons)
1	2020	1	27	300
		2	24	300
		3	12	300
		4	84	300
2	2021	1	50	300
		2	34	300
		3	7	300
		4	9	300

Description: 1 (January, February, March), 2 (April, May, June), 3 (July, August, September), 4 (October, November, December).

Cold storage role assessment calculation:

$$\text{Length of interval class} = \frac{\text{range}}{\text{many interval class}}$$

Description:
Range = Highest score – The lowest score

Highest score = total number x highest score
= 15 x 5
= 75

Lowest score = total number x lowest score
= 15 x 2 (government) 1 (private)
= 30 (government)
15 (private)

Based on the formula, the length of the interval class is:

$$\text{Length of the interval class} = \frac{75-30}{5} = 9 \text{ and } \frac{75-15}{5} = 12$$

$$\text{Average score of the government's cold storage role} = \frac{(12x5)+(8x4)+(27x3)+(28x2)+(0x1)}{5} = 43{,}6$$

$$\text{Average score of the role of private cold} = \frac{(12x5)+(8x4)+(27x3)+(28x2)+(0x1)}{5} = 45{,}8$$

Analysis of the role of cold storage capacity is also carried out using a Likert scale based on the parameters observed by looking at the secondary data obtained. All parameters are arranged in the form of a matrix with a score of 1 to 5. Each parameter will be assessed according to the criteria that have been compiled. The results of the assessment of the role of cold storage can be seen in the table below.

The results of the assessment of the role of government cold storage obtained a calculation score of 45,8, while private cold storage amounted to 43,6 (Table 3). The score states that the role of cold storage is still not maximized to store fish in PPN Prigi.

Meanwhile, private cold storage shows the same thing as cold storage owned by the government; no production reaches a capacity of 300 tons or the highest 100% storage value, namely 84 tons (Figure 7). Fish availability in quarters 1 to 3 in 2019 was below 50%. This also happened in the 2nd quarter to the 4th quarter of 2020, where fish availability was below 50%.

The total comparison of cold storage production with the total cold storage capacity at the Nusantara Prigi Fishing Port from 2020 - 2021, government-owned and privately owned, does not even reach 100% of the total cold storage capacity. The highest production occurred in the 4th quarter of 2020, namely 84 tons. This production still did not even reach 50% of the total cold storage capacity. The lowest production occurred in the 2020 – 2021 period, quarter 3, with a production capacity of 22 tons, with production not reaching 20% of cold storage capacity.

The role of cold storage in PPN Prigi can be increased by looking at the large fish production and seasonal factors of superior fish species to stabilize prices. There are 3 superior fish groups, the first group is tuna and skipjack. The fishing season only occurs during the eastern season and can be released for the transitional season II, in the same season the second group of superior fish consisting of swallow, Lemuru, and Layur fish can be stored in the transitional season II and released during the western season, while for the third group of superior fish consists of Slengseng fish, Tembang fish and Selar fish, the fishing season occurs throughout the year from the western season to the eastern season, this third group of superior fish can be released in every season.

Meanwhile, private cold storage shows the same thing as cold storage owned by the government; no production reaches a capacity of 300 tons or the highest 100% storage value, namely 84 tons (Figure 7). Fish availability in quarters 1 to 3 in 2019 was below 50%. This also happened in the 2nd quarter to the 4th quarter of 2020, where fish availability was below 50%.

The total comparison of cold storage production with the total cold storage capacity at the Nusantara Prigi Fishing Port from 2020 - 2021, government-owned and privately owned, does not even reach 100% of the total cold storage capacity. The highest production occurred in the 4th quarter of 2020, namely 84 tons. This production still did not even reach 50% of the total cold storage capacity. The lowest production occurred in the 2020 – 2021 period, quarter 3, with a production capacity of 22 tons, with production not reaching 20% of cold storage capacity.

Table 2. Cold Storage Capacity Role Assessment

No.	Criteria	Assessment Score	
		Cold storage government	***Cold storage* private**
1	Fish production in cold storage increases every year	3	2,8
2	Every eastern season (fish season) the cold storage is always full	2,4	2,4
3	Cold storage production reaches capacity every fish season	2,2	2,4
4	Cold storage production reaches capacity every fish season	2,4	2,4
5	Every month the cold storage sells/releases fish	2,4	3
6	In the western season, cold storage continues to operate	2,4	2,8
7	Fish availability remains during the lean season	2,4	1,3
8	Every year per quarter cold storage production reaches 50%	2,4	2
9	Cold storage can slow down the spoilage of stored products	5	4,8
10	The fish stored are large pelagic fish.	4	2,4
11	Cold storage industry business opportunities are getting better	3	3
12	The quality of fish stored in cold storage is fresh	2,6	4,6
13	The production that cold storage does is sufficient	2,4	2,4
14	Market demand for fish in cold storage is always met	2,4	2,2
15	Fish prices increase during the lean season	4,8	4,6
Total		45,8	43,6

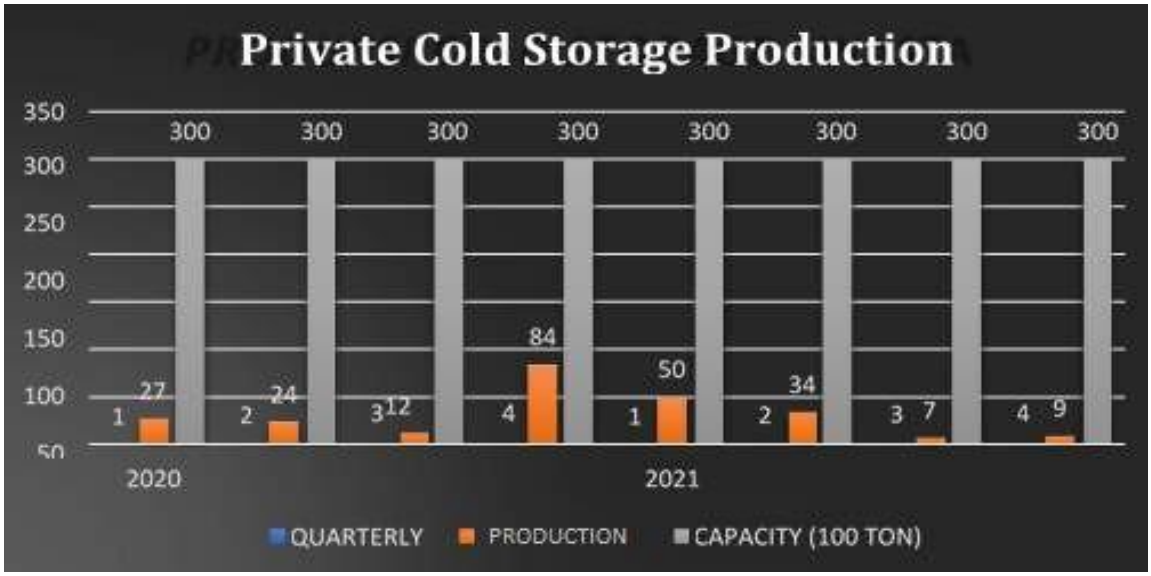

Figure 7. Private Cold Storage Production

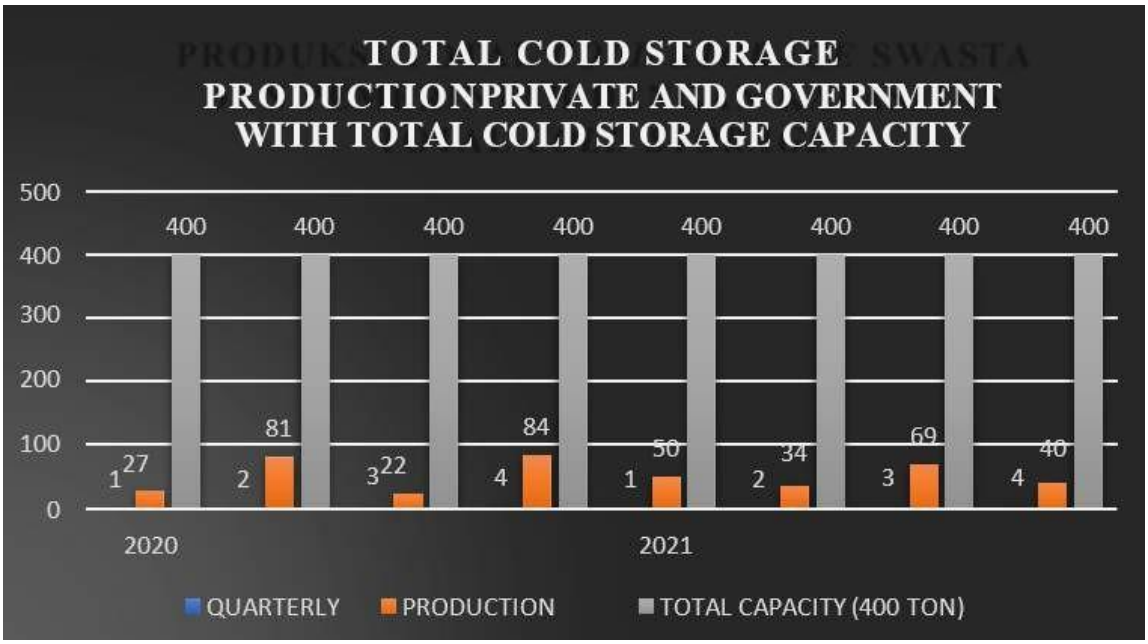

Figure 8. Total Production with Cold Storage Capacity 2020 – 2021

Comparison of private cold storage production with total cold storage capacity (Figure 9). It can be seen from the graph above that the comparison of private cold storage production with the total cold storage capacity in the Prigi fishing port states that no production has reached 50%. The highest production occurred in 2017 in the 4th quarter with a production of 72 tons. The lowest production occurred at the end of 2020 and the beginning of 2021, with a production of 0. With this factor, it is possible that fishermen stored their catch in the cold storage government property. This can be seen in Figure 6, where the government cold storage produces fishery products.

The assessment of the role of government cold storage obtained a calculation score of 45.8, while for private cold storage, it is 43.6. This score states that the role of cold storage is still not optimal in terms of availability to support the capture fisheries industry in PPN Prigi. This is because many local fish entrepreneurs buy the fish they catch and market it directly at that time. This social phenomenon means that cold storage in PPN is not optimally utilized according to its function. Efforts to develop fisheries businesses by improving the quality of products marketed at regional to international levels certainly require the role of cold storage in its operations.

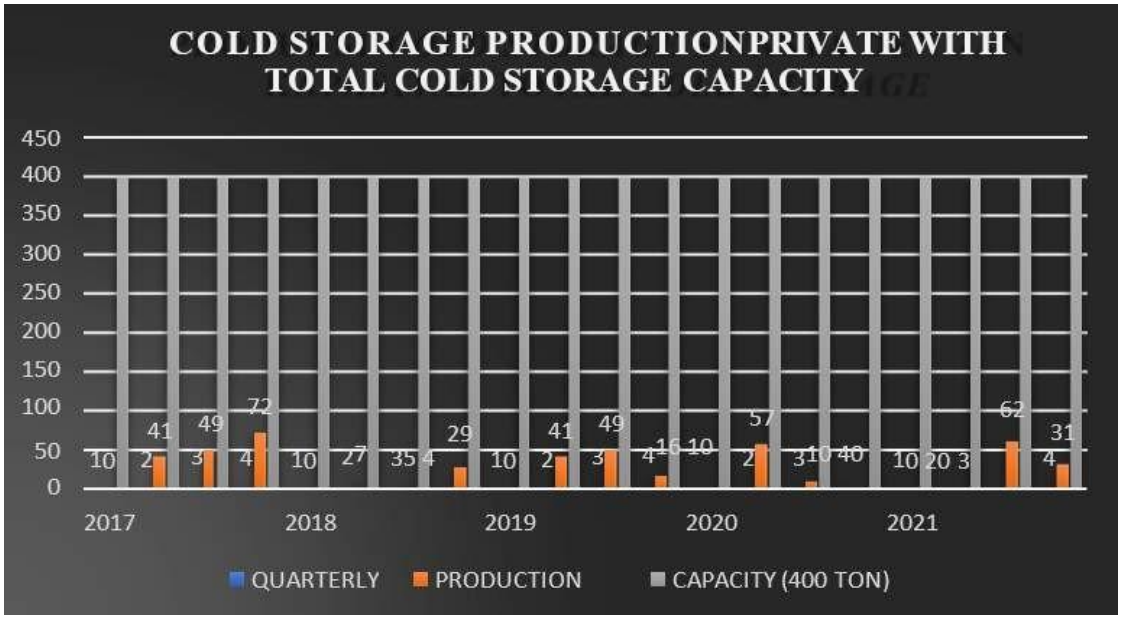

Figure 9. Comparison of Private Cold Storage Production with Cold Storage Capacity in 2017 – 2021

Conclusion

From the research that has been done, the following conclusions are obtained: Mapping the supply chain management process of the distribution system from the cold storage factory to the Tulungagung market and surrounding areas using a Thermo King truck with a capacity of 6 tonnes. Mapping of the supply chain management process using land routes (Existing), starting from the cold storage factory to the Tulungagung market, for a frozen processed fish product. Mapping the identification of distribution costs from the PPNPrigi cold storage factory using truck Thermo King transportation with a total cost of Rp 173,382,000 / year, including operational costs of Rp 82,950,000 / year and vehicle travel costs of Rp 90,432,000 / year. Based on the production and capacity of cold storage and assessment of the role obtained, numbers 45.8 and 43.6 indicate that the role of cold storage in PPN Prigi is not optimal.

Acknowledgments

We would like to express our deepest gratitude to all those directly involved in this research, as well as other parties involved indirectly. Our deepest gratitude to PPN Prigi, the Prigi community, the Tulungagung Regency fish market, and the market residents where we conducted our research. We would also like to thank the Prigi and Tulungagung Regency Fisheries Service for helping us with the data.

References

[1] Ashok A., Brison M. and LeTallec Y., 2017. Improving cold chain systems: Challenges and solutions. Vaccine. Vol. 35, No. 17 (2017) pp. 2217-2223 DOI: https://doi.org/10.1016/j.vaccine.2016.08.045

[2] Hongxia Z., Sheng L., Changging T., Gang Y. and Da W. An overview of current status of cold chain in China. International journal of refrigeration. Vol. 88, (2018) pp. 483-495. https://doi.org/10.1016/j.ijrefrig.2018.02.024

[3] Badia-Melis R., Mc Carthy U., Ruiz-Garcia L., Garcia-Hierro, J. and Villalba, J.I.R. New trends in cold chain monitoring applications-A review. Food Control. Vol. 86, (2018)pp.170182.https://doi.org/10.1016/j.foodcont.2017.11.022

[4] Pusporini P. and Dahdah S.S. The conceptual framework of cold chain for fishery products in Indonesia. Journal of Food Science and Technology. Vol. 8, No. 2 (2020) pp. 28-33. DOI: https://doi.org/10.13189/fst.2020.080202

[5] Lailosa, G.W. The New Paradigm Of Cold Chain Management Systems and it's Logistics on Tuna Fishery Sector in Indonesia. Aquaculture, Aquarium, Conservation and Legislation Vol. 8, (2015) pp. 381-389.

[6] Arista G., Jahroh S. and Indrawan D. Mapping Fisheries Cold Chain in Western Java Using a Value Chain Perspective. Jurnal Managemen & Agribisnis. Vol. 19, No. 1 (2022) pp. 129-138. DOI: https://doi.org/10/17358/jma.19.1.29

[7] Yihang, O. Towards Ensuring the Safety and Viability of Seafood: the Regional Guidelines on Cold Chain Management of Fish and Fishery Products in the ASEAN Region. Fish for the People. Vol. 18, No. 2 (2020) pp. 29-31.

[8] Guritno A.D., Ushada M., Kristanti N.E., Dharmawati M.S. and Putro N.A.S. Development of Quality Evaluation Model for Supply Chain of Capture Fisheries in Southern Coast of Java. Agricultural Engineerng International: CIGR Journal. Vol. 3, No.4 (2021) pp. 183-197

[9] Hartono, Laporan Statistik Time Series 5 Tahunan *Statistic Report Of Prigi Fishing Port* (2019).

[10] Mubarok A.S., Perdana A.W., Sasmito B.B., Kusuma B., Waluyo E., Aji M.T. and Sulthoniyah S.T.M. Study of Fishery Commodities Cold Chain System at Malang City. JFMR (Journal of Fisheries and Marine Research). Vol. 5, No. 2 (2021) pp. 350-35. DOI: https://doi.org/10.21776/ub.jfmr.2021.005.02.20

[11] Budiyanto E.H., Gurning R.O.S. and Cahyagi, D. The analysis of port integration on fishing cold chain: The Case of collaboration between general port and fish operator. Proceeding of Marine Safety and Maritime Installation (2018).

Date of Received:
June 25, 2024

Date of Accepted:
July 10, 2024

Date of Published:
September 1, 2024
DOI: doi.org/10.30649/ijmea.v1i1.367

INTERACTION ANALYSIS HULL AND PROPELLER AND IMPROVEMENT OF EFFICIENCY PROPELLER ON FISHING VESSELS

Mohammad Abu Jami'in[1*], Abi Primanjaya[2]

[1] Politeknik Perkapalan Negeri Surabaya, 60111, Indonesia
[2] PT. Federal International Finance, 60175, Indonesia

*Corresponding Author: jammy@ppns.ac.id

ABSTRACT

The determination of propeller and hull adjustment of both small and large fishing vessels is indeed very important; in general, fishing vessels at the port of Lamongan only use hereditary techniques. many weaknesses in the problem of synchronization between the hull, the main propulsion engine, and the propeller. therefore, after analysis, it can be concluded that at the coastal port of Lamongan, an Ijon-Ijon type fishing boat, with a main size of 5-10 GT. In one ship using the Mitsubishi Fuso 120 ps 2 engine type, using 2 gearbox advance ratio 3.1 rated input speed 1000- 2500 r/min and rated trans capacity 0.039 kW/min with a total resistance value of 17.599 kN, wake fraction value 0.235, value thrust deduction 0.197 and using a propeller with type B-series B3-35 with a diameter of 1.54 with a KT value of 0.31, a value of 10KQ 0.37, a value of J 0.52 and an average efficiency value of 0.48. By changing the propeller diameter to 1.75 and changing the gearbox ratio with the same engine, a comparison can be made between the efficiency of the propeller previously and the efficiency after changing the propeller diameter, with a KT value of 0.30, a value of 10KQ 0.345, a value of J 0.55, and an average efficiency value of 0.565.

Keywords: Fishing boat, hull shape, propulsive coefficient

Introduction

Determining the propeller and adjusting the hull of both small and large fishing boats is very important; in general, fishing boats in Lamongan harbor only use techniques passed down from generation to generation. This traditional shipbuilding is far from modern technology and has many weaknesses that must get more attention, especially the synchronization problem between the hull, main engine, and propeller [1]. Therefore, after analysis, it can be concluded that Kranji Village, Lamongan Regency, is one of the fish-producing areas in East Java. The characteristics of the Kranji Village area are coastal areas with fisheries activities as the dominant activity in areas located along the coast.

However, the research will raise several problems, including analyzing the type of ship engine, gearbox, and propeller type that is appropriate and optimal, and by the obstacles of traditional fishing boats. Based on observations made in the field, there are fishing boats that have three main engines. The fishermen there get engines for ships from trucks or buses whose engines are no longer in use. In ships that exist in this modern era, there is a fairly sophisticated drive system. Some components of the drive system on the ship are the main drive engine, gearbox, and propeller shaft, which will later be analyzed for characteristics to find the efficiency of performance of the propeller [2].

While in general the optimal characteristics of fishing boat propellers are with Ae/Ao = 0.550; P/D = 1.3; J = 0.5, the reason for using several propellers is so that fishing boats can operate at high speeds for the fishing process, based on the main size ratio

of standard fishing boats, namely the value of the L/B ratio of 4.30 - 4.50; L/D 10.00 - 11.00; B/D 2.10 - 2.15. If the B/D value is getting bigger, the ship's stability and ship's motion are getting better, and the relationship between the B/D ratio value and the engine power and net size of the fishing boat means that the weak or low thrust of the ship can be supported by large engine power. stated that the driving force used by fishing boats must be calculated properly and correctly [3].

Based on these conditions, it can be concluded that in planning the propulsion system of fishing boats on the Lamonga coastline, using the right calculations and studies to determine the use of engines and propulsion systems on ships can produce optimal ship performance according to existing standards [4].

Methodology

a. Location and Time of Research

This research was conducted on the coast of Lamongan for the collection of ship data to be tested, as well as photographic images of ships that will be examined. This will strengthen the objectives of this study for the time of the data to be taken after obtaining the requirements of the supervisor.

b. Fishing Boat Data

On this page, we will explain the data of the fishing boat to be examined, along with the type of engine and gearbox on the fishing boat. This data collection is based on the results of a survey of the Lamongan shipport located in East Java. The ship data used is the main Nabila fishing boat data.

Table 1. Principal dimensions

Principal Dimensions	
Ship Type	Ijon ijon
Ship Name	Nabila Utama
The overall length of the vessel (LOA)	12.70 m
Waterline length (LWL)	12 m
Ship width (B)	5.00 m
Ship height (D)	2.80 m
Ship draft (T)	1.30 m
Displacement	62,34256 Ton
Cb	0,779769
Ship speed	7 knots
CB wl	0,758
CM	0,8557
CP wl	0,6520
Cwp	0,837
Fishing gear	Fishing rod
Owner ship	Warsujud
Phone number	081212342548

Table 2. Main engine

Main Engine	
Mitsubishi Fuso, Engine 4D34-2AT8 Fuso	
Number of machines	2
Machine type	4 water-cooled cycle
Maximum power	228 kW/2900 rpm
Maximum torque	33 kg.m/2800 rpm
Emissions	Non-emissions
Bore x stroke	104 x 115 mm
Displacement	11.945
Length	1473 mm
Width	881 mm
Height	1209 mm
Dry weight	1000 kg
Cylinder	4 cylinder
Cylinder diameter	104 mm
Cylinder length	115 mm

Table 3. Gearbox data

Gearbox Data	
Brand	*Advance*
Model	16A-1
Input speed	1000-2000r/min
Reduction ratio	2.07,2.48, 2.95, 3.35, 3.83
Trans capacity	0.012kw/r/min
Control method	Manually
L x W x H	422 x 325 x 563 mm
Thrust value	3,5 kn
Net weight	84 kg

Table 4. Propeller data

Propeller Data	
Propeller type	B3-35
D_b(m)	0,54 m
(P/D_b)	0,745
η propeller	0,480
RPM propeller	228 rpm
Control method	Manually

Figure 1. Propeller

c. Simulation

Simulation, or what is commonly called the process of knowing with this engineering form, is calculated using the Holtrop mathematical system and simulated with the KT-KQ-J method and using the ANOVA method, where this method can find ship efficiency, ship thrust, and drive motor power.

The conclusions received after using the ANOVA method can be filtered again to find the maximum results in an analysis.

The simulation I made was a model that fits the real size that was scaled, and then I added other model variations that changed the radius of the propeller as a comparison to get a thrust value, and used AUTOCAD software to make a more optimal propeller model.

Result and Discussion

a. Holtrop Mathematical Resistance

In Holtrop's mathematical calculations, by entering the main data on the ship, the calculation of the total resistance of the ship is obtained.

Rtotal = RF (1+k1) + RApp + RW + RTR + RB + R

RF = frictional resistance according to the ITTC-1957 formula

1 + k1 = form factor of the hull

RAPP = appendage resistance

RW = wave resistance

RB = additional pressure resistance of the bulbous bow near the water surface

RTR = additional pressure resistance due to transom immersion

RA = model-ship correlation resistance

Rtotal = RF(1+k1) + RApp + RW + RTR + RB + RA
= 1,621 kN + 1,390 kN + 0,010 kN + 14,9488822 kN + 0 kN + 0 kN + 0,388 kN
= 17,599 Newton

Therefore, the wake fraction

W = C9 x C20 x Cv x L/T (0.050776 + 0.93405 x C11 x CV/1 – Cp1)) + 0.27951 x C20 √ ((B/(L(1-CP1))) + C19.C20
= 12.561 x 0.988 x 0.000559624 x (11/1,3) x (0.050776 + 0.93405 x 1.538 x 0.000559624/ (1 – 0,652) + 0.27951 x 0.988 √ (5/ (11 (1- 0.652)) + (0.072 x 0.988)
= 0,235

b. Calculating Trust Deduction Factor (t)

t = 0,25014 (B/L) 0.2896 (√((B.T)/D) 0.2646 / (1- CP + 0,225LCB) 0.01762 + 0.0015 CSTERN
= 0.25014 (5/11) 0.2896 (√(5x1,3)/0,8) 0.2646 / (10. 652 + 0.0225 x 0.068) 01762 + 0.0015 x (-8)
= 0,197

c. Hull-Propeller Interaction

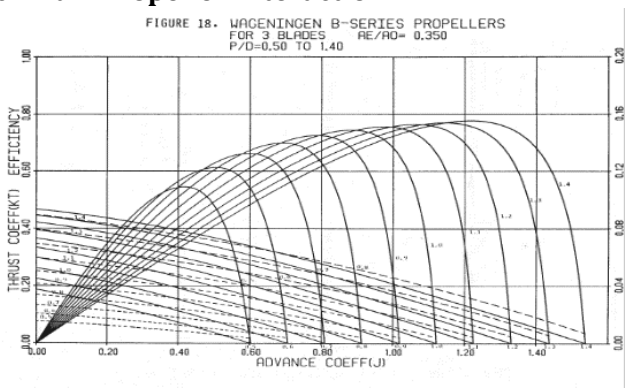

Figure 2. Wagening diagram of B3-35

Propeller-hull interaction describes the correlation between ship resistance and propeller performance characteristics. Ship resistance is transformed into the form of a propeller loading curve, and propeller performance characteristics are shown by the results of propeller testing called the propeller open water test. The characteristics of the open-water test propeller are approximated by the B-series propeller type through the B-series propeller polynomial equation.

The mathematical formulation of the open-water test propeller performance is as follows:

$$J = \frac{Va}{nD}$$

$$Kt = \frac{T}{\rho.N^2.D^4}$$

$$Kq = \frac{Q}{\rho.N^2D^5}$$

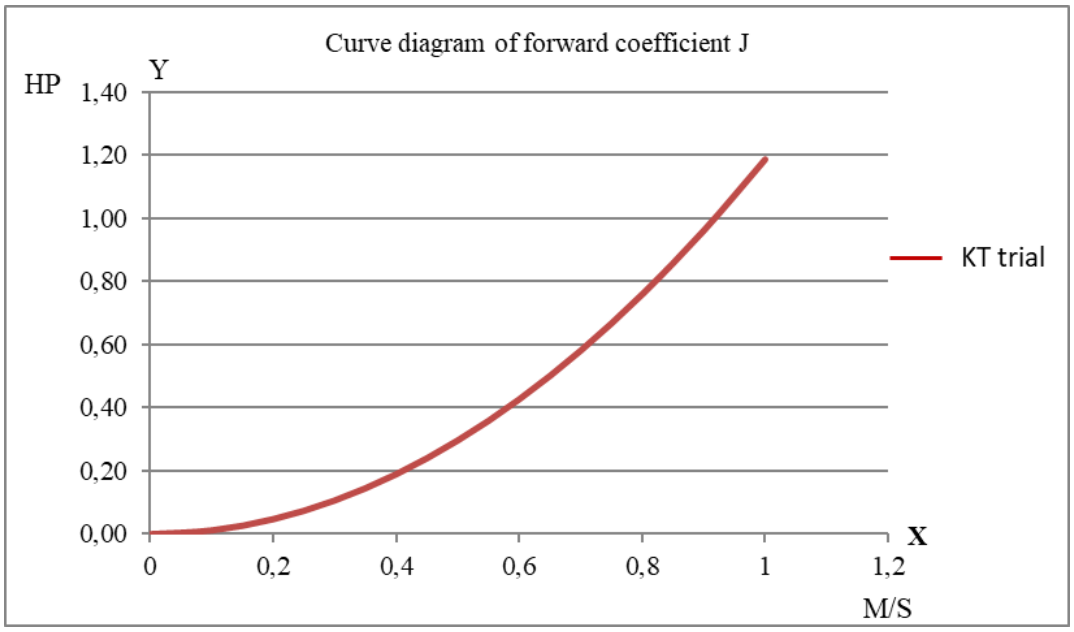

Figure 3. Diagram of forward coefficient

$$\pi_0 = \frac{Pt}{Pd} = \frac{T.Va}{2.\pi.n.Q} = \frac{J.Kt}{2.\pi.Kq}$$

Where:

J	=	Propeller forward coefficient,
Va	=	Forward speed (m/s),
D	=	Propeller diameter (m),
n	=	Propeller rotation (rpm),
Kt	=	Propeller thrust coefficient,
T	=	Propeller thrust force (N),
Kq	=	Propeller torque coefficient,
Q	=	Torque propeller (N.m),
ηo	=	Open water efficiency,

The mathematical description of ship resistance characteristics converted to a propeller loading curve is:

$$R = c.V^2$$

$$T.(1-t) = c.\left[\frac{Va}{(1-w)}\right]^2$$

$$Kt.\rho.n^2.D^4 = \frac{c}{(1-t).(1-w)^2}Va^2$$

$$Kt = \frac{c}{\rho.(1-t).(1-w)^2.D^2}\left[\frac{Va}{n.D}\right]^2$$

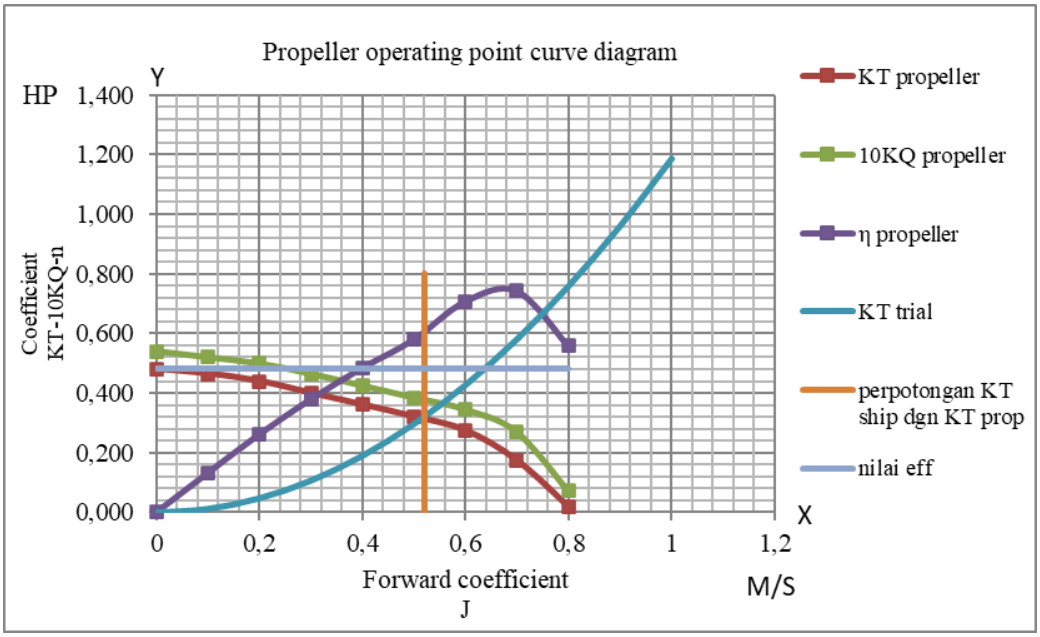

Figure 4. Propeller operating point diagram

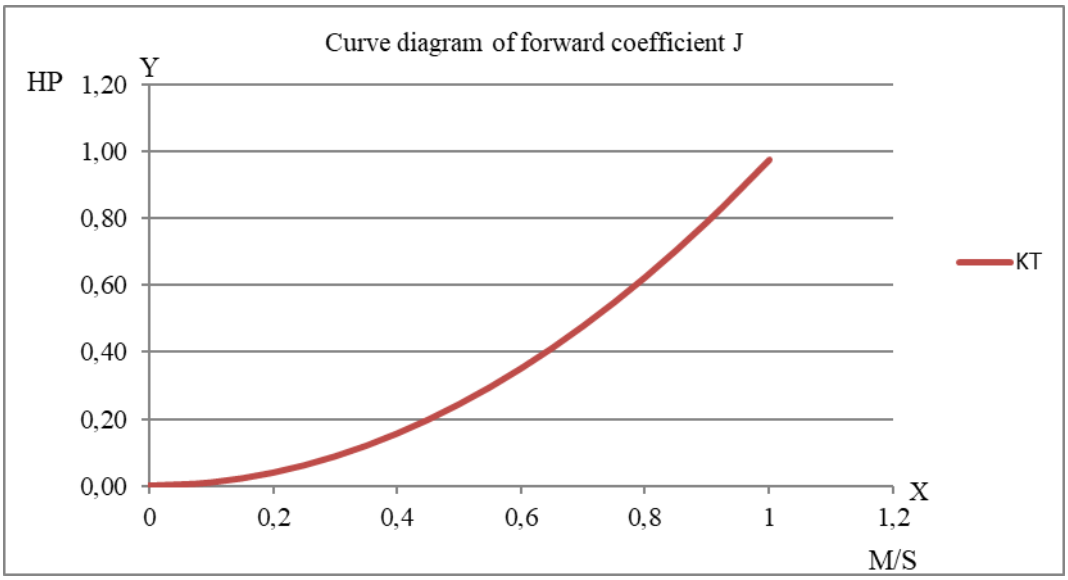

Figure 5. Diagram of forward coefficient

$Kt = Constan\,t\,.J^2$

Where:

W = Wake fraction coefficient,
t = Thrust deduction coefficient,
Kt = Propeller thrust coefficient,
c = Constant,
ρ = Density of seawater (kg/m3).

d. Calculating the coefficient α

$R = c.V^2$
= 17,599 x 3,601= 1357,35 In the unfilled position

Calculating the coefficient

$$Kt = \frac{c}{\rho.(1-t)(1-w)^2 D^2}\left[\frac{Va}{nD}\right]$$

$$= 1.19$$

e. Create an open water test diagram

After calculating the value of the constant coefficient, the next fishing boat will be able to create an open water test curve as follows: with the open water test curve that has been made from a speed of 7 knots and plotted to the open water test image, you can also create a thrust coefficient (KT) diagram when the ship is in an empty hull position and get the propeller operating point of 0.54 m propeller diameter.

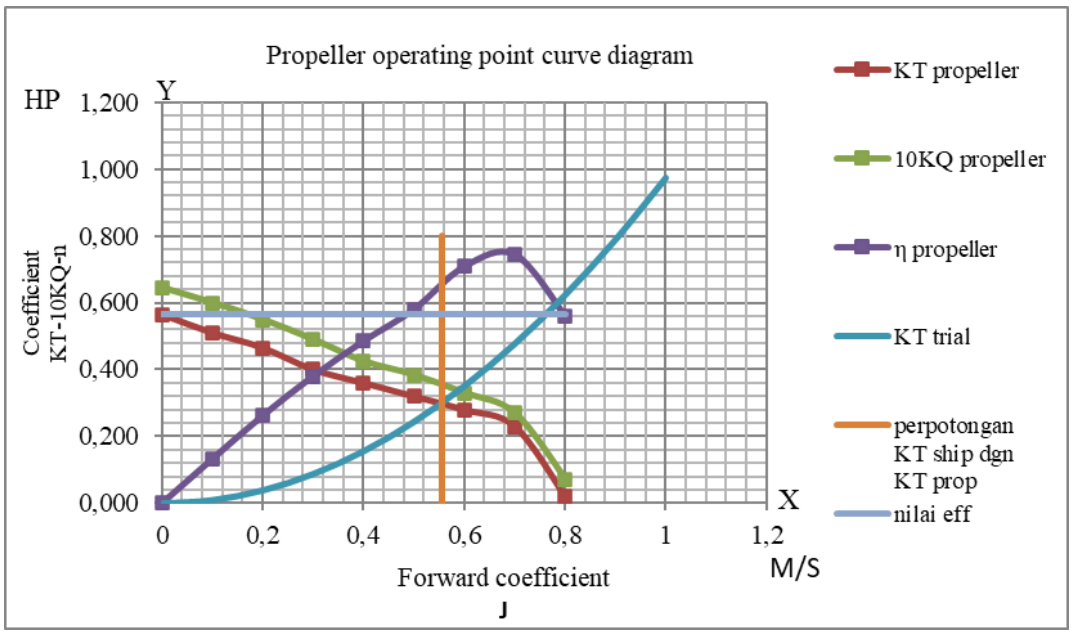

Figure 6. Propeller operating point diagram

Furthermore, from the results of these calculations, the KT design can be made at a speed of 7 knots and plotted against the open water test image to get the value of the intersection point of the curve. After looking for the KT trial value, it can then make a curve diagram of the table value accordingly and accurately.

From the results of Figure 4 above, we can determine the X-axis value of the forward coefficient (J), as well as the Y-axis value of the propeller thrust coefficient (KT propeller) and the propeller torque coefficient (10KQ) at the intersection of the KT design. At a speed plot of 7 knots, the resulting forward coefficient (J) value is 0.52 m/s, the propeller coefficient (KT) value is 0.31 HP, and the propeller torque coefficient (10KQ) value is 0.37 HP by determining the efficiency on the ship of 0.48%.

f. Changing the propeller diameter

To find out the optimal propeller performance, it is necessary to change the diameter of the propeller to find a more efficient propeller.

This propeller data comes from a type

Propeller type = B3-35
Db(m) = 0.75 m
(P/Db) = 0.745
η propeller = 0.565
Propeller rpm = 228 rpm

Calculating the coefficient α

$$R = c.V^2$$

$$= 17{,}599 \text{ x } 3{,}601 = 1357{,}35$$

Calculating the coefficient

$$Kt = \frac{c}{\rho.(1-t)(1-w)^2 D^2}\left[\frac{Va}{nD}\right]$$

$$= 0{,}82$$

Diagram of an open water test after calculating the constant coefficient value on the next fishing boat, it will be able to create an open water test curve as follows: with the open water test curve that has been made from a speed of 7 knots and plotted to the open water test image, it can also create a thrust coefficient (KT) diagram when the ship is in an empty hull position and when the hull is fully loaded.Getting the propeller operating point of 0.74 m propeller diameter from the results of Figure 4.7. Above, we can determine the X-axis value of the forward coefficient (J) from the highest point to the lowest point value of the forward coefficient (J), following the explanation in Table 5.

From the results of Figure 6 above, we can determine the X-axis value of the forward coefficient (J), as well as the Y-axis value of the thrust coefficient (KT) and the torque coefficient (10KQ) at the intersection of the design KT. At a speed plot of 7 knots, the forward coefficient (J) value of 0.55 m/s is obtained, the value of the intersection of the thrust coefficient (KT) with the KTtrial is 0.30 Hp, and the value of the intersection of the torque coefficient (10KQ) with the KTtrial is obtained by 0.345 Hp by determining the efficiency of the ship by 0.565%.

Table 4. Comparison of old and new propellers

Old propeller	New propeller
Tipe B3-35	Tipe B3-35
D 0,54 m	D 0,74 m
(P/D) 0,745	(P/D) 0,745
J 0,52 m/s	J 0,55 m/s
KT 0,31 Hp	KT 0,30 Hp
KQ 0,37 Hp	KQ 0,345 Hp
η 0,48 %	η 0,565 %

Conclusion

The ship uses a propeller type B-series B3-35 with a diameter of 0.54 m and an average efficiency value of 0.48% based on the initial efficiency value of 0.48%. At a speed plot of 7 knots, the resulting forward coefficient (J) value is 0.55 m/s, with the value of the intersection of the thrust coefficient (KT) of 0.30 HP and the value of the intersection of the torque coefficient (10KQ) of 0.345 HP by determining the efficiency on the ship of 0.565%. By increasing the diameter and also changing the angle of the propeller, the best propeller data results are a 0.74 m diameter propeller with an angle change of 20% for the B3-35 propeller type.

The results of this study are the calculation of engine estimation with a propeller to find efficiency on the fishing boat under study. We need to make a 3-dimensional image of the best propeller calculation results to be able to easily study them.

References

[1] Paska A., Hadi E.S., Kiryanto, Analisa Engine Propeller Matching pada Kapal Perintis Baru Type 200 Dwt Untuk Medapatkan Sistem Propulsi yang Optimal. Kapal: Journal of Marine Science and Technology Vol. 4, No. 3 (July 2016) pp. 576-585. ejournal3.undip.ac.id/index.php/naval/article/view/13831

[2] Abdillah M.A., Winarno A., Riyadi M., Pengaruh Propeller tidak Center dengan Linggi Terhadap

Arah Gerak Pada Km. Sri Mulyo di Brondong Lamongan. Seminar Nasional Kelautan XIV "Implementasi Hasil Riset Sumber Daya Laut dan Pesisir Dalam Peningkatan Daya Saing Indonesia", (11 July 2019) C4. 80-89. prosidingseminakel.hangtuah.ac.id/index.php/jurnal/article/view/118

[3] SetyaBudi P.B., Chrismianto D., Rindo G., Analisa Nilai thrust dan Torque Propeller Tipe B-Series Pada Kapal Selam Midget 150m Dengan Variasi Skew Angle dan Blade Area Ratio (Ae/Ao) Menggunakan Metode CFD. Kapal: Journal of Marine Science and Technology Vol. 13 No. 3 (Oct 2016) pp. 109-117. DOI: https://doi.org/10.14710/kpl.v13i3.12352

[4] Report F., The Specialist Committee on Cavitation Erosion on Propellers and Appendages on High Powered / High Speed Ships Final Report and Recommendations to the 24th ITTC. II, (2004) 509–542.

[5] Risma D.R., Implementasi Penggunaan Aplikasi AutoCAD dalam Meningkatkan Kompetensi Dasar Menggambar teknik bagi Masyarakat. Briliant: Jurnal Riset dan Konseptual Vol. 3 No. 2 (May 2018) pp. 184-189. DOI:10.28926/briliant.v3i2.174

[6] Habibi, Nurhadi, Analisa Pemilihan Propeller Tipe B-Series Pada Kapal Feri Ro-Ro 600 GT dengan Menggunakan Aplikasi Matchpro Jurnal Wave Vol. 9 No. 2 (Dec 2016) pp. 75-81. DOI: 10.29122/jurnalwave.v10i2.2643

[7] Mustofa A., Jokosisworo S., Budi W.,A., Analisa Kekuatan Tarik, Kekuatan Lentur Putar dan Kekuatan Puntir Baja ST 41 sebagai Bahan Poros Baling-baling Kapal (Propeller Shaft) setelah Proses Quenching Jurnal Teknik Perkapalan Vol. 6 No. 1 (Jan 2018) pp. 199-206. ejournal3.undip.ac.id/index.php/naval/article/view/19940.

[8] Niam A,W., Hasanudin, Desain Kapal Ikan di Perairan Laut Selatan Malang, Jurnal Teknik ITS Vol. 6 No.2 (2017) G246-G251, DOI: 10.12962/j23373539.v6i2.26112

[9] Ahmad M., Habibie I., Nofrizal, Teknik Pemasangan Perangkat Mesin Kapal Perikanan, Jurnal Perikanan dan Kelautan 14,2 (2009) pp. 191-197.

[10] Putra A.G., Winarno A., Studi Pengaruh Variasi Bentuk Wave-Piercing Terhadap Hambatan Pada Kapal Katamaran Untuk Meningkatkan Efisiensi Pemakaian Bahan Bakar, Zona Laut: Jurnal Inovasi Sains dan Teknologi Kelautan Vol. 3 No.1 (2022) pp. 24-31.

[11] Winarno A., Ciptadi G., Iriany A., Widodo S.A., Experiment Study of the Resistance on Nusantara Ship Hull Modification with Fishing Boat in Pantura East Java, International Journal on Engineering Applications Vol. 11 No. 2 (2023) pp. 111–120.

[12] Winarno A., Ciptadi G., Iriany A., Widodo S.A., Experimental and Numerical Study of Ship Resistance on the Combination of Traditional Nusantara Fishing Vessel Hull Forms, International Review of Mechanical Engineering Vol. 17 No.4 (2023) pp. 190–196.

[13] Yunita N.D., Winarno A., Analisa Teknis Pengaruh Jumlah Sudu Propeller Bebas Putar Terhadap Gaya Dorong Kapal Tunda DPS IX, Seminar Nasional Kelautan XIV: Implementasi Hasil Riset Sumber Daya Laut dan Pesisir Dalam Peningkatan Daya Saing Indonesia (2019).

[14] Rozi F.M., Winarno A., Riyadi M., Pengaruh Variasi Jarak Poros Propeller Yang Berbeda Pada Kapal Ikan Tradisional KM. Sri Mulyo di Brondong Lamongan, Seminar Nasional Kelautan XIV: Implementasi Hasil Riset Sumber Daya Laut dan Pesisir Dalam Peningkatan Daya Saing Indonesia (2019)

[15] Hermawan R.A.M., Winarno A., Kajian Teknis Propeller Tipe B - Series Dan Kaplan Dengan Variasi Sudut Rake Pada Kapal Offshore Supply Vessel 80 (OSV 80), Zona Laut: Jurnal Inovasi Sains dan Teknologi Kelautan Vol. 4 No. 3 (2023) pp. 309-318.

[16] Winarno A., Widodo S.A., Ciptadi G., Iriany A., The Effect of Sail Layout on Fishing Vessels Hydrodynamics in the North Coast of Java using Computational Fluids Dynamic, Semarak Ilmu: CFD Letter Vol. 16 Issue. 1 (2024) pp. 107-120.

International Journal of Marine Engineering and Applications
Volume 1, Number 1, September 2024
e-ISSN: 3063-640X

Date of Received:
July 2, 2024

Date of Accepted:
August 4, 2024

Date of Published:
September 1, 2024
DOI: doi.org/10.30649/ijmea.v1i1.372

TECHNICAL ANALYSIS OF ENGINE PROPELLER MATCHING KRI X AFTER MAIN ENGINE REPOWERING

Imron Achmadi Fajar[1*], Miftakhul Jannah Dwi Ratna[2]

[1] Marine Water Resources Development Installation, Human Resource Development and Counseling Agency, Ministry of Maritime Affairs and Fisheries, 10110, Indonesia
[2] PT. Vinilon Jaya Sakti, 61353, Indonesia

*Corresponding Author: Iachmadifajar@gmail.com

ABSTRACT

The gas turbine, which is one of the main engines of KRI X, is not used anymore because of the amount of damaged material. In 2017, it was decided to replace its main engine. Ships that previously used gas turbines and two diesels as the main engines are replaced with four MTU diesel engines with 4000 HP power and 2100 rpm rotation per engine. With a fixed propeller and a power change on the main engine, the matching point of the main engine also changes. Referring to the problem, this study conducted an assessment of engine propeller matching obtained after repowering the main engine, by calculating the pricing of the ship and calculating the power required by the ship. The calculation of ship resistance is done in two ways: with the help of running software Maxsurf with the Holtrop method, and by using an empirical formula. Having known the price of the ship's resistance and power required, then calculated the speed of the ship with the new main engine and the variation of the pitch propeller. The result of this research obtained the operating point (matching point), which resulted in optimum speed obtained at the main rotation condition of 1974 rpm, propeller rotation 452,666 rpm, with 85% power loading that is 6152,426 kW, ship speed reached 17,855 Knot, and in this condition is deemed to be by the operation of the continuous service rating.

Keywords: Engine propeller matching, repowering, pitch propeller

Introduction

KRI X previously used a CODOG (Combined Diesel or Gas) model thruster system. But in 2009, the gas turbine, which is one of the main engines of this ship, was no longer used because of the many damaged materials. Due to the age of this ship, in 2017, it was decided that a complete overhaul of KRI X would be carried out due to material fatigue on the plates, buildings, and engines.

Due to the difficulty of obtaining spare parts, expensive maintenance costs, and wasteful fuel, the relevant parties finally decided to repower the main engine. The ship, which previously used one gas turbine and two diesels as main engines, was replaced with four MTU brand diesels and used the CODAD (Combined Diesel and Diesel) system.

With a fixed propeller and a change in the power of the main engine, the matching point of the main engine also changes. Referring to these problems, this study examines the engine propeller matching obtained after repowering the main engine by calculating the price of ship resistance in two ways, namely with the help of running Maxsurf software with the Holtrop method and calculations using empirical formulas. After knowing the price of ship resistance and the required power, the calculation of ship speed with the new main engine and variations in the magnitude of the propeller pitch are carried out. The object that will be used in this research is KRI X.

Methodology

a. Controllable Pitch Propeller

A controllable Pitch Propeller is a propeller whose pitch can be adjusted. Pitch is the axial distance traveled or taken by the propeller at one full rotation (3600). In general, the CPP system consists of several components:

1. A propeller hub with a blade whose pitch can be moved from full ahead to full astern.
2. Propeller shaft with oil distribution box.
3. Hydraulic system.
4. Remote control system

Its operation can be done with two systems, namely the pull-push rod system and the hub piston system. In the pull-push rod system, a long rod is used, which is connected from the ship's shaft to the propeller hub. In the hub piston system, the piston rod is placed on the propeller hub. The advantages of using a controllable pitch propeller, namely:

1. It can be used to accelerate, stop, and process ship movements properly.
2. The thrust force can be kept constant under changing load conditions.
3. It is economical for ships working at different speeds and load conditions.

The disadvantages of using a controllable pitch propeller namely:

1. CPP construction is quite complicated.
2. The price is relatively high.
3. Requires more attention in terms of maintenance than a regular propeller. This is due to the complexity of the hub construction and the hydraulic system.

b. Ship Resistance

According to Harvard (1992) [1], Ship resistance is the fluid force acting on the ship in such a way that it opposes the ship's motion. The total resistance itself is broken down into several different components that result from a variety of causes and interact with each other in a truly complex way.

The faster the movement of the ship, the greater the resistance it receives. So, to keep moving at its speed, the ship must be able to overcome these obstacles with the thrust generated by the performance of the propeller. Which thrust comes from the brake force (PB), which is the power released by the propulsion motor and is channeled to the ship's propeller and then converted into thrust (PT).

By using the Holtrop method, the total resistance of the ship can be obtained with the equation as follows:

$$RT = \frac{1}{2} x\ \rho\ x\ V^2\ x\ S_{tot}\ x\ (C_F(1+K)C_A) + \frac{R_W}{W}$$

c. Drive Motor Power

In general, a ship that moves in the water medium at a certain speed will experience a drag (resistance) that is opposite to the direction of motion of the ship. The amount of drag that occurs must be able to be overcome by the thrust of the ship (thrust) resulting from the work of the ship's propulsion device (propulsor). The power supplied (PD) to the ship's propulsion is derived from the shaft power (PS), while the shaft power itself comes from the brake power (PB), which is the output power of the ship's propulsion motor. Several notions of power are often used in estimating the power requirements of ship propulsion systems, among others:

- Effective Horse Power (EHP)

  Is the amount of power needed to overcome the drag force of the hull so that the ship can move from one place to another with a service speed of VS. This effective power is a function of the total drag and ship speed. To get the effective power of the ship, the following equation can be used:

  $$EHP = R_T\ x\ V_S$$

- Thrust Horse Power (THP)

  Is the amount of power generated by the work of the ship's propulsion device (propulsor) to push the ship's body. Thrust is a function of the thrust force and fluid flow rate that occur when the ship's propulsion device works. The equation. Thrust can be written as follows:

  $$THP = \frac{EHP}{\eta \mathrm{HULL}}$$

- Delivery Horse Power (DHP)

  Is the power absorbed by the ship's propeller to produce thrust of PT, or, in other words, PD, the power supplied by the propulsion motor to the propeller, which is then converted into the ship's thrust (PT).

  The variables that affect this power are the torque delivered and the propeller turn, so the equation for calculating PD is as follows:

  $$PD = 2\pi \text{ x } QD \text{ x } nP$$

- Shaft Power (Ps)

  The power is measured up to the area in front of the stern tube bearing of the ship's propulsion system. For ships powered by gas turbines, in general, the power used is PS. Meanwhile, the term brake power (PB) refers to the power generated by the main engine motor with a type of PS. motor (main engine) in marine diesel engines.

- Efficiency in ship propulsion systems

  Ship propulsion systems have several definitions of transmitted power, ranging from the power released by the propulsion motor to the power delivered by the ship's propulsion to the surrounding fluid. The ratio of these powers is often expressed by the term efficiency, although in some cases it is not a direct power conversion value. In assessing propulsion efficiency, other technical factors are taken into account due to the operation of the propeller and the shape of the ship, so that propulsion efficiency can be viewed from several aspects, namely:

  - Hull Efficiency ($\eta HULL$)

    It is the ratio between effective power (PE) and thrust (PT). Hull efficiency is a measure of the suitability of the hull design (stern) to the propulsor arrangement, so this efficiency is not a form of actual power conversion. So even though this Hull Efficiency value can be more than one, generally a number around 1.05 is taken.

    Calculations that are often used in obtaining hull efficiency are as follows:

    $$\eta\text{HULL} = \frac{(1-tt)}{(1-w)}$$

  - Propeller Efficiency (ηPROP)

    It is the ratio between the thrust (PT) and the power supplied (PD). This efficiency is power conversion, and the difference in value that occurs is located where the propeller torque measurement is carried out. Specifically, whether in open water conditions (Q0) or conditions behind the ship (QD), the following equation shows both conditions of propeller efficiency, as follows:

    Efficiency propeller of open water

    $$\eta_0 = \frac{T\ x\ V_A}{2\ x\ \pi\ x\ Q_0\ x\ n}$$

    The efficiency propeller behind the ship

    $$\eta_B = \frac{P_T}{P_D} = \frac{T\ x\ V_A}{2\ x\ \pi\ x\ Q_0\ x\ n}$$

    Because there are two conditions, an efficiency ratio appears, known as Relative-Rotative Efficiency, $\eta\eta RR$, which is a comparison between the Propeller Efficiency in conditions behind the ship with the Propeller Efficiency in conditions in open water, as follows:

    $$\eta_{RR} = \frac{\eta_B}{\eta_0} = \frac{T\ x\ {V_A}/{2}\ x\ \pi\ x\ Q_D\ x\ n}{T\ x\ {V_A}/{2}\ x\ \pi\ x\ Q_D\ x\ n} = \frac{Q_0}{Q_D}$$

    Therefore, ηRR is not a property of the actual efficiency (not a power conversion). This efficiency is only a comparison of different efficiency values. So, the magnitude of relative rotative efficiency can also be greater than one, but generally, the value is taken to be around one.

  - Shaft Transmission Efficiency (ηS)

    Shaft Transmission Efficiency, ηS, can generally be defined mechanically with more than one type of efficiency, which is highly dependent on the configuration of the stern arrangement. This efficiency is the product of the overall efficiency of each component installed. Efficiency can be expressed as an equation, as follows:

    $$\eta_S = \frac{P_D}{P_S}$$

  - Overall Efficiency (ηP)

    Also known as propulsive efficiency, or propulsive coefficient, is the result of the overall efficiency of each power phase that occurs in the ship's propulsion system. The overall efficiency can be obtained with the equation as follows:

    $$\eta_P = \frac{P_E}{P_T} x \frac{P_T}{P_D} x \frac{P_D}{P_S} = \eta\text{HULL x } \eta_B\ x\ \eta_S$$

    $$= \eta\text{HULL}\ x\ \eta_0\ x\ \eta_{RR}\ x\ \eta_S$$

- Installed Motor Power

According to S. W. Adji (2005) [2], the ship propulsion motor power (PB) in question is brake power, or power received by the transmission shaft of the ship propulsion system (PS), which is then operated continuously to move the ship at its service speed (VS). If the amount of mechanical efficiency in the gearbox arrangement, which serves to reduce and reverse the rotation of the drive motor, is 98 percent, Then the driving motor power ship can be calculated, as shown in the equation below:

$$P_B - CSR = \frac{P_S}{0{,}98}$$

The power on the PB-MCR can then be used as a reference in carrying out the drive motor selection process (Engine Selection Process).

- Hull and Propeller Characteristics

According to S. W. Adji (2005) [2], one of the most influential stages in carrying out the engine-propeller matching analysis process is the modeling stage of the characteristics of the designed or observed ship body. This is because the characteristics of the ship's body have a direct effect on the characteristics of the propeller.

❖ Characteristics of Ship Propellers

In general, the characteristics of ship propellers under open water test conditions are as represented in Diagrams KT- KQ - J. Each type of ship propeller has different performance curve characteristics. So, the study of the characteristics of ship propellers cannot be generalized for the entire shape or type of propeller. The equation model for propeller characteristics is as follows:

$$K_T = \frac{T_{prop}}{\rho \; x \; n^2 \; x \; D^4}$$

$$K_Q = \frac{Q_{prop}}{\rho \; x \; n^2 \; x \; D^5}$$

$$J = \frac{V_A}{n \; x \; D}$$

$$\eta_O = \frac{J \; x \; K_T}{2\pi \; x \; K_Q}$$

❖ Hull-Propeller Interaction

Hull and Propeller Interaction is an on-paper approach to efforts to obtain the performance characteristics of the propeller when operating in behind-the-ship conditions. The method is to process the equation as follows:

$$T_{SHIP} = \frac{\alpha \, V_A^2}{(1-t)(1-w)^2}$$

$$T_{prop} = K_T \; x \; \rho \; x \; n^2 \; x \; D^4$$

$$\mathbf{T_{Ship} = T_{Prop}}$$

$$K_T = \frac{\alpha \, V_A^2}{(1-t)(1-w)^2 \; \rho \; n^2 \; D^4}$$

$$\beta = {}^{\alpha}/_{(1-t)(1-w)^2 \rho D^2} \; \ldots\ldots\ldots (2.84)$$

Then it becomes,

$$K_T = \beta \; x \; \frac{V_A^2}{n^2 D^2}$$

So that the equational relationship is obtained as follows:

$$K_T = \beta \; x \; J^2$$

The next step is to make a 'tabulation'. The "J" price is taken from the open water test diagram of the propeller that will be used on the ship, which is from the lowest number, moving gradually to the highest number. Then, the tabulated results are plotted on the open-water test diagram of the propeller, as illustrated in the figures below. illustrated in the following figures below.

$$\beta = {}^{\alpha}/_{(1-t)(1-w)^2 \rho D^2}$$

Then it becomes,

$$K_T = \beta \; x \; \frac{V_A^2}{n^2 D^2}$$

So that the equation relationship is obtained as follows:

$$K_T = \beta \; x \; J^2$$

❖ Propeller Load Characteristics

In developing the 'trend' propeller load characteristics, the variables involved are propeller torque and propeller speed. For propeller torque is the result of graphically processed from the hull & propeller interaction, namely KQ and KQ-SM, which are then developed as the equation below:

$$Q_{Prop} = K_Q \times \rho \times n^2 \times D^5$$

$$Q_{Prop} = K_{Q-SM} \times \rho \times n^2 \times D^5$$

From the two equations above, the characteristic trend of propeller power (∞ Propeller Load) can be obtained as follows:

[Power] = [Torque] * [Speed]

The next step is to tabulate the trend of propeller power characteristics with the inputs of "propeller speed," which is obtained from "engine speed" after being reduced by mechanical gears (note the gear ratio). The figure below illustrates the tabulation and trend of the propeller power developed.

- Drive Motor Characteristics Ship

The method of combustion and atomizing of fuel in diesel motors is not the same as in gasoline motors. In gasoline motors, a mixture of fuel and air through the carburetor is put into the cylinder and burned by an electric flame from the spark plug. In diesel motors, which are sucked by the piston and put into the combustion chamber, only air is compressed until it reaches a high temperature and pressure. A few moments before the piston reaches the top dead point (TMA), diesel fuel is injected into the combustion chamber. With a high enough temperature and air pressure in the cylinder, the fuel particles will ignite by themselves to form a combustion process. For the diesel fuel to burn itself, it must have a compression ratio of 15–22 and an air temperature of approximately 600ºC.

- Combination of Engine and Propeller Characteristics

Matching Point According to S. W. Adji (2005) [2], the operating point of the ship's propulsion motor rotation (engine speed) is such that it matches the character of the propeller load, namely the operating point of the motor rotation, where the power absorbed by the propeller is equal to the power produced by the engine and produces a ship speed that is close to (the same) as the planned ship service speed. Propeller characteristics are as shown in Figure 2.6, while engine characteristics are represented in Figure 2.9. To be able to equate the two trendlines into the same plotting means, first, the price of the two trendlines is expressed in a percentage (%). At engine speed, n is the operating point of the propulsion motor rotation that corresponds to the propeller load condition, because the power generated by the propulsion motor is equal to the power absorbed by the propeller. This will certainly provide optimal consequences for the use of fuel consumption by the propulsion motor of the ship against the desired service speed of the ship.

Result and Discussion

a. Calculating Ship Resistance

Of the two methods used to get the value of the total resistance of the ship, the results obtained are:

1. Determining the value of ship resistance with help from Maxsurf software, 64-bit resistance resulted in a total resistance of 265.1 kN.
2. Calculation of the ship resistance value with an empirical formula resulted in a total resistance value of 286.375 kN.

b. Calculation of KT, KQ, J

The next step after calculating the value of ship resistance is to get the values of KT, KQ, and J. Where KT is the thrust coefficient, KQ is the torque coefficient, and J is the advance coefficient. The first step is to use interpolation taken from the open-water test propeller diagram. The second, by calculating the value of the thrust coefficient during trial conditions (KT-trial) and the thrust coefficient during service conditions (KT-SM). when service conditions (KT-SM).

- Open water test propeller KT - KQ - J value

It can be seen that the pitch ratio (P/D) value on the controllable pitch propeller can change, but it is still one type of propeller (B.5-75). By looking at the Wageningen B-Screw series propeller open-water test diagram, a table is made showing the KT-KQ-J value interpolated from the open-water test propeller diagram with a pitch ratio value variation from 0.6 to 1.21 with an increase of 0.1 per level of variation, as shown in tables 4.3 to 4.9, respectively. After obtaining the KT - KQ - J value, a graph is made showing the value of the open water test propeller diagram tabulation, which is shown in Figures 4.10 to 4.16, respectively.

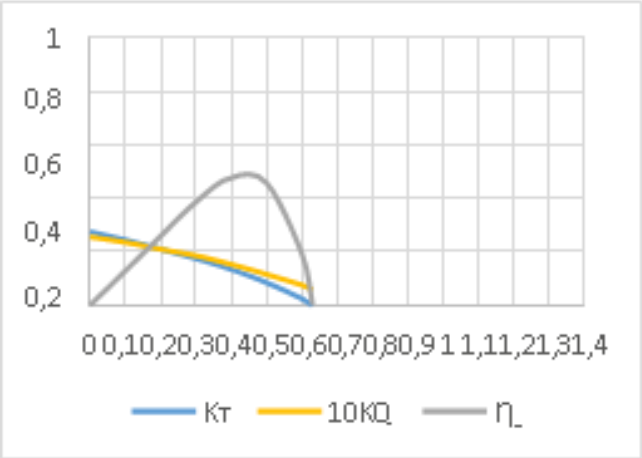

Figure 1. Graph of Openwater Test Propeller at P/D 0.6

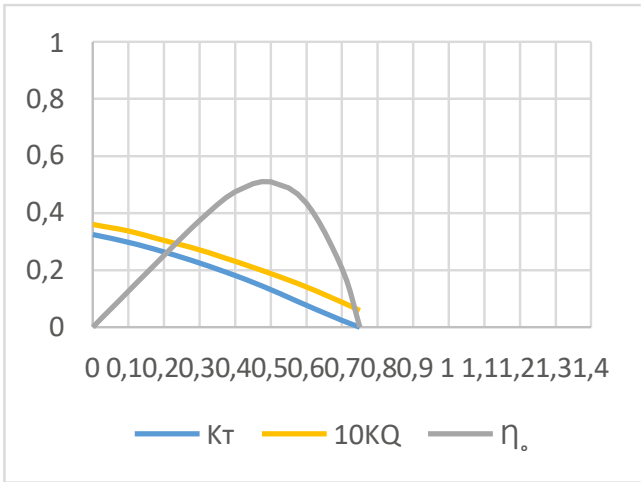

Figure 2. Graph of Openwater Test Propeller at P/D 0.7

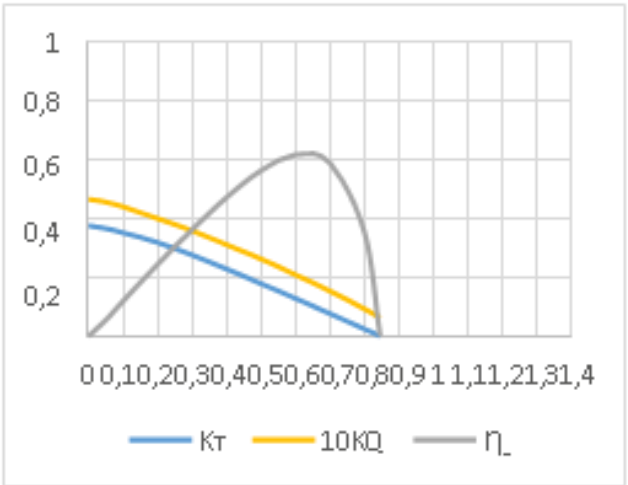

Figure 3. Graph of Openwater Test Propeller at P/D 0.8

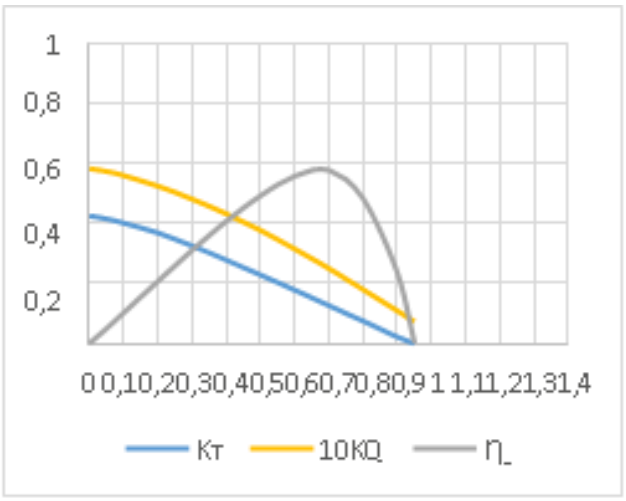

Figure 4. Graph of Openwater Test Propeller at P/D 0.9

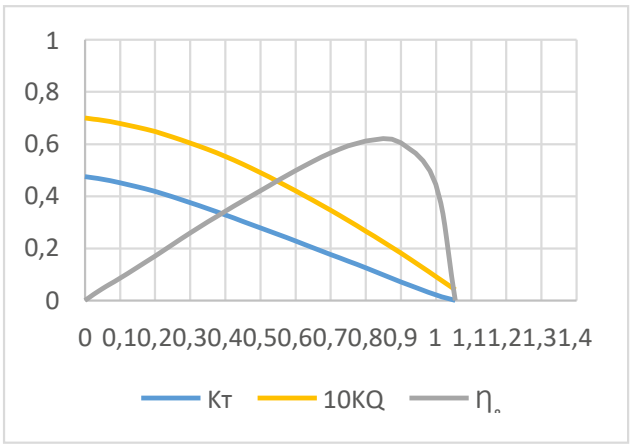

Figure 5. Graph of Openwater Test Propeller at P/D 1.0

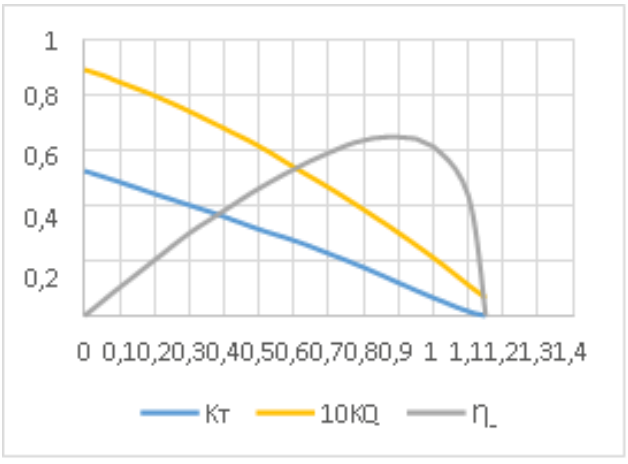

Figure 6. Graph of Openwater Test Propeller at P/D 1.1

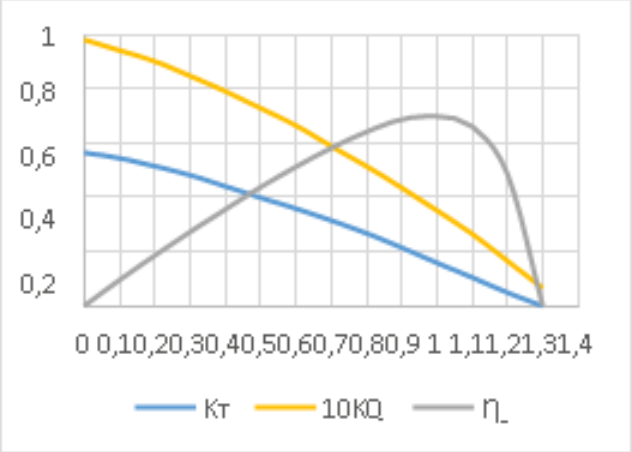

Figure 7. Graph of Openwater Test Propeller at P/D 1.2

- Calculation of KT-trial and KT-SM Values

  The calculation of the thrust coefficient value is carried out under trial conditions (KT-trial) and service margin conditions (KT-SM). By using equations 2.86 and 2.87, the KT and KT-SM values are obtained:

$$KT = \beta \; x \; J^2$$
$$= \frac{\alpha}{(1-t)(1-w)^2 \; x \; \rho \; x \; D^2} x \; J^2$$
$$= 1{,}274 \; x \; J^2$$
$$K_{T-SM=120\% \; x \; \beta \; x \; J^2}$$
$$= 120\% \; x \; 1{,}274 \; x \; J^2$$

The next step is to calculate the value of KT and KT-SM by varying the advanced coefficient (J). The J value is taken from the open-water test propeller diagram, which moves from the lowest number to the highest number. Then the results of the tabulation of the KT and KT-SM values are plotted in a graph that shows the trendline of the thrust trial condition coefficient (KT) and the thrust service margin coefficient (KT-SM), as shown in Figure 8.

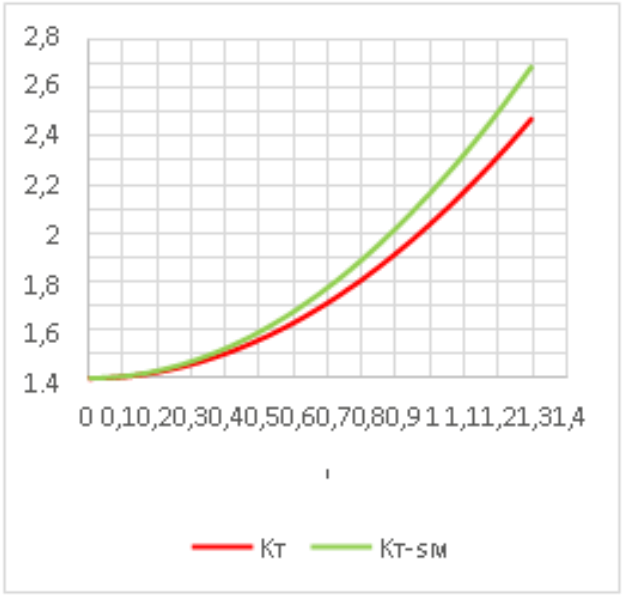

Figure 8. Graph KT-trial and KT-SM

From the graph above, the trendlines of the trial condition thrust coefficient (KT) and service margin thrust coefficient (KT-SM) can be seen. The greater the value of the advanced coefficient (J), the higher the value of KT and KT-SM.

- Relationship graph of KT, KQ, J, and ηo

  To determine the relationship between KT, KQ, J, and ηo, obtained from the intersection of the KT and KT-SM graphs and the open-water test propeller graph with variations in pitch ratio (P/D), the next step is to determine the intersection point between the KT open-water test propeller curve and the KT-SM curve. After obtaining the intersection point, a vertical line is drawn until it intersects the KQ curve. After that, a horizontal line is drawn from the KQ curve, and the value of the torque coefficient (KQ) is obtained. The same steps are also carried out on the KT curve of the open-water test propeller, and the KT curve in the trial conditions is shown in Figures 9 to 15, respectively.

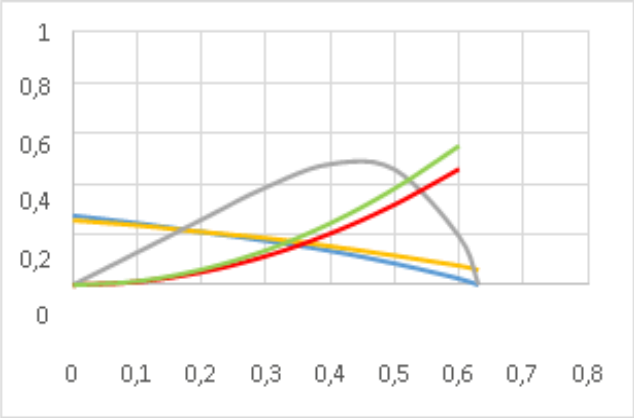

Figure 9. Openwater Test Propeller at P/D 0,6

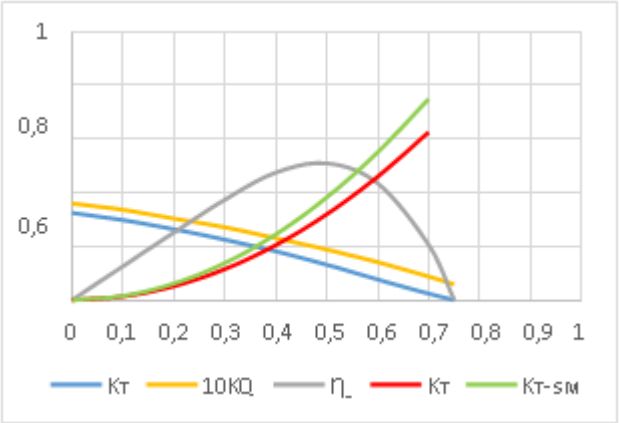

Figure 10. Openwater Test Propeller at P/D 0,7

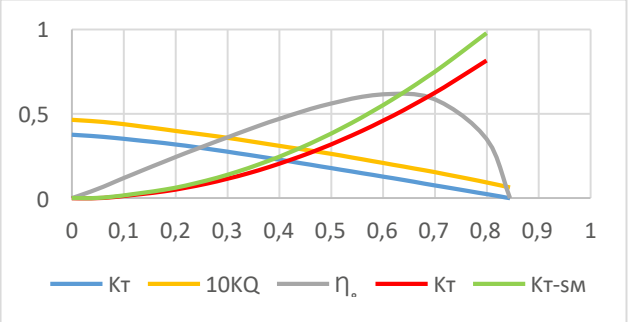

Figure 11. Openwater Test Propeller at P/D 0,8

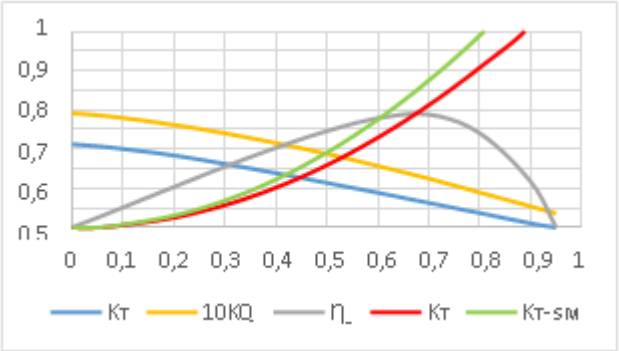

Figure 12. Openwater Test Propeller at P/D 0,9

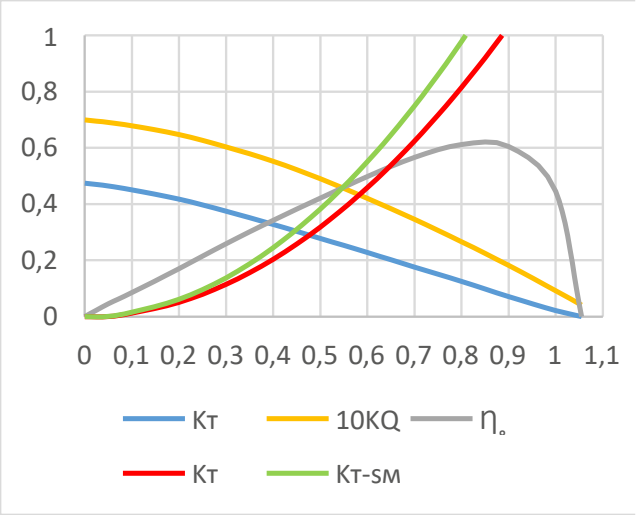

Figure 13. Openwater Test Propeller at P/D 1.0

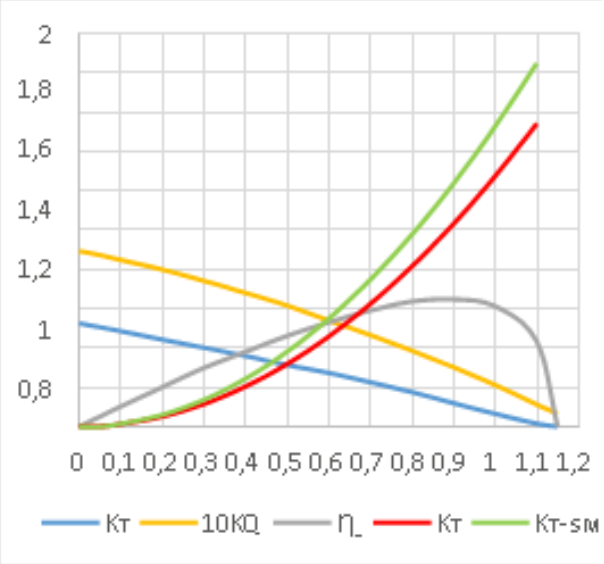

Figure 14. Openwater Test Propeller at P/D 1.1

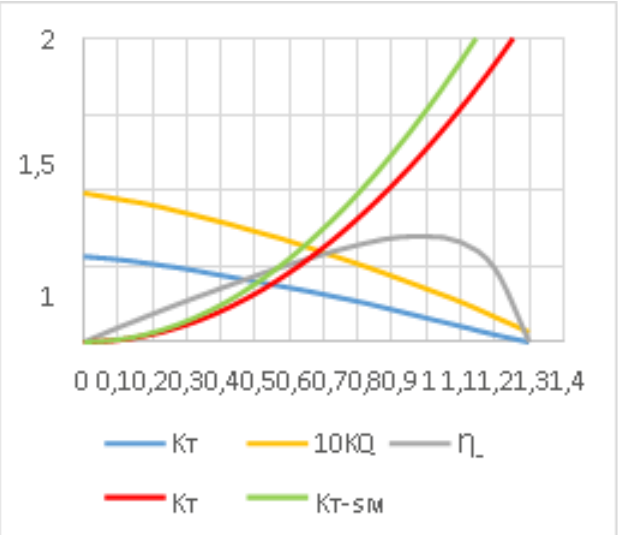

Figure 15. Openwater Test Propeller at P/D 1.2

From the intersection of the KT and KT-SM graphs with the open-water test propeller graph shown in Figures 9 to 15, the obtained torque coefficient (KQ) data on trial and service conditions are presented in Table 1.

c. Engine Power Calculation

By knowing the values of J and KQ above, it can be calculated the amount of torque (Q), power (DHP), and BHP produced by the propeller using the equation that has been mentioned. The next step is to tabulate the results of the equation with variations in engine rpm, as shown in Tables 4.12 and 4.13. Then, the tabulated results are made into a graph showing the relationship between power (BHP) and engine RPM, as shown in Figure 16.

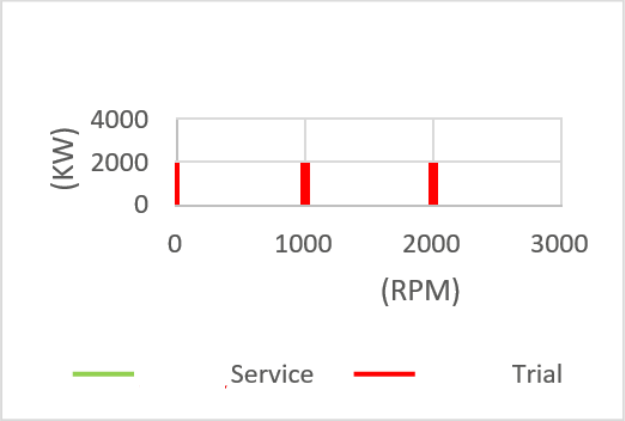

Figure 16. Graph of Power Relationship with Engine RPM

From the graph of the relationship between power and engine rpm above, it can be seen that the greater the engine speed, the higher the power. In other words, engine speed is proportional to the value of the power produced.

d. Matching Point

Because of the difference between engine speed and propeller speed, the matching process assumes that the magnitude of engine speed is equal to propeller speed, or that 100% engine speed is equal to 100% propeller speed. To plot the propeller load curve in the working area of the main engine, the curve is the amount of engine speed and propeller rotation expressed on the abscissa axis of the curve, expressed in percentage scale (%) [3]. The results of depicting the propeller curve into the main engine characteristics are shown in Figure 17, and after the matching points are found, each of these points is analyzed to find out: Motor power, engine speed, propeller speed, and propeller load. Ship speed achieved from the graph above, several matching points are obtained between the old propeller and the new main engine after repowering, as follows:

Titik	Kondisi	Rpm *Engine*	Rpm *Propeller*	% Rpm	% Daya	Daya (kW)	Vs
A	*Service* CSR	1974	452,666	94	85	3076,213	17,855
B	*Trial* CSR	1911	438,666	91	85	3076,213	17,461
C	*Service* MCR	2100	466,666	100	98	3925,158	20,582
D	*Trial* MCR	2100	466,666	100	92	3684,843	20,122

Figure 17. Matching point result

From the matching points that have been obtained, which are analyzed only under service conditions and are expressed as follows:

1. Point A is the propeller load point at 3076.213 kW, or 85% (service rating), with a propeller rotation of 452.666 rpm. Produces a speed of 8.927 knots, which corresponds to the speed in free-running conditions. In this condition, the matching point is in the engine envelope working area. So, this condition is considered safe for continuous service rating (CSR) operations.
2. Point C is the propeller load point at 3925.158 kW, or 85% (service rating), with a propeller rotation of 466.666 rpm. Resulting in a speed of 10.291 knots. In this condition, the matching point is in the maximum working area of the engine envelope. Therefore, this condition is only permitted during sea trials.

Conclusion

Based on the analysis and discussion, The matching point obtained after repowering the main engine between the old propeller and the new main engine on KRI X which produces the optimum speed of two engines and one propeller is obtained under the condition that the main engine rotation is 1974 rpm, the propeller rotation is 452.666 rpm reaching 94% of its maximum rotation, with a power loading of 85% which is 6152.426 kW, the ship's speed reaches 17.855 Knots, in this condition it is considered by the continuous service rating operation and by the desired speed. This thesis can be developed by conducting further studies on the re-planning of the engine mount construction due to changes in the main engine dimensions.

References

[1] Harvald, Sv, Aa. Tahanan dan Propulsi Kapal. Surabaya: Airlangga University Press, 1992.
[2] S. W. Adji. Engine Propeller Matching. 2005.

[3] A. Khanif Firdianto. Analisa Teknis Pengaruh Kecepatan Pada Kapal KMP. Sms, Swakaya Setelah Dilakukan Penambahan Dek [Skripsi]. Surabaya: Universitas Hang Tuah Surabaya, 2017.

[4] Alfan Dicky Firmansyah, Agoes Santoso, dan Edy Djatmiko. Perancangan Controllable Pitch Propeller pada Kapal Offshore Patroli Vessel 80 (OPV80). Jurnal Teknik Its Vol. 1, No. 1, ISSN: 2301-9271, 2012.

[5] Frederico SC, dan Wibowo H.N. Kajian Unjuk Kerja Mesin Induk Kapal Cepat Pascar Re-Powering. Surabaya., 2005.

[6] Hartono Yudo. Engine Matching Propeller Pada Kapal Untuk Mendapatkan Optimalisasi Pemakaian Mesin Penggerak Kapal Dan Baling – Baling Sebagai Alat Pendorong Kapal [Skripsi]. Semarang: Prodi Teknik Perkapalan FT-Universitas Diponegoro.

[7] Satria Perdana Sakti. Analisa Pemilihan P/D Ratio Propeller Jenis CPP Pada Kapal Dengan Shaft Generator Akibat Variasi Kecepatan Kapal [Skripsi].

[8] Untung Budiarto, dan M. Abdurrohman Raup. 2011. Engine Matching Propeller Pada Kapal Mt. Nusantara Shipping Line IV Akibat Pergantian Sistim Propulsi. KAPAL- Vol. 8, no.1. pp 24-28.

[9] Yoga Febrianto. 2017. Engine Propeller Matching Pada Kapal Tunda DPS IX Dengan Mesin Induk CUMMINS NTA855-M [Skripsi]. Surabaya: Universitas Hang Tuah Surabaya.

[10] Putra A.G., Winarno A., Studi Pengaruh Variasi Bentuk Wave-Piercing Terhadap Hambatan Pada Kapal Katamaran Untuk Meningkatkan Efisiensi Pemakaian Bahan Bakar, Zona Laut: Jurnal Inovasi Sains dan Teknologi Kelautan Vol. 3 No.1 (2022) pp. 24-31.

[11] Winarno A., Ciptadi G., Iriany A., Widodo S.A., Experiment Study of the Resistance on Nusantara Ship Hull Modification with Fishing Boat in Pantura East Java, International Journal on Engineering Applications Vol. 11 No. 2 (2023) pp. 111–120.

[12] Winarno A., Ciptadi G., Iriany A., Widodo S.A., Experimental and Numerical Study of Ship Resistance on the Combination of Traditional Nusantara Fishing Vessel Hull Forms, International Review of Mechanical Engineering Vol. 17 No.4 (2023) pp. 190–196.

[13] Yunita N.D., Winarno A., Analisa Teknis Pengaruh Jumlah Sudu Propeller Bebas Putar Terhadap Gaya Dorong Kapal Tunda DPS IX, Seminar Nasional Kelautan XIV: Implementasi Hasil Riset Sumber Daya Laut dan Pesisir Dalam Peningkatan Daya Saing Indonesia (2019).

[14] Rozi F.M., Winarno A., Riyadi M., Pengaruh Variasi Jarak Poros Propeller Yang Berbeda Pada Kapal Ikan Tradisional KM. Sri Mulyo di Brondong Lamongan, Seminar Nasional Kelautan XIV: Implementasi Hasil Riset Sumber Daya Laut dan Pesisir Dalam Peningkatan Daya Saing Indonesia (2019)

[15] Hermawan R.A.M., Winarno A., Kajian Teknis Propeller Tipe B - Series Dan Kaplan Dengan Variasi Sudut Rake Pada Kapal Offshore Supply Vessel 80 (OSV 80), Zona Laut: Jurnal Inovasi Sains dan Teknologi Kelautan Vol. 4 No. 3 (2023) pp. 309-318.

[16] Winarno A., Widodo S.A., Ciptadi G., Iriany A., The Effect of Sail Layout on Fishing Vessels Hydrodynamics in the North Coast of Java using Computational Fluids Dynamic, Semarak Ilmu: CFD Letter Vol. 16 Issue. 1 (2024) pp. 107-120.

International Journal of Marine Engineering and Applications
Volume 1, Number 1, September 2024
e-ISSN: 3063-640X

Date of Received:
June 27, 2024

Date of Accepted:
July 4, 2024

Date of Published:
September 1, 2024
DOI: doi.org/10.30649/ijmea.v1i1.370

THE EFFECT OF FLUID FLOW RATE ON THE CORROSION RATE OF THE PIPE OF SEAWATER SYSTEM

Kriyo Sambodho[1*] Kurnia Kusherminto Priyo Pratomo[2*]

[1] Ocean Engineering 1, Sepuluh Nopember Institute of Technology, Surabaya, Indonesia
[2] Nissandi Kompresindo, Cilegon, Indonesia
*Corresponding Author: kriyosambodho@gmail.com

ABSTRACT

Corrosion is a process of decreasing the quality of a material because it reacts with the environment. The corrosion process takes place spontaneously and is a natural event that cannot be avoided. This research was carried out to determine the relationship between the fluid flow rate of seawater flowing in the channels of API 5L grade B standard galvanized pipe and seamless pipe specimens on the corrosion rate using flow modeling for 4 months. The research variations used were variations in flow rate, namely 50%, 75%, and 100%. Corroded pipe specimens were cleaned, weighed, and photomicrography. From this research, it was found that the higher the flow rate, the higher the corrosion rate that occurs, and the corrosion that occurs is abrasion corrosion and pitting corrosion.

Keywords: Abrasion corrosion, corrosion rate, erosion corrosion, galvanized and seamless pipe

Introduction

Corrosion is an event that reduces the quality of metal materials due to interaction with the environment [1]. The operation of a large ship is always equipped with a cooling system and a ship balancing system with fluid using seawater, so a piping system is needed to circulate the cooling fluid [2]. The flow rate of a corrosive fluid can initially increase the corrosion rate by bringing a lot of oxygen to the surface of the material. At high speeds, only a few oxygen ions can reach the surface of the material, resulting in a slowdown in the corrosion rate. If this happens, the corrosion rate will decrease after the initial increase. On the other hand, high flow rates can also increase the rate of corrosion by damaging the protective layer or causing mechanical damage [3].

Since there is no discussion regarding the relationship between the rate of seawater fluid flowing in steel pipes and the rate of corrosion in steel pipes transmitting seawater, for this reason, the author examines this relationship.

Corrosion comes from the Latin word "Corrodere," which means metal destruction or rust due to the environment [4]. Corrosion is a process of degradation/deterioration/destruction of materials caused by chemical, physical, and biological environmental influences [5]. The corrosion mechanism cannot be separated from electrochemical reactions, which involve the transfer of electrons as a result of reduction-oxidation (redox) reactions. The main elements of corrosion are anode, cathode, electrolyte, and conducting medium [6].

Factors that influence corrosion:

1. Material factors, including material purity, material structure, crystal form, material trace elements, and material mixing techniques.
2. Environmental factors, including the level of air pollution, temperature, humidity, and the presence of corrosive substances.

3. Electrical factors that influence metal elements in chemical processes that will produce corrosion.

Erosive corrosion or abrasion is a combination of corrosive fluids and high flow speeds. Erosive corrosion occurs because erosion and corrosion support each other [7]. Erosive corrosion can also be caused by impingement corrosion as a result of very fast fluid speeds and eroding the protective layer on the metal. Damage to pipes in systems that use seawater caused by corrosion can cause various bigger problems, both in construction, such as ship hulls or other marine construction, and in systems on ships, including engines that use seawater cooling, which is very dependent on pipe resistance to corrosion [8].

Methodology

This study used flow rate variations of 0%, 50%, 75%, and 100% for 4 months. Each treatment is marked with the type of pipe, valve opening size, and test duration. For example: PG.075.04, which means PG for galvanized pipe and PN for seamless pipe, 075 is the size of the valve opening, and 04 is the length of the month of testing.

a. Specimen

The specimens used are galvanized pipe and seamless pipe standard API 5L grade B, NPS ¾ inch, SCH 40.

b. Test equipment

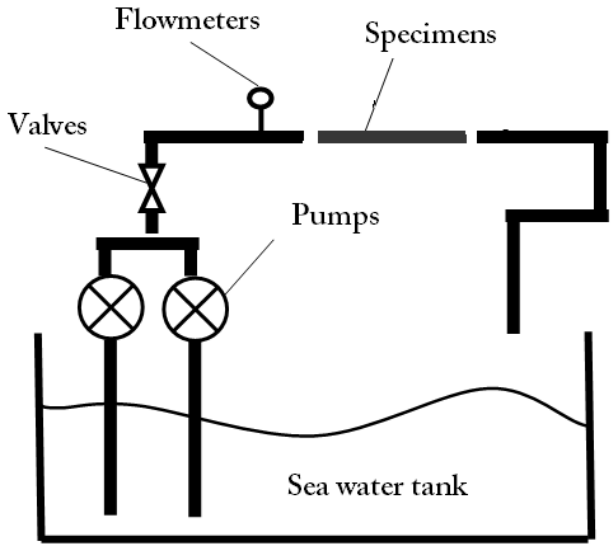

Figure 1. The side view of the scheme of corrosion test equipment

c. Fluid Flow Calculations

Flow rate:

$$V = \frac{Q}{A}$$

where:

V: flow rate (m^2/sec)
Q: flow rate (m^3/sec)
A: surface area (m^2)

Reynolds number:

$$\mathrm{Re} = \frac{VxD}{\nu}$$

where:

V: flow speed (m^2/sec)
D: pipe diameter (mm)
v: viscosity of water
- Re < 2300, laminar flow
- 2300 < Re < 4000, transition flow
- Re > 4000, turbulent flow

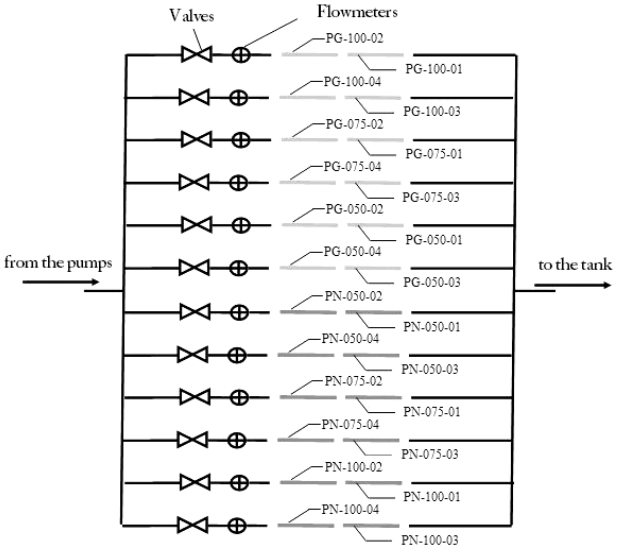

Figure 2. The top view of the scheme of corrosion test equipment

d. Corrosion Rate Calculation

The corrosion rate in this study is defined as the increase in the amount (weight) of corrosion that occurs as a function of time. Measurement of the weight of corrosion that occurs is carried out by cleaning the corroded specimen until it is clean, then weighing it. The weighing results are used to reduce the initial weight of the specimen before the experiment.

Corrosion weight = initial weight – final weight

$$\% \text{ corrosion } = \frac{\text{corrosion weight}}{\text{intitial weight}} \times 100\% \quad [1]$$

e. Metallography

Metallographic observations are carried out to determine the microstructure of the test specimen; in this case, micrographic observations are carried out.

f. Micrographic Photo Observation Process

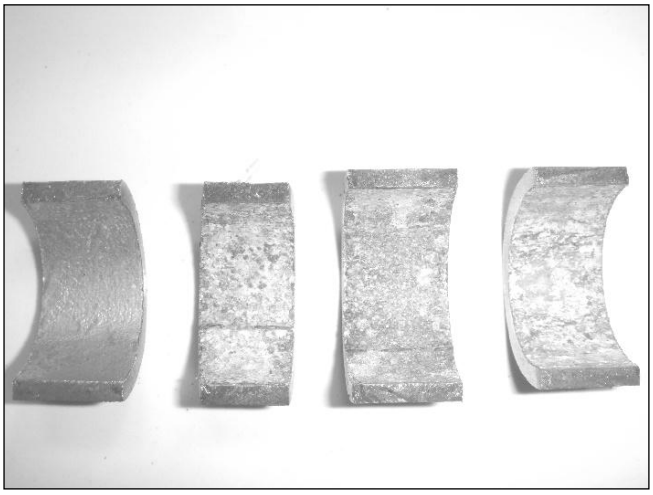

Figure 3. Specimen section for micro photos

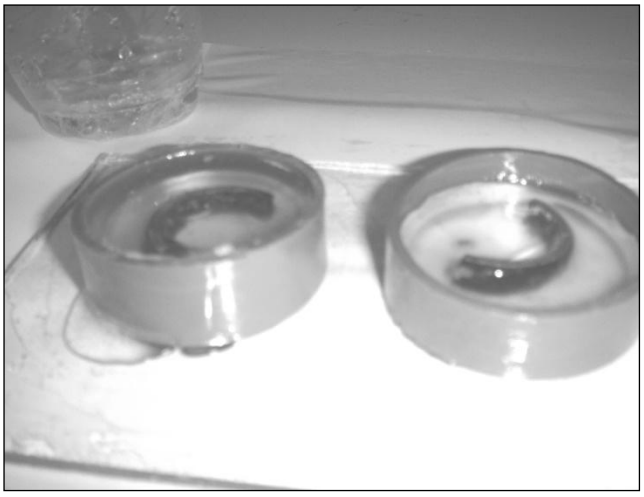

Figure 4. Fiber printing process

Figure 5. Material polishing

Figure 6. Polishing results

Figure 7. Micrography process

Result and Discussion

a. Corrosion Rate

Using the method described previously, the necessary data and calculations are carried out to obtain the corrosion rate, both on galvanized and non-galvanized pipes, with variations in seawater fluid flow rates, which are regulated by valve openings. The research results are presented and explained in the following tables, figures, and descriptions

Table 1. Data on dissolved content in the seawater fluid used Data on dissolved content in the seawater fluid used

No.	Type of analysis	Content
1.	Salinity	29,45 ‰
2.	Chlorinity	16,3 ‰
3.	pH	7,6
4.	Dissolved O_2	1,76 mlO_2/lt

Table 2. Data from the testing results of pipe material composition

No.	Type of Pipes	Content (%)				
		Fe	Mn	Ni	Si	Zn
1.	Galvanized	93.85	0.19	0.01	0.03	4.96
2.	Non-Galvanized	99.80	0.16	-	0.01	-

Table 3. Data on the percentage of galvanized pipe corrosion

		Flow rate (valve opening)		
		50%	75%	100%
Corrosion Rate after:	1 month	0.02%	0.03%	0.05%
	2 months	0.07%	0.09%	0.15%
	3 months	0.14%	0.22%	0.24%
	4 months	0.23%	0.57%	0.85%

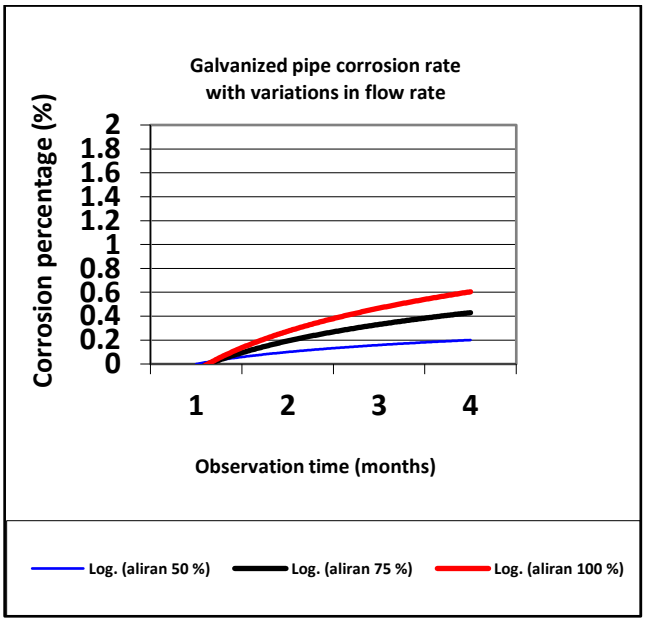

Figure 8. Comparison of corrosion rate with variations in fluid flow rate in the galvanized pipes

Figure 8 shows a comparison between the corrosion rates that occur between each flow rate, where the corrosion rate of galvanized pipe at a flow rate of 100% occupies the highest position, followed by a flow rate of 75% and a flow rate of 50%, or in other words the more The higher the flow rate through the galvanized pipe, the greater the rate of corrosion that occurs in the pipe.

Table 3. Data on the percentage of non-galvanized pipe corrosion

		Flow rate (valve opening)		
		50%	75%	100%
Corrosion Rate after:	1 month	0.47%	0.49%	0.52%
	2 months	1.39%	1.36%	1.50%
	3 months	2.63%	2.84%	3.18%
	4 months	4.52%	5.02%	5.11%

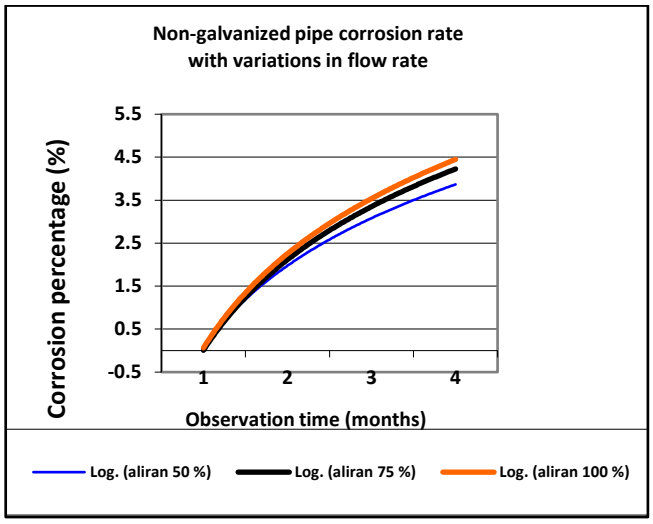

Figure 9. Comparison of corrosion rate with variations in fluid flow rate in the non-galvanized pipes

Figure 9 shows a comparison between the corrosion rates that occur between each flow rate, where the corrosion rate of non-galvanized pipe at a flow rate of 100% occupies the highest position, followed by a flow rate of 75% and a flow rate of 50%, or in other words the more The higher the flow rate through the galvanized pipe, the greater the rate of corrosion that occurs in the pipe.

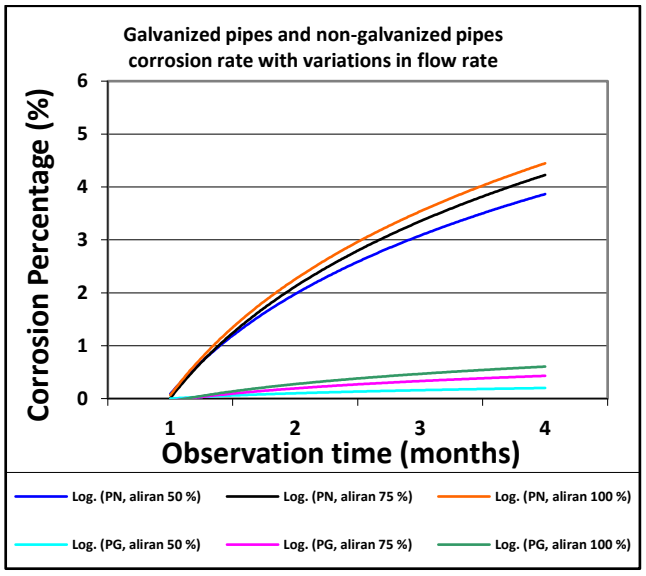

Figure 10. Comparison of corrosion rate with variations in fluid flow rate for galvanized and non-galvanized pipes

From 10, it can be seen that, for both galvanized and non-galvanized pipes, the fluid flow rate influences the pipe corrosion rate. The higher the fluid flow rate in the pipe, the higher the rate of corrosion in the pipe. The corrosion rate due to fluid flow in non-galvanized pipes is higher than the corrosion rate in galvanized pipes for the same fluid flow rate.

b. Microstructure Observations

Observation of the microstructure of pipes, both galvanized pipes and non-galvanized pipes, is carried out by carrying out micrographic observations, which is one of the metallographic observation methods.

Observations were made on each variation of the specimen after being subjected to corrosion testing. The aim is to find out whether corrosion also occurs on the inside of the pipe or only in the part exposed to the fluid flow of seawater. This will help in determining the type of corrosion that occurred on the specimen. The final goal is to determine the protection or protection against corrosion that will occur in pipes in systems that use seawater.

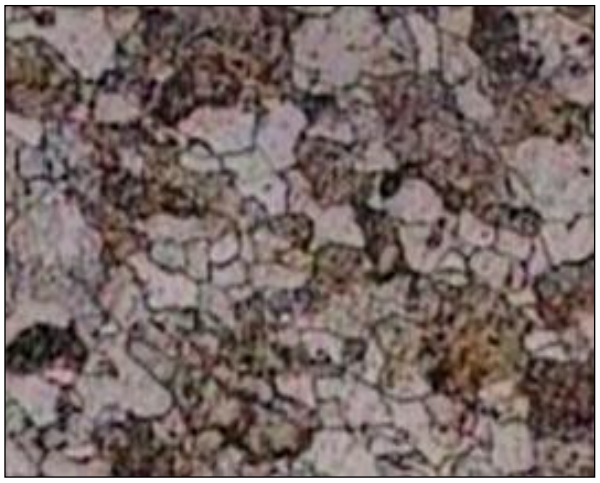

(a)

(b)

Figure 11. Photo of the microstructure of the galvanized pipe specimen before the corrosion

test, (a) 100x magnification, (b) 500x magnification

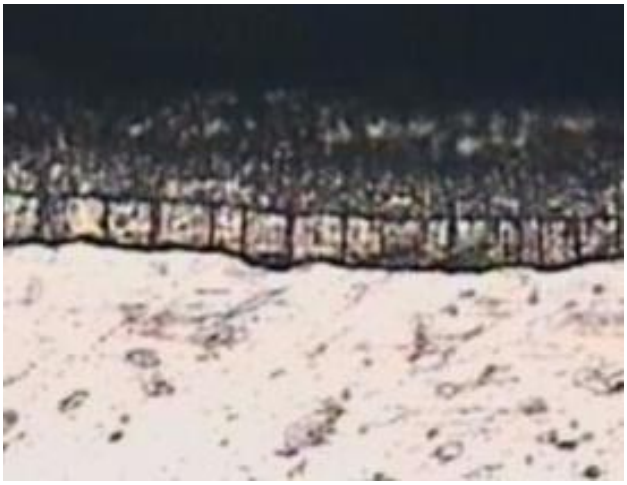

(a)

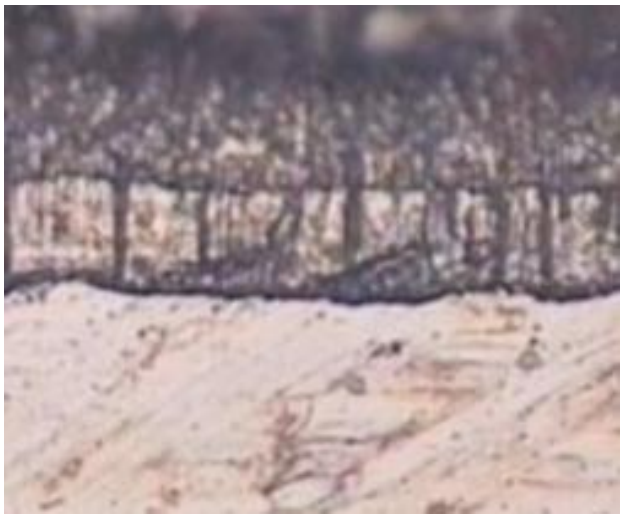

(b)

Figure 12. Photo of the microstructure of the galvanized pipe specimen, with a fluid flow rate of 0%, (a) 50x magnification, (b) 200x magnification

(a)

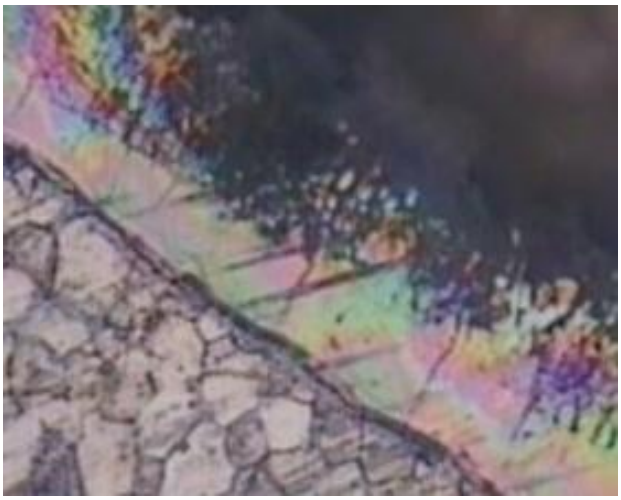

(b)

Figure 13. Photo of the microstructure of the galvanized pipe specimen, with a fluid flow rate of 50%, (a) 50x magnification, (b) 200x magnification

(a)

(b)

Figure 14. Photo of the microstructure of the galvanized pipe specimen, with a fluid flow rate of 75%, (a) 50x magnification, (b) 200x magnification

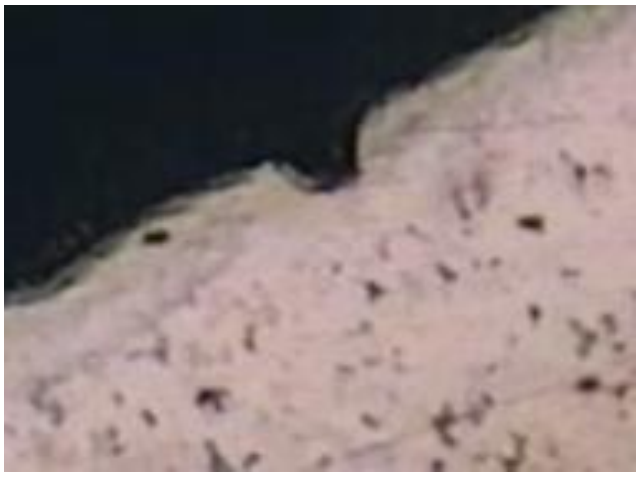

(a)

(b)

Figure 15. Photo of the microstructure of the galvanized pipe specimen, with a fluid flow rate of 100%, (a) 50x magnification, (b) 200x magnification

(a)

(b)

Figure 16. Photo of the microstructure of the non-galvanized pipe specimen before the corrosion test, (a) 100x magnification, (b) 500x magnification

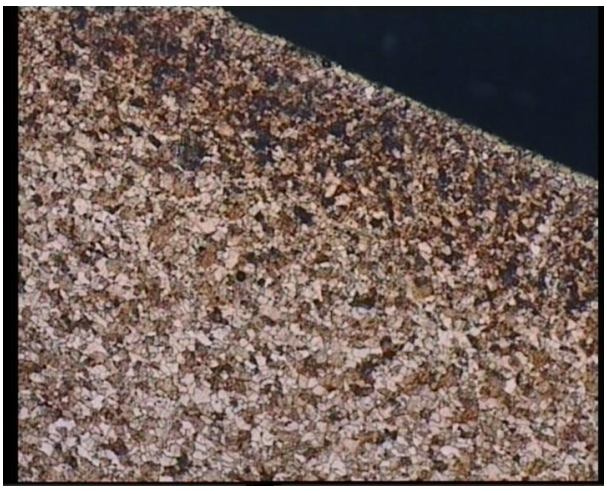

(a)

(b)

Figure 17. Photo of the microstructure of the non-galvanized pipe specimen, with a fluid flow rate of 0%, (a) 50x magnification, (b) 200x magnification

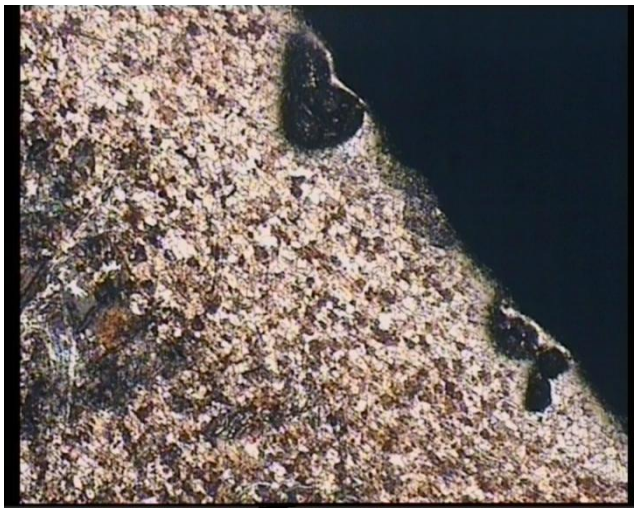

(a)

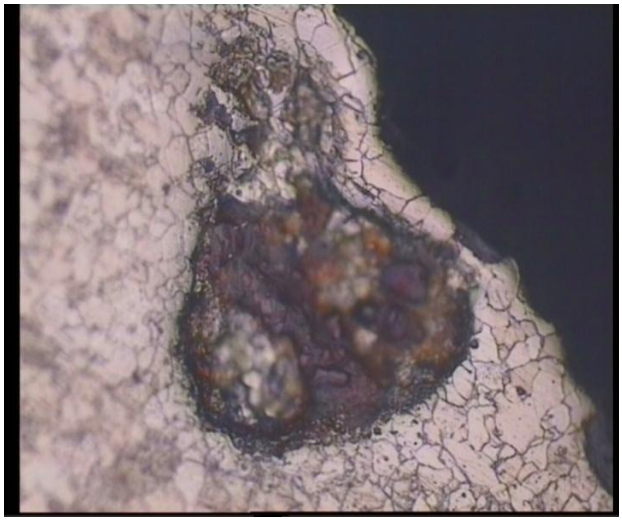

(b)

Figure 18. Photo of the microstructure of the non-galvanized pipe specimen, with a fluid flow rate of 50%, (a) 50x magnification, (b) 200x magnification

(a)

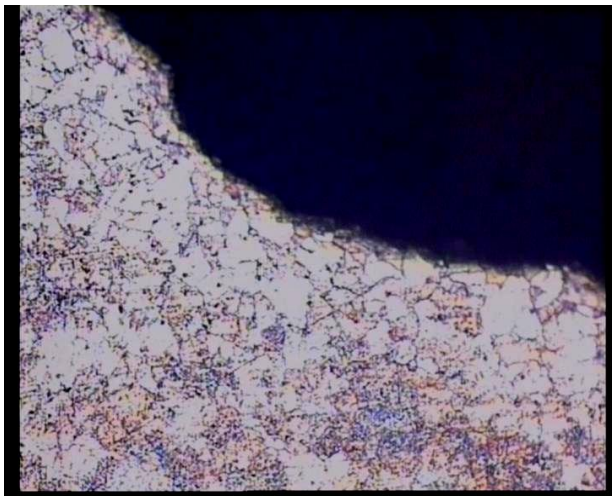

(b)

Figure 19. Photo of the microstructure of the non-galvanized pipe specimen, with a fluid flow rate of 75%, (a) 50x magnification, (b) 200x magnification

(a)

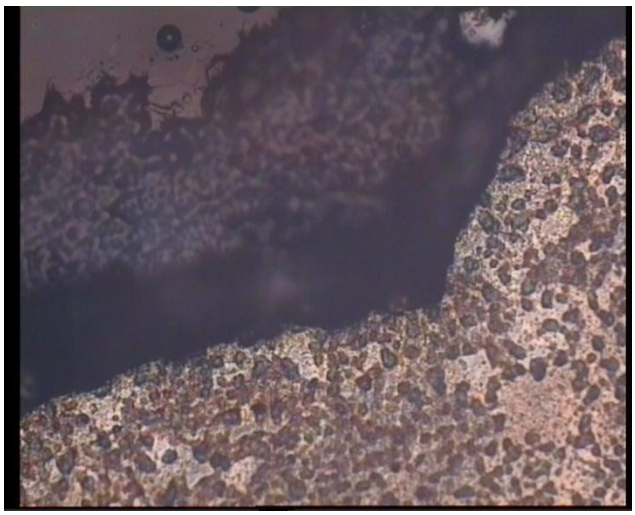

(b)

Figure 20. Photo of the microstructure of the non-galvanized pipe specimen, with a fluid flow rate of

100%, (a) 50x magnification, (b) 200x magnification

From metallographic observations, there is no visible intergranular corrosion or corrosion at the grain boundaries of the microstructure. Meanwhile, on visual observation, some specimens showed pitting and abrasion marks on the pipe surface, both galvanized and non-galvanized pipes. From this observation, we can conclude that the corrosion that occurs is abrasion and pitting corrosion.

Conclusion

From the tests and observations that have been carried out, it can be concluded that:

1. The relationship between seawater fluid flow rate and corrosion rate in this experiment is that the higher the flow rate, the higher the corrosion rate that occurs.
2. The corrosion that occurs is abrasion corrosion and pitting corrosion.

References

[1] Dwisetiono, D. Laju Korosi Pelat Baja Lunak "Grade A" Di Perairan Laut Surabaya Dengan berbagai Tingkat Sandblasting. Jurnal Sains dan Teknologi vol. 5 no.2. [2007].

[2] Fachroini T.A., Dwisetiono D. Penerapan MGPS (Marine Growth Prevention System) Pada Lambung Kapal. Hexagon Vol. 3 No. 1. 2022 Jan 28. Pp.53-5. DOI: https://doi.org/10.36761/hexagon.v3i1.1523

[3] Suhartanti, D. Laju Korosi Baja di Kawasan Udara PLTP Kamojang Jawa Barat. Seminar Fakultas Matematika dan Ilmu Pengetahuan Alam, Universitas Indonesia, Depok [2005].

[4] Agustini D, Fitriah L, Fahrurrozi F. Pemodelan Matematika pada Sistem Korosi Logam. Lombok Journal Of Science Vol. 5 No. 1 [2023] Apr 29. pp.33-41.

[5] Moelyo M. Tingkat Korosifitas Air Terhadap Infrastruktur Sumber Daya Air Menurut DIN 4030 dan Langelier Saturation Index. Jurnal Sumber Daya Air Vol. 8 No. 2 [2012] pp.187-200.

[6] Suharlinah, L., Sonjaya, H.G. Kerusakan Akibat Korosi Pada Komponen Baja Jembatan. Batam: Dinas Pekerjaan Umum [2008].

[7] Dwisetiono, D., Sambodho K., Winarno, A., Prayogi, U., Felayati, F.M., Karyatanti, I.D.P., Kristiono. T.A., Korosi Di Lingkungan Laut. Hang Tuah University Press. Surabaya, Indonesia (2024).

[8] Dwisetiono, D., Asmara, R.G. Analisa Kegagalan Sistem Bahan Bakar Kapal Dengan Menggunakan Metode Preliminary Hazard Analysis (PHA) dan Fault Tree Analysis (FTA). Hexagon Vol. 3 No. 1 [2022] Jan 28. pp. 34-9. DOI: https://doi.org/10.36761/hexagon.v3i1.1348